METHOD OF APPROXIMATE PARTICULAR SOLUTIONS FOR THE SOLUTION OF ELECTROCHINETIC FLUIDS IN MICRO AND NANOCHANNELS

DENIS ALBERTO CASTRO RODRIGUEZ

UNIVERSIDAD PONTIFICIA BOLIVARIANA
ESCUELA DE INGENIERIA
DOCTORADO EN INGENIERIA
MEDELLIN
2019

METHOD APPROXIMATE PARTICULAR SOLUTIONS FOR THE SOLUTION OF ELECTROCHINETIC FLUIDS IN MICRO AND NANOCHANNELS

DENIS ALBERTO CASTRO RODRIGUEZ

Thesis submitted for the degree of Doctor en Ingenieria

Advisor
Whady Felipe Floréz Escobar
PhD in Engineering

UNIVERSIDAD PONTIFICIA BOLIVARIANA
ESCUELA DE INGENIERIA
DOCTORADO EN INGENIERIA
MEDELLIN
2019

11 de marzo de 2020

DENIS ALBERTO CASTRO RODRIGUEZ

“Declaro que este trabajo de grado no ha sido presentado con anterioridad para optar a un título, ya sea en igual forma o con variaciones, en esta o en cualquiera otra universidad”. Art. 92, parágrafo, Régimen Estudiantil de Formación Avanzada.

Firma

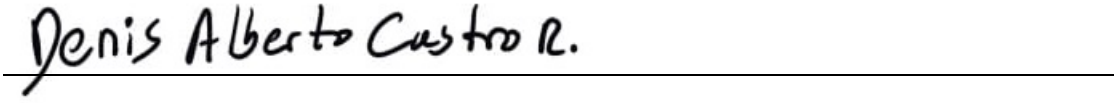

A mi esposa:
La cual ha sido mi ayuda idónea
A mis padres y mi hermano
A Dios todo poderoso
por su amor y misericordia incondicional ...

ACKNOWLEDGMENTS

First of all I want to thank God, creator of heaven and earth, for life, health and direction of my life throughout this doctoral process. I also want to thank my wife Sandra Patricia Rivas Bonilla for her unconditional support and for always being by my side. I also want to thank Professor Whady F. Florez, for his direction and teachings, comments and recommendations and above all his patience. Also thank my colleagues from CIFASIS - CONICET (Rosario, Argentina) especially Nahuel Caruso and Margarita Portapila for all the time dedicated and for having received me and allowing me to work with them and their friendship.

Finally, I would like to thank the Department of Chocó and COLCIENCIAS for the funds provided to carry out my doctorate through the royalty fund and the Technological University of Chocó, for facilitating and allowing me to carry it out.

Table of Contents

List of Figures

List of Tables

ABSTRACT

This work develops a global version of the Method of Approximate Particular Solutions (MAPS) as [17] or in the works of Bustamante [12], who have been researching and applying this method in different investigations and problems. This is due to its characteristics such as RBF Collocation system, its mesh-free environment, great efficiency and precision in its approaches, easy to implement and its easy adaptation to different types of boundary conditions making it a powerful and robust numerical method for solution of partial differential equations. Two MAPS formulations are studied here, in the first one particular solutions of non-homogeneous linear Poisson equations for scalar problems are used and in the second one particular solutions of a non-homogeneous Stokes system for multivariate problems.

The results obtained are accurate, due to the integration process that it has incorporated, which provides a smoothness in the solution unlike the derivation process that is carried out in other methods. Hence the problem variable is not approximated as in Kansa's method, The RBFs are approximated by the differential operator and the particular solutions obtained are used to approximate the variables of the given problem. When multivariate flow problems occur, the components for velocity and pressure in the momentum equation are approximated by the particular solutions of the non-homogeneous Stokes equation system, which means that an integration strategy that links velocity-pressure is not needed, since the particular solution of pressure is in terms of speed.

Initially, two problems are solved to verify the implementation of the MAPS in order to solve boundary value problem, the first one is a scalar problem whereas the second one is non-homogeneous Stokes flow problem, and results are compared with their respective exact solutions. Then the work is focused on identifying the influence of the different boundary conditions in the MAPS, where the easy adaptation of the method to arbitrary boundary conditions is evidenced. For this, a scalar problem is solved, then a homogeneous vector problem and finally an inhomogeneous vector problem. These results are compared with the exact different solutions for each case. Thirdly, electrokinetic fluids in microchannels are studied, which allows us to know the physical nature of the problem while showing the great development and research interest in this subject.

Finally, pressure-driven fluids, electroosmotic flows and mixed flows are studied; These fluids are initially developed in micro channels and finally in nanochannels through the implementation of the MAPS.

In summary, the main contribution of this work is the development of a meshless numerical method based in RBFs which is implemented to solve the flow problem within and between the interface of two nanochannels of a proton exchange membrane in a fuel cell, which becomes an advance in the field of mathematics since a meshless method is developed to solve mixed electro-kinetic fluids (pressure driven flow and electro-osmotic flow) that are not reported in the literature to solve this type of problem, as well as a contribution to the field of applied mathematics.

KEYWORDS:

Radial Basis Functions, meshless methods, MAPS, Stokes system, electrokinetic fluid, micro and nanochannel

INTRODUCTION

In recent decades, the use and development of meshless methods has increased, as is the case of RBF collocation methods, which have recently been applied to a variety of problems within science and engineering. These allow to eliminate the difficulties of the traditional methods of preprocessing the mesh and its efficiency. But nevertheless, we are interested in this type of methods with RBF collocation because of its ease of implementation to solve problems in two and three dimensions, its rapid convergence and its flexibility when applying arbitrary boundary conditions. In addition, interpolations with RBF have shown to be quite robust, although this contradicts their dependence on the shape parameter, current research topic to find its optimal value. On the other hand, this work used a global RBF scheme to solve PDEs and, like the literature, it was evident that the matrix of the system is affected by the accuracy of the solution, a situation that arises when the number of nodes increases of the system in search of a better precision which is related to the bad conditioning of the matrix.

Meshless methods using radial basis functions (RBF) have been studied in recent years due to their simplicity of implementation, high rates of onvergence and flexibility. RBF have been widely used in continuous interpolation [11] and global dispersed data sets. This interpolation strategy has become the basis of meshless methods for solving PDEs through the development of the Kansa method [44]. Kansa used the Multiquadric (MQ) function to obtain an accurate solution meshless for the advection-diffusion equations and Poisson Chen in [16], although the Kansa method was used by many authors to solve Laplace equations [15, 45, 62], [21, 61, 62] Poisson equation, Helmholtz equation [19] and Parabolic [17] which show better accuracy compared to the traditional methods [15, 19, 57, 100]. In [45] the authors concluded that the bad conditionality of the matrix worsens as the number of nodes increases.

The Method of Approximate Particular Solutions (MAPS) was developed initially by Chen to solve PDE for linear problems in two dimensions (see [17, 21, 72]) with the purpose of finding a set of coefficients that are approximated by numerical schemes based on radial basis function to approximate a particular solution. In [17] the authors solve scalar problems with elliptic PDE as Poisson type [76], Helmholtz and Biharmonic [29] and in [16] presents the method to solve elliptic PDEs with variable coefficients

(see [28, 75]), showing how simple and easy is to apply the MAPS. During the last two decades, the MAPS have been used extensively in diverse investigations to solve problems of convection-diffusion [39, 92, 28], In [84] uses RBF trigonometric for the solution of PDEs, elipticos problems [103] and at local level [97, 96, 66], see also [51, 59, 54]. It is important to note that the scheme developed by Chen is based on particular Poisson solutions to approximate the PDEs. On the other hand, Bustamante et al. [13] develop a MAPS scheme to solve a vector equation of a Stokes flow, which was also implemented to solve the Navier-Stokes equations in [14, 30, 31, 25, 101], and elasticity problems [12].

The MAPS presented previously, is intended to be used to solve electrokinetic fluids in nanochannels, which are important in various chemical and biomedical analyzes. We are based on the theory developed by [56] and [46] with respect to the electrokinetic flows, [36, 73, 32], which have been studied in two major subtopics: the first one, are the pressure-driven fluids [93, 63, 40, 38], which occurs when a liquid is forced through a channel under applied hydrostatic pressure, resulting in an electric current in the direction of flow pressure-driven, see also [67, 77, 35]. The second ones are the electonic fluxes [102, 55, 88], which consist of those fluids that move under the influence of an applied electrical force, that is, the electroosmosis that allows the pumping of fluids and the flow control using electric fields. In addition, the velocity profiles for this type of flow are mostly uniform; this type of fluid was initially studied in microchannels [74, 43, 87, 91], but in recent years has been growing greatly investigations in nanochannels [98, 20, 64, 68], see also the works [47, 71, 77, 99].

We are interested in the phenomenology of PEM membranes, since these constitute an important factor in the operation of fuel cells. It is for this reason that the modeling of fuel cells is very useful for the developers of these technologies, as it can lead to improvements in the design of fuel cells. The improvements necessary for the operation and operation of the fuel cell require one in design, materials and optimization. There are many published models for PEM fuel cells in the literature, but it is often a daunting task to begin to understand the complexity of current models [34, 5]. According to [24] the multi-scale models lose too much precision compared to those that focus on a specific component, see also [50]. Research in this type of technology has used different types of approaches for the modeling and simulation of the PEM membranes, such as the work done by [37, 90, 47]. They present results that use molecular dynamics [1, 26, 46], consider that the larger radius leads to faster diffusion of the proton, in the same way [42, 33, 4, 83] obtained similar procedures and approaches, see also [80, 41].

Peighambardoust et al. [69], it shows us a detailed review of the evolution in investigations carried out on proton exchange membranes and the importance they have for the operation of a fuel cell, while in [89], they consider that high temperature proton exchange membrane fuel cells (HT-PEMFC) It has several advantages, such as high proton conductivity, low fuel permeability, low electroosmotic drag coefficient, good chemical

/ thermal stability, good mechanical properties and low cost. Similarly [23] shows the different materials that are currently considered for membrane manufacturing, see also [89], [85] and [52].

One of the most interesting studies regarding the investigation of the phenomenology of the transport of flow of loaded fluid, is the one proposed by [48] which propose a hydrodynamic model that allows them to describe the flow of charged fluid and the change of pore morphology due to mechanical deformations, solve a set of numerical coupled nonlinear equations, based on the experiments of [9, 81, 86]. Berg et al. [10], the equilibrium form of the interface representing the lateral limit of a channel of the pore embedded in an elastomer is studied. In the models proposed by [48, 49] they affirm that an ohmic resistance is observed between the interfaces of two electrolyte membranes of joint polymer, of which no theoretical explanation is found. Also they propose a new model for the flow of fluid loaded in and between the nanochannels and investigated numerically, they solve it for velocity, pressure, electrical potential and proton concentration. Finally the work of [7] by means of an uncoupled continuous model studies the distribution and the flow of protons inside a cylindrical nanopore filled with water of a PEM, in it the Poisson-Nernst-Planck equations are modified.

From the review shown above we can see the importance of the electrokinetic flows and the role they play when investigating the flow of fluid in PEM membranes, besides it is evident that these have not been solved with the MAPS method. Taking into account the importance of developing new numerical methods and diversifying its field of applications, in this work we set out as the main objective the following:

OBJECTIVES

To develop a meshless numerical method of RBFs with approximate particular solutions to solve the 2-D Stokes flow problem in and between the interface of two nanocanales of a proton exchange membrane (PEM) in a fuel cell, allowing the identification and characterization of the factors that generate the electro-ohmic resistance in the transport of protons in a nanochannel.

For the development of the overall objective the following specific objectives are proposed:

- Study the characteristics of the meshless numerical method of radial basis functions with approximate particular solutions.
- Solve the linear and non-linear scalar problems for the Poisson equations for the electric potential and Nernst-Planck equations in the proton concentration of the

proposed model.

- Solve Stokes' flow problem, coupled with the equations of the electric potential and proton concentration.
- Validate the results obtained and the efficiency of the meshless numerical algorithm based on RBFs with approximate particular solutions identifying the effects generated by the electro-ohmic resistance in the transport of protons in a PEM membrane.

THESIS OUTLINE

This work the method of approximate particular solutions global in two dimensions, where we study numerically the solution of electrokinetic fluids and their application to proton exchange membranes (PEM) in a fuel cell. This document is organized as follows: in Chapter 1, the MAPS is presented for scalar problems as in [16] and it is also presented for multivariable problems as in [13]; once the results are presented of implementing the global MAPS, some general observations are made. In Chapter 2, the influence of boundary conditions in the MAPS is presented, for this, three types of problems are solved, the first a "Slip Flow" for a homogeneous Stokes fluid, second a connective laminar flow between parallel vertical plates this for a non-homogeneous Stokes and finally a scalar problem is solved and the results are compared in these three situations. In Chapter 3, a general theory of electro-kinetic fluids is shown as in [46], a formulation of these fluids for cylindrical and rectangular microchannels is presented which is done for two general cases for pressure-driven fluids and for electro osmotic fluids. Finally, in Chapter 5 the MAPS is applied to solve problems of electro-kinetic fluids in two nanochannels of a PEM membrane of a fuel cell, a solution that is made for a mixed flow driven by pressure and electro osmotic.

Chapter 1

GLOBAL METHOD APPROXIMATE PARTICULAR SOLUTIONS

In this section we show the theoretical foundations of the method of approximate particular solutions (MAPS), which was developed by [17] to solve PDE for linear problems in two dimensionswith the purpose of finding a set of coefficients using RBF numerical schemas and approximate a particular solution. The authors solve a elliptic equations for a problem of Poisson type. In addition, they solve the equations of Helmholtz and Biharmonic and in [16] they presents the method to solve Elliptic PDEs with variable coefficient, showing how simple and easy to apply is the MAPS.

Unlike the contributions of [17] and [16], Bustamante et al. [14] and [13] particular solutions of Stokes are used to approximate velocity and pressure, We use this procedure to solve a scalar problem and a vector problem. The particular solutions of Stokes and Poisson are used to study the problem of electro-osmotic flow in a membrane channel PEM, given by the model Kimmerle et al. [48]formed by the steady state Poisson-Nernst-Planck-Stokes equations.

1.1 Global MAPS for Linear PDEs

Now we present the global MAPS scheme which was proposed by [17]. Consider a boundary value problem, where L and B are linear partial differential operators that apply in the Ω domain of the problem and its Γ boundary, such as:

$$L(u(\vec{x})) = f(\vec{x}) \quad \forall x \epsilon \Omega \tag{1.1}$$

$$B(u(\vec{x})) = g(\vec{x}) \quad \forall x \epsilon \Gamma \tag{1.2}$$

where f and g are known functions. The unknown variable u can be approximated by RBF using the MAPS, such as:

$$u(\vec{x}) = \sum_{k=1}^{N} \alpha_k \widehat{u}_k(r) \tag{1.3}$$

where $\widehat{u}$ is the corresponding particular solution, then we have,

$$L(u(\vec{x})) = \sum_{k=1}^{N} \alpha_k L(\widehat{u}_k(r)) = \sum_{k=1}^{N} \alpha_k \phi(r_k) = f(\vec{x}) \tag{1.4}$$

since,

$$L(\widehat{u}(\vec{x})) = \phi(r_k) \tag{1.5}$$

then, if $\widehat{u}$ satisfies the boundary conditions 1.2, we have the expression

$$B(u(\vec{x})) = \sum_{k=1}^{N} \alpha_k B(\widehat{u_k}(r)) = g(\vec{x}) \tag{1.6}$$

Thus, we obtain the following system of equations

$$\sum_{k=1}^{N} \alpha_k B(\widehat{u}(r)) = g(\vec{x}) \tag{1.7}$$

$$\sum_{k=1}^{N} \alpha_k \phi(r_k) = f(\vec{x}) \tag{1.8}$$

The implementation of the MAPS is reduced to solving the following linear system of algebraic equations:

$$\begin{pmatrix} B[\hat{u}(\vec{x}_1, \vec{\xi}_1)] & \dots & B[\hat{u}(\vec{x}_1, \vec{\xi}_N)] \\ \vdots & \ddots & \vdots \\ B[\hat{u}(\vec{x}_{N_b}, \vec{\xi}_1)] & \dots & B[\hat{u}(\vec{x}_{N_b}, \vec{\xi}_N)] \\ \phi(|\vec{x}_{N_b+1} - \vec{\xi}_1|) & \dots & \phi(|\vec{x}_{N_b+1} - \vec{\xi}_N|) \\ \vdots & \ddots & \vdots \\ \phi(|\vec{x}_N - \vec{\xi}_1|) & \dots & \phi(|\vec{x}_N - \vec{\xi}_N|) \end{pmatrix} \begin{pmatrix} \alpha_1 \\ \vdots \\ \alpha_{N_b} \\ \alpha_{N_b+1} \\ \vdots \\ \alpha_N \end{pmatrix} = \begin{pmatrix} g(\vec{x_1}) \\ \vdots \\ g(\vec{x_{N_b}}) \\ f(\vec{x_{N_b+1}}) \\ \vdots \\ f(\vec{x_N}) \end{pmatrix}$$

For N_b points at the boundary and N_i interior points, with $N = N_b + N_i$. The solution of the previous boundary value problem is achieved after solving the resulting algebraic system for the coefficients α.

The particular solution $\widehat{u}$ of (1.5), has previously been used in connection with the numerical solution of a linear boundary value problem using classical decomposition in terms of its particular and homogeneous solutions, combined with The Fundamental Solution Method [29] and with the Boundary Element Method (BEM) [27] to find the corresponding homogeneous solution.

1.2 Global MAPS for scalar problems

According to [16]. Give the boundary value problem in two dimensions of the form:

$$\nabla^2 u + b_1(x,y)\frac{\partial u}{\partial x} + b_2(x,y)\frac{\partial u}{\partial y} + c(x,y)u = f(x,y), \quad (x,y) \in \Omega \tag{1.9}$$

$$Bu = g(x,y), \quad (x,y) \in \partial\Omega \tag{1.10}$$

The equation (1.9) is a Poisson type equation, which we can see if we rearrange, as

$$\nabla^2 u = h\left(x, y, u, \frac{\partial u}{\partial x}, \frac{\partial u}{\partial y}\right) \tag{1.11}$$

where

$$h\left(x, y, u, \frac{\partial u}{\partial x}, \frac{\partial u}{\partial y}\right) = -b_1(x,y)\frac{\partial u}{\partial x} - b_2(x,y)\frac{\partial u}{\partial y} - c(x,y)u + f(x,y) \tag{1.12}$$

Using the RBF, we have that a particular approximate solution of the solution is given

by

$$\widehat{u}_p = \sum_{i=1}^{N} \alpha_i \Phi(r_i) \tag{1.13}$$

Where Φ is obtained by the analytical solution of the expression

$$\nabla^2 \Phi = \phi \tag{1.14}$$

so,

$$\Phi(r) = \frac{1}{9}(4c^2 + r^2)\sqrt{r^2 + c^2} - \frac{c^3}{3} \ln\left(c + \sqrt{r^2 + c^2}\right) \tag{1.15}$$

where $\phi(r) = \sqrt{r^2 + c^2}$ and $r = \sqrt{(x - x_i)^2 + (y - y_i)^2}$

Now the solution of the problem (1.9)-(1.10) can be approximated by

$$u(x, y) \simeq \widehat{u} = \sum_{i=1}^{N} \alpha_i \Phi(r_i) \tag{1.16}$$

Therefore of (1.14) we have to,

$$\nabla^2 u \simeq \nabla^2 \widehat{u} = \sum_{i=1}^{N} \alpha_i \nabla^2 \Phi(r_i) = \sum_{i=1}^{N} \alpha_i \phi(r_i), \quad \text{in} \Omega \tag{1.17}$$

so we have the expression

$$h\left(x, y, u, \frac{\partial u}{\partial x}, \frac{\partial u}{\partial y}\right) = \sum_{i=1}^{N} \alpha_i \phi(r_i) \tag{1.18}$$

As the derivatives of the solution can be approximated by the particular solution $\widehat{u}$ we have,

$$\frac{\partial u}{\partial x} \simeq \frac{\partial \widehat{u}}{\partial x} = \sum_{i=1}^{N} \alpha_i \frac{\partial \Phi}{\partial x}(r_i) \tag{1.19}$$

$$\frac{\partial u}{\partial y} \simeq \frac{\partial \widehat{u}}{\partial y} = \sum_{i=1}^{N} \alpha_i \frac{\partial \Phi}{\partial y}(r_i) \tag{1.20}$$

Therefore we have the following formulation:

$$\sum_{i=1}^{N} \alpha_i \left(\phi(r_i) + \delta(x, y)\frac{\partial \Phi(r_i)}{\partial x} + \beta(x, y)\frac{\partial \Phi(r_i)}{\partial y} + \gamma(x, y)\Phi(r_i)\right) = f(x, y) \tag{1.21}$$

This expression is completed with the boundary condition and we have the system:

$$\sum_{i=1}^{N} \alpha_i \Psi(r_{ij}) = f(x_j.y_j) \tag{1.22}$$

$$\sum_{i=1}^{N} \alpha_i B\Phi(r_{ij}) = g(x_j.y_j) \tag{1.23}$$

where

$$\Psi(r_{ij}) = \phi(r_{ij}) + \delta(x_j, y_j)\frac{\partial \Phi(r_{ij})}{\partial x} + \beta(x_j, y_j)\frac{\partial \Phi(r_{ij})}{\partial y} + \gamma(x_j, y_j)\Phi(r_{ij}) \tag{1.24}$$

1.3 Global MAPS for the Stokes equation

In [13] the MAPS procedure is used, as presented above, to solve elasticity problems modeled by the Navier equations. A linear combination of the particular displacement solutions is used to approximate the problem variables, that is, the displacement components in this case.

The procedure proposed by [17], is used in the global Stokes MAPS, but the particular solutions solve a Stokes system. In addition, the definition of a particular solution, in terms of an auxiliary potential, leads to satisfy the continuity equation automatically.

Consider a two-dimensional arbitrary region Ω with boundary Γ. The steady-state equations of Navier-Stokes in its primitive variable formulation, with a low Reynolds number, a system of nonlinear equations for incompressible fluid flow is reduced to the Stokes linear system:

$$\frac{\partial u_i}{\partial x_i} = 0 \tag{1.25}$$

$$\mu\frac{\partial^2 u_i}{\partial x_j \partial x_j} + \frac{\partial p}{\partial x_i} = 0 \tag{1.26}$$

With $i = 1, 2$ for a problem in two dimensions. The natural boundary conditions are defined by the speed and/or surface tension given by,

$$u_i = \vec{u}_{ib} \quad \forall x \in \Gamma_u \tag{1.27}$$

$$t_i = \sigma_{ij} n_j = -p n_i + \mu \left(\frac{\partial u_i}{\partial x_j} + \frac{\partial u_j}{\partial x_i} \right) \quad \forall x \in \Gamma_t \tag{1.28}$$

The particular solution $(\widehat{u}_i^l, \widehat{p}^l)$ are given by the following non-homogeneous Stokes system, from the equations (1.26) and (1.25):

$$\mu \frac{\partial^2 \widehat{u}_i^l(\vec{x}, \vec{\xi})}{\partial x_j \partial x_j} + \frac{\partial \widehat{p}^l(\vec{x}, \vec{\xi})}{\partial x_i} = \phi(r) \delta_{il} \tag{1.29}$$

$$\frac{\partial \widehat{u}_i^l(\vec{x}, \vec{\xi})}{\partial x_i} = 0 \tag{1.30}$$

Where the field variables $\widehat{u}_i^l$ and $\widehat{p}^l$ are known as Stokes' particular velocities and pressures, respectively. The inhomogeneous term in the momentum equation (1.29) is given by the function ϕ for our case defined as the Multiquadric RBF (MQ), $\phi(r) = (r^2 + c^2)^{1/2}$, which depends on r given by the Euclidean distance between a field point $\vec{x}$ and a test point $\vec{\xi}$ and the shape parameter c.

Making use of the decomposition formula of Oseen [70] to find the corresponding fundamental solution of the Stokes equations. First, we define the particular speeds in terms of an auxiliary potential ψ, as

$$\widehat{u}_i^l(\vec{x},\vec{\xi}) = \frac{\partial^2\psi(r)}{\partial x_m \partial x_m}\delta_{il} - \frac{\partial^2\psi(r)}{\partial x_i \partial x_l} \tag{1.31}$$

Substituting the velocity representation formula (1.31) in the equation (1.26), the following expression is obtained

$$\mu\frac{\partial^4\psi(r)}{\partial x_j \partial x_j \partial x_m \partial x_m}\delta_{il} - \mu\frac{\partial^4\psi(r)}{\partial x_i \partial x_l \partial x_m \partial x_m} - \frac{\partial p^l(\vec{x},\vec{\xi})}{\partial x_i} = \phi(r)\delta_{il} \tag{1.32}$$

By multiplying certain terms by δ_{il} leaving aside those that coincide in the subscripts, we obtain a non-homogeneous biharmonic equation for the potential ψ, with the RBF ϕ as an inhomogeneous term, next to an expression that relates $\widehat{p}$ with ψ, that is

$$\mu\frac{\partial^4\psi(r)}{\partial x_m \partial x_m \partial x_k \partial x_k} = \phi(r) \tag{1.33}$$

$$\mu\frac{\partial^4\psi(r)}{\partial x_m \partial x_m \partial x_i \partial x_l} + \frac{\partial p^l(\vec{x},\vec{\xi})}{\partial x_i} = 0 \tag{1.34}$$

By directly integrating the first of these two previous equations, you get the following expression for ψ in terms of r.

$$\psi(r) = \frac{1}{12\mu}\left[\frac{1}{75}\phi(r)(4r^4 + 48r^2c^2 - 61c^4) - c^3\ln(c)r^2 - \frac{1}{5}(5r^2 - 2c^2)c^3\ln(c+\phi(r))\right] \tag{1.35}$$

Substituting (1.35) in (1.31) and (1.34), you get expressions for $\widehat{u}_i^l$ and $\widehat{p}^l$, in terms of r, then the expressions for the flow field (u, p) is given as:

$$\widehat{u}_i^l(\vec{x}, \vec{\xi}) = \frac{1}{\mu}\left\{\left(\frac{\psi}{r} + \psi^{''}\right)\delta_{il} - \left[\frac{\psi^{'}}{r}\left(\delta_{il} - \frac{\widehat{x}_i\widehat{x}}{r^2}\right) + \psi^{''}\frac{\widehat{x}_i\widehat{x}}{r^2}\right]\right\} \tag{1.36}$$

Where $\widehat{x}_i = x_i - \xi_i (i = 1, 2)$, with its corresponding directional derivative

$$\frac{\partial \widehat{u}_i^l(\vec{x}, \vec{\xi})}{\partial x_j} = \frac{1}{\mu}\left\{\left[\left(\frac{\psi^{'}}{r^2} - \frac{\psi^{''}}{r}\right) + \psi^{'''}\right]\frac{\widehat{x}_j}{r}\delta_{il} + \left(\frac{\psi^{'}}{r^2} - \frac{\psi^{''}}{r}\right)\left(\frac{\widehat{x}_l}{r}\delta_{ij} + \frac{\widehat{x}_i}{r}\delta_{lj}\right) - \left[3\left(\frac{\psi^{'}}{r^2} - \frac{\psi^{''}}{r}\right) + \psi^{'''}\right]\frac{\widehat{x}_i\widehat{x}_j\widehat{x}_k}{r^3}\right\} \tag{1.37}$$

The particular pressure solution is given by the following equation obtained after integrating and expressing in radial terms the equation (1.34):

$$\widehat{p}^l = -\mu\frac{\widehat{x}_l}{r}\left[\psi^{'''} - \left(\frac{\psi^{'}}{r^2} - \frac{\psi^{''}}{r}\right)\right] \tag{1.38}$$

Then, we have that for this case the velocity field u and pressure p of Stokes, are approximated by the expressions:

$$u_i(\vec{x}) \approx \sum_{k=1}^{N} \alpha_k^l \widehat{u}_i^l(r_k) \tag{1.39}$$

$$p(\vec{x}) \approx \sum_{k=1}^{N} \alpha_k^l \widehat{p}^l(r_k) \tag{1.40}$$

Substituting these expressions in the momentum equation (1.26), we have the representation of the approximate momentum equation:

$$\sum_{k=1}^{N} \alpha_k^l \left[\mu \frac{\partial^2 \widehat{u}_i^l(r_k)}{\partial x_j \partial x_j} - \frac{\partial \widehat{p}^l(r_k)}{\partial x_i} \right] = \sum_{k=1}^{N} \alpha_k^l [\phi(r_k)\delta_{il}] = 0 \tag{1.41}$$

Then, by replacing the equations (1.39) and/or (1.40) in the boundary conditions (1.27) and/or (1.28), the placement process is completed by obtaining the following matrix system:

$$\begin{bmatrix} B^1[\hat{u}_1^1, \hat{u}_2^1, \hat{p}^1] & B^1[\hat{u}_1^2, \hat{u}_2^2, \hat{p}^2] \\ B^2[\hat{u}_1^1, \hat{u}_2^1, \hat{p}^1] & B^2[\hat{u}_1^2, \hat{u}_2^2, \hat{p}^2] \\ [\phi] & [0] \\ [0] & [\phi] \end{bmatrix} \begin{bmatrix} [\alpha^1] \\ [\alpha^2] \end{bmatrix} = \begin{bmatrix} [g(\vec{x})_1] \\ [g(\vec{x})_2] \\ [0] \\ [0] \end{bmatrix}$$

Here, it is generally used the boundary condition $B^k[u_1, u_2, p] = g(\vec{x})_k$, where B^k is a boundary operator and g_k the corresponding value of the boundary condition. In the case that a pressure boundary condition is imposed, it would be necessary to prescribe one of the components of the velocity field, according to the physics of the problem.

It is important to note that the expressions obtained for the particular solution of the velocity (1.36), its derivatives (1.37) and the pressure (1.38), although there are terms $1/r^n$, the particular solution obtained it is not singular anywhere in the delimited domain since the singularities in the terms $\frac{\psi'}{r^2}$ and $\frac{\psi''}{r}$ are canceled in the expression $\frac{\psi'}{r^2} - \frac{\psi''}{r}$. The following expressions for radial derivatives of ψ, required for the last equations, are obtained from (1.35).

$$\frac{\psi}{r} = \frac{4r^6 + 36r^4c^2 + 39r^2c^4 + 7c^6}{180(r^2+c^2)^{(3/2)}} - \frac{(5r^4 + 3r^2c^2 - 2c^4)c^3}{60(r^2+c^2)^{(3/2)}\left[c + (r^2+c^2)^{(1/2)}\right]} - \frac{1}{6}c^3 \ln\left[c + (r^2+c^2)^{(1/2)}\right] - \frac{1}{6}c^3 \ln(c)$$

$$\psi'' = \frac{16r^6 + 84r^4c^2 + 96r^2c^4 + 7c^6}{180(r^2+c^2)^{(3/2)}} - \frac{(20r^4 + 25r^2c^2 - 2c^4)c^3}{60(r^2+c^2)^{(3/2)}\left[c + (r^2+c^2)^{(1/2)}\right]} + \frac{(5r^2 - 2c^2)c^3r^2}{60(r^2+c^2)\left[c + (r^2+c^2)^{(1/2)}\right]^2} - \frac{1}{6}c^3 \ln\left[c + (r^2+c^2)^{(1/2)}\right] - \frac{1}{6}c^3 \ln(c)$$

$$\psi''' = \frac{76r^4 + 176r^2c^2 + 285c^4}{300(r^2+c^2)^{(3/2)}} - \frac{(4r^4 + 48r^2c^2 - 61c^4)c^3}{300(r^2+c^2)^{(5/2)}} + \frac{(10r^4 + 15r^2c^2 - 2c^4)c^3r}{20(r^2+c^2)^2\left[c + (r^2+c^2)^{(1/2)}\right]} + \frac{(5r^2 + 22c^2)c^3r}{20(r^2+c^2)^{(3/2)}\left[c + (r^2+c^2)^{(1/2)}\right]} + \frac{(-5r^2 + 2c^2)c^3r^3}{20(r^2+c^2)^{(5/2)}\left[c + (r^2+c^2)^{(1/2)}\right]} + \frac{(-5r^2 + 2c^2)c^3r^3}{30(r^2+c^2)^{(3/2)}\left[c + (r^2+c^2)^{(1/2)}\right]^3}$$

Finally, due to the relationship between the expressions of the particular velocity solution and the pressure in the equation (1.34), it is not necessary to look for a velocity-pressure coupling. In addition, the formulation fulfills the mass conservation, since the particular solution exactly satisfies the continuity equation.

1.4 Numerical Results

In this section we solved some problems that helped us to implement generic codes for the MAPS. At the beginning, the main intention was to verify the performance of the method, review its behavior to solve scalar and vector problems.

To determine the accuracy obtained, the errors are evaluated in terms of the relative root-mean-square error (RMSE) which are given by:

$$RMSE = \frac{\sqrt{\frac{1}{N}\sum_{i=1}^{N}|u_i - \widehat{u}_i|^2}}{max|u|} \tag{1.42}$$

where $\widehat{u}_j$ is the approximate solution and u_j the analytic solution.

1.4.1 Scalar problem

We present a scalar problem given by a 2D Poisson equation with Dirichlet boundary conditions (for more details see [82]) given by:

$$\begin{aligned} \triangle u &= \sin(\pi x)\sin(\pi y), \qquad 0 \leq x, y \leq 1 && (1.43)\\ u(x,y) &= 0, \quad \text{along the boundaries} && (1.44) \end{aligned}$$

Which has the exact solution $u_e(x,y) = -1/(2\pi^2)\sin(\pi x)\sin(\pi y)$

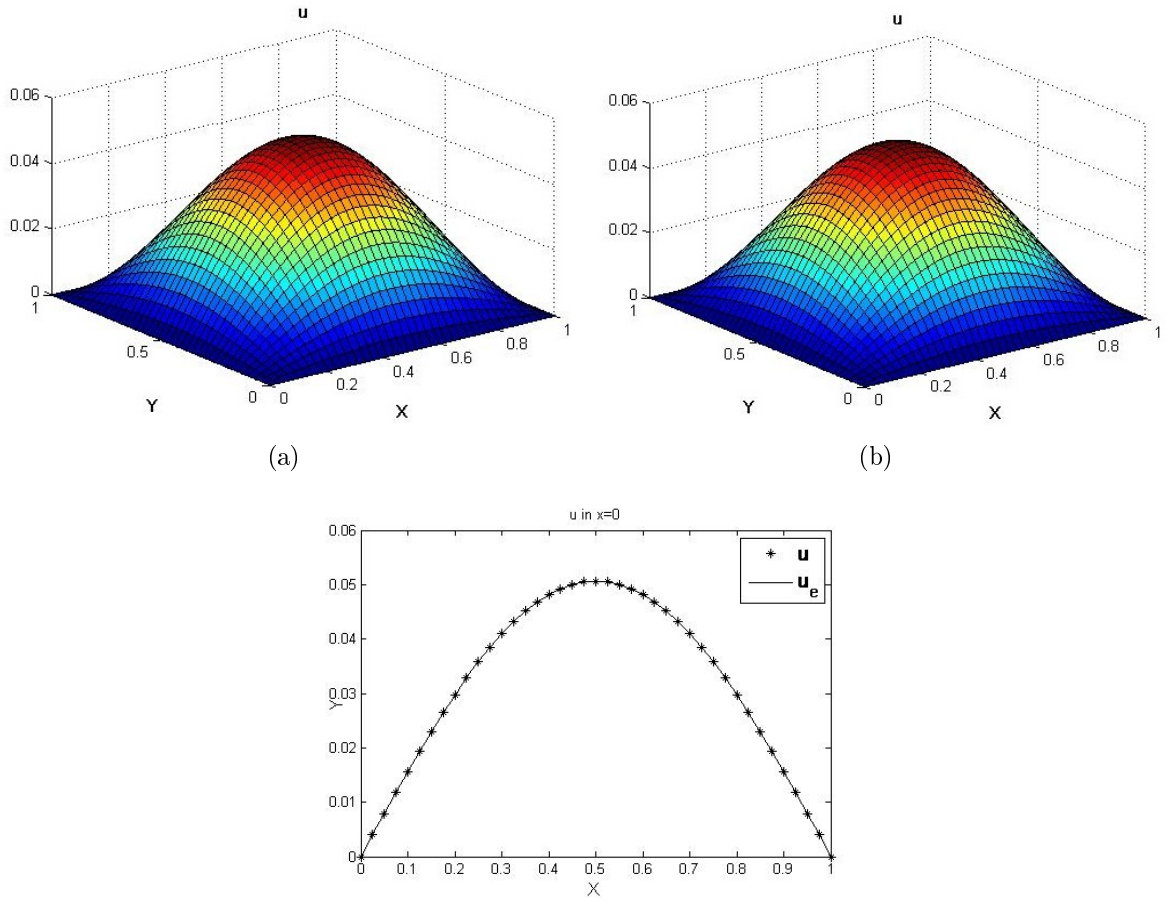

(a) (b)

(c)

Figure 1.1: Results (a) u for $c = 1.2e^{-1}$, (b) u for $c = 1.2e^{-3}$, and (c) u in $x = 0.5$ for $c = 1.2e^{-1}$

N	$c = 1.2e^{-1}$	$c = 1.2e^{-3}$
441	$1.3402e^{-5}$	$7.1950e^{-5}$
961	$3.2996e^{-6}$	$2.5842e^{-5}$
1681	$5.6170e^{-7}$	$1.2755e^{-5}$

Table 1.1: RMSE errors according to discretization size and shape parameter

The figure 1.1 shows the results for two different values of the shape parameter, there is not a noticeable difference between them. However, the 1.1 table shows the errors for various discretization and the two values of shape parameters.

In the table 1.1 it can be seen how for the large shape parameter better solutions are obtained, however in both cases good approximations are achieved, see for example [16] and [14].

1.4.2 Vector problem

Secondly, we solve a vector problem similar to the one in [18], which solves an inhomogeneous Stokes equation on the domain $\Omega = (0,1) \times (0,1)$. For our case, we apply Dirichlet boundary conditions over the entire bounday $\partial\Omega$. The differential equation is given by:

$$-\mu(\nabla u + \nabla u^T) + \nabla p = f \tag{1.45}$$

$$\nabla \cdot u = 0 \tag{1.46}$$

Along with the boundary condition

$$u = u_{Analytical}, \quad \text{on} \quad \partial\Omega \tag{1.47}$$

Where the exact solution is given by the following expression:

$$\vec{u} = (x^3 + 8x^2y - 6xy^2 + 10y^3, 10x^3 - 3x^2y - 8xy^2 + 2y^3)^T \tag{1.48}$$

$$p = 4x^3 - 6xy^2 \tag{1.49}$$

The solution to this problem allowed us to verify the operation of the code for the solution of vector problems. In the figure 1.2, we show the results for velocity "u" and in the figure 1.3 for velocity "v", on the lines $x = 0$ and $x = 1$.

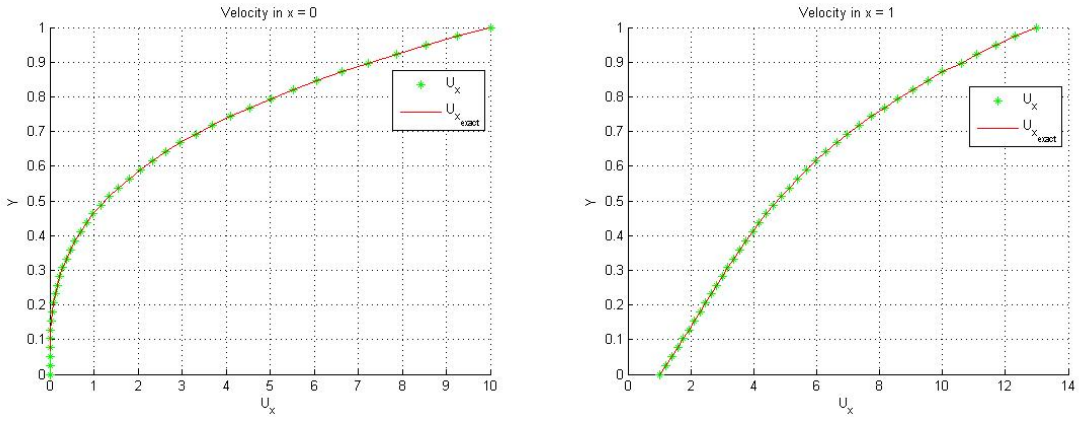

(a) (b)

Figure 1.2: x-Velocity component comparison in: a) $x = 0$, b) $x = 1$

To verify the operation of the method when performing the reconstruction of the derivatives, we calculate the derivative $\frac{du}{dy}$ which was compared with the derivative of the analytical solution, which can be seen in the figure 1.4.

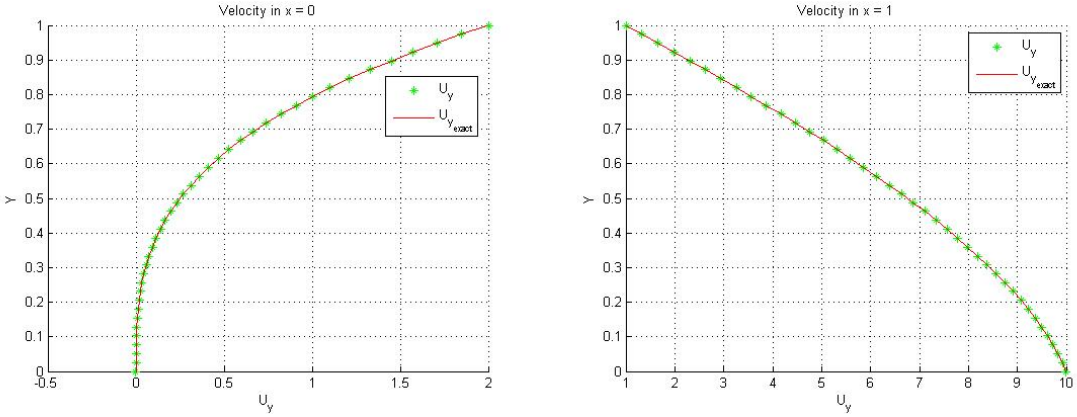

(a) (b)

Figure 1.3: y-Velocity component comparison: a) $x = 0$, b) $x = 1$

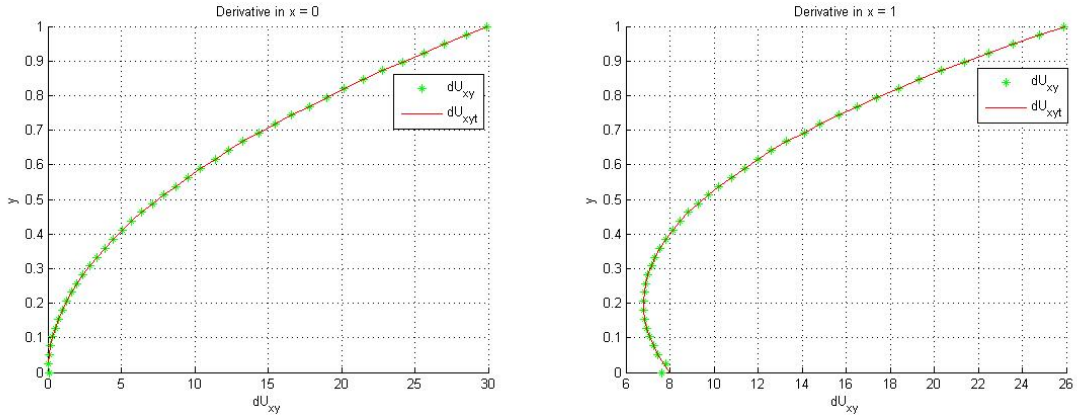

(a) (b)

Figure 1.4: Derivative from the solution: a) $x = 0$, b) $x = 1$

Finally we perform the reconstruction of the traction, whose y-component is shown on both $x = 0$ and on $y = 0$ lines, In figure 1.5. The other components are not illustrated since they show a constant behavior.

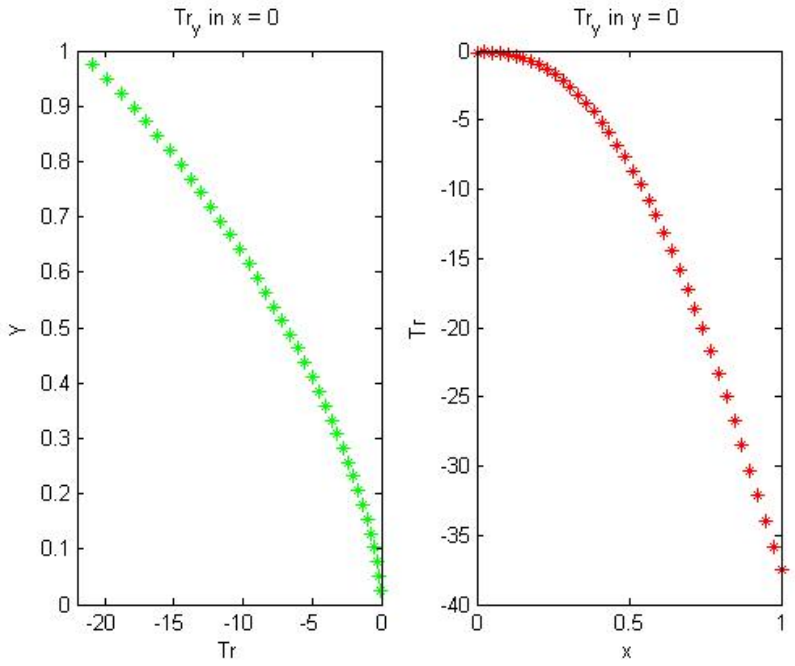

Figure 1.5: Traction

1.5 Final Remarks

In this section, we solved two problems using MAPS, which allowed us to create generic codes for both scalar problems and vector problems. The solution of these verification problems demonstrate the good behavior of the MAPS and is novel and little has been used to solve PDEs.

In the following chapters we will show how the choice of a type of boundary condition can influence the MAPS, and we use it to solve a problem that models the flow of gates through a PEM membrane.

Chapter 2

INFLUENCE OF THE BOUNDARY CONDITION IN THE MAPS

For the solution of differential equations many numerical methods have been developed such as finite difference method (FDM), finite element method (FEM), boundary elements method (BEM) and some recent meshless methods base on radial basis functions (RBF), such as the Method Approximate Particular Solutions (MAPS) (see [17] and [14]). However, one factor to be taken into account is how (BC) affect the computational domain and the application of the method, since these are mathematical approximations and simplifications of the reality.

Ataie-Ashtiani et al. [3], the influence of boundary conditions on density-dependent fluid is investigated, the authors state that more research is required to evaluate the impacts of BCs and demonstrate that the choice of BCs for dependent flow problems the density, more care should be taken in the studies and simulations made. On the work [22] the authors propose a strategy for choosing effective boundary conditions in the solution of compressible flow problems, they claim that it is possible to get better approximation when Dirichlet boundary conditions are applied and also the computational cost is reduced. While [6] study numerically the effects of different boundary conditions on the surfaces of the computational domain extended over a

natural convection flow in an open cavity, they conclude that BCs have a sensitive effect within the cavity, since they observed changes in the characteristics of flow and heat transfer within the cavity occurred due to the different BC.

The work done by Madhavan in [60] studied the sensitivity of cardiovascular flow under the influence of different boundary conditions on entry and exit in a patient-specific aorta model, affirming that most researchers choose to guess this type of condition because it is difficult and expensive to measure. In addition, they found that entry velocity conditions affect significantly only the flow region near the entrance and their study indicates that the exit conditions influences a greater percentage of the domain solution. On the other hand [65] try to show that for arbitrary boundaries of a computational region in a subsonic flow and shock waves, the numerical treatment of such limits can be physically defective and suggests what actions to take, when these situations arise.

As is affirmed in [60], this type of decisions does not only affect this type of situations, it is also presented when using a numerical method to solve a problem, due to simplification made to the models.

In this chapter we intend to show the influence of the choice of these boundary conditions in the MAPS with RBFs.

Now we consider two problems which are solved with the MAPS. We study the effects of the number of nodes and type of boundary condition can on the precision of the method. The results are compared with the respective analytical solution.

2.1 Problem 1: Solution of Slit flow problem

We solve the Slit flow problem, in a straight channel of length $L = 4$, applying different types of boundary conditions in the entrance and exit of the channel, over the domain $\Omega = [0, 4] \times [-1, 1]$, presented in figure 2.1. The governing equation for the Slit flow problem is given by:

$$\mu\Delta\vec{u} - \frac{\triangle P}{L} = 0 \quad \text{on} \quad \Omega \tag{2.1}$$

$$\nabla \cdot \vec{u} = 0 \tag{2.2}$$

If the fluid velocity is $\vec{u} = [u, 0]$ and assuming slip wall boundary condition. Which can be reduced to the expression:

$$\mu\frac{\partial^2\vec{u}}{\partial y^2} - \frac{\triangle P}{L} = 0 \quad \text{on} \quad \Omega \tag{2.3}$$

$$u = 0 \quad \text{in} \quad y = w \tag{2.4}$$

$$\frac{du}{dy} = 0 \quad \text{in} \quad y = 0 \tag{2.5}$$

Figure 2.1: Domain of the Problem

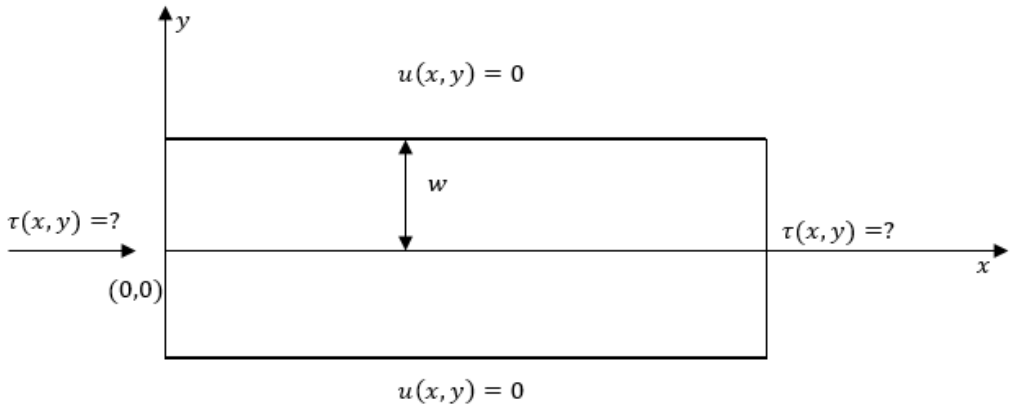

The problem that arises in the equations (2.3) y (2.5), has as an exact solution:

$$u = \frac{\triangle P}{2\mu L}(y^2 - w^2) \tag{2.6}$$

Where $\triangle P$ is the pressure gradient with a value of $-90Pa$, where P=100 on channel input y P=10 on output , $w = 1$ is the distance from the center of the channel to stop, and $\mu = 1$ is the viscosity. In addition, for this problem we use two types of

	Type 1: Traction	Type 2: Dirichlet	Type 3: Mixed	Type 4: Analytical Traction
IN	$\binom{P}{0}$	$\binom{u_E}{0}$	$\binom{v}{\tau_x} = \binom{0}{P}$	$\binom{\mu\frac{du}{dy}}{\tau} = \binom{-\mu\frac{du}{dy}}{P}$
OUT	$\binom{-P}{0}$	$\binom{u_E}{0}$	$\binom{v}{\tau_x} = \binom{0}{-P}$	$\binom{\mu\frac{du}{dy}}{\tau} = \binom{\mu\frac{du}{dy}}{-P}$

Table 2.1: Types of boundary conditions (IN, OUT channel input and output, u_y component 'y' of the speed, τ_x component 'x' of the traction and $\frac{du}{dy}$ is derived)

discretization: one performed with a distribution of uniform nodes, and another with a distribution of nodes adapted in the direction of the axis "x" towards inlet and outlet boundaries.

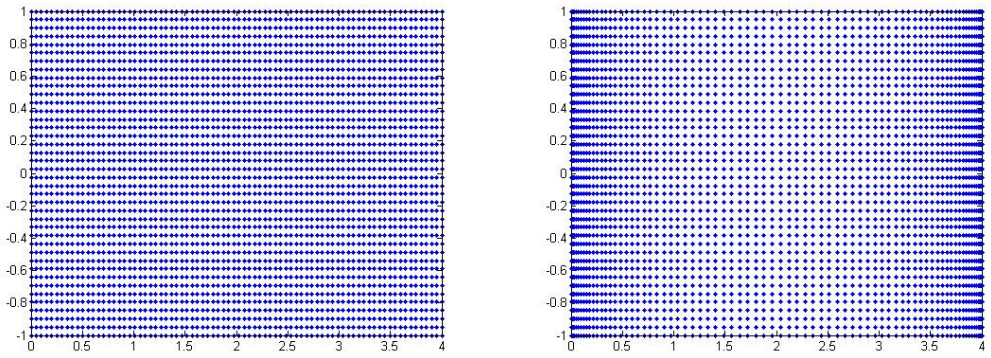

(a) Uniform discretization (b) Refined nodal distribution

Figure 2.2: Domain discretization, N = 3200

The table 2.1 shows the types of boundary conditions used in this problem. It is important to note that the Type 1, is taken as in [48] in which traction is imposed as the pressure in the component 'x' and zero speed in the component 'y'.

The figure 2.3 shows the velocity profiles for a uniform point discretization of the boundary conditions used in this problem, and in the figure 2.4 the profiles for an refined point discretization at x are shown.

The figure 2.5 shows the velocity profiles at the entrance ($x = 0$), exit ($x = L$) and in the middle of the channel ($x = L/2$), the comparison with the analytical solution shows a good approximation obtained with the MAPS, and table 2.2 shows the dogs for each type of BC with a uniform discretization.

For this problems, it is important to reconstruct the derivative $\frac{\partial u_x}{\partial y}$ and the traction,

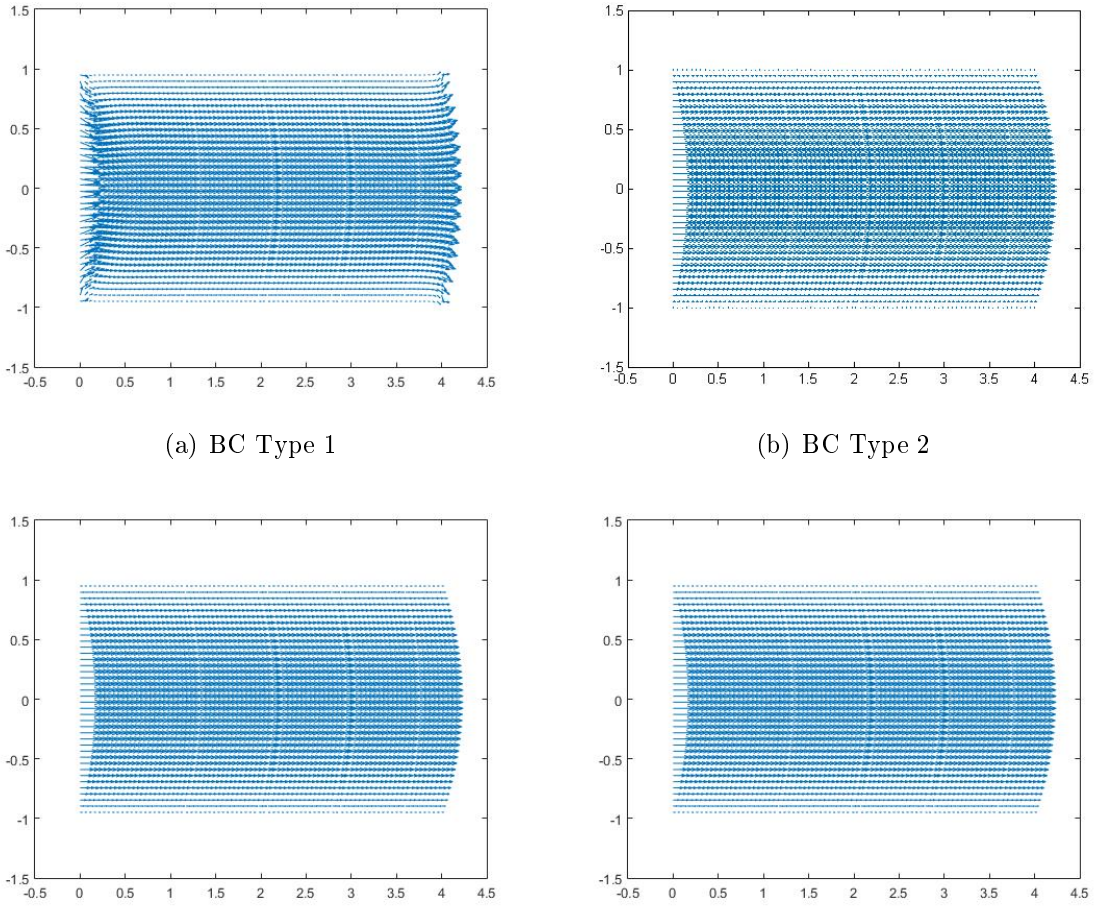

(a) BC Type 1

(b) BC Type 2

(c) BC Type 3

(d) BC Type 4

Figure 2.3: Velocity profiles for uniform points (N=3200) for different boundary conditions

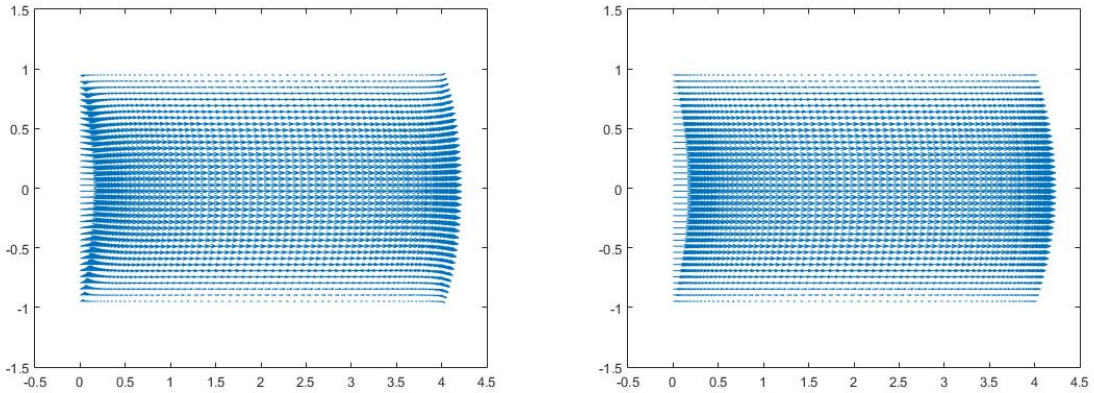

(a) BC Type 1

(b) BC Type 2

(c) BC Type 3

(d) BC Type 4

Figure 2.4: Velocity profiles for adaptive in x points (N=3200) for different boundary conditions.

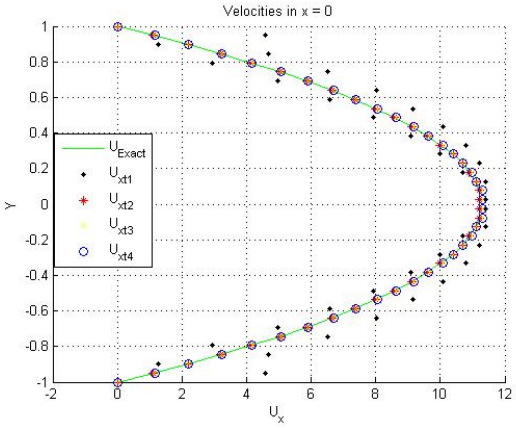

(a) Profiles in x = 0

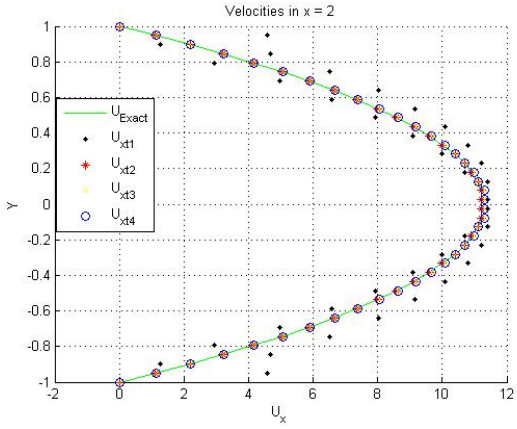

(b) Profiles in x = 2

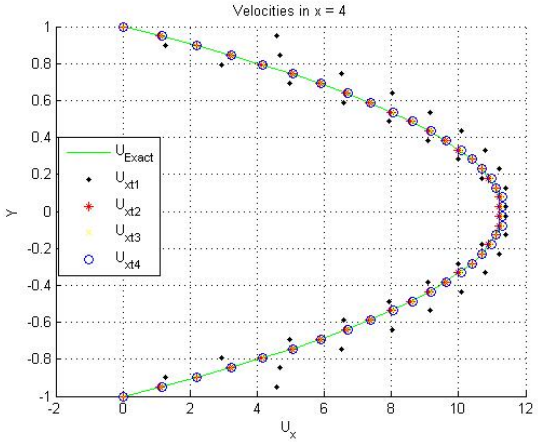

(c) Profiles in x = 4

Figure 2.5: Velocity profiles of BC for N = 3200

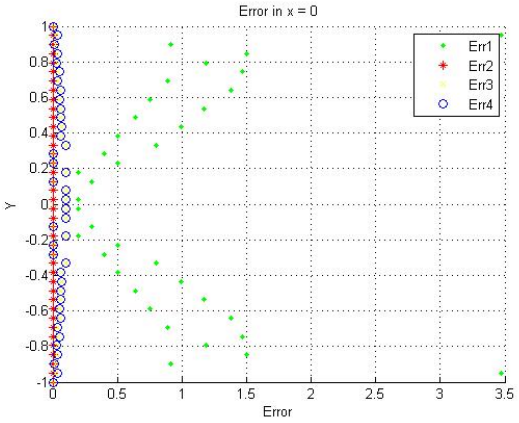

(a) Error u in x = 0

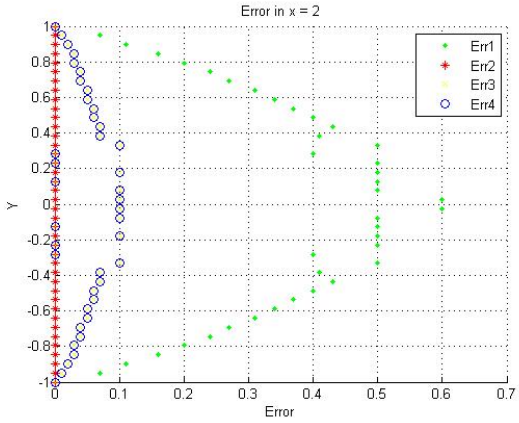

(b) Error u in x = 2

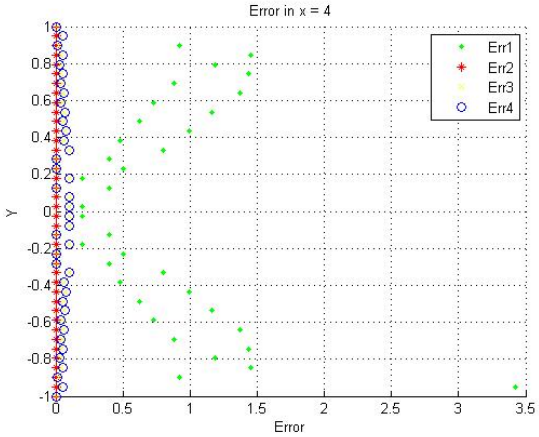

(c) Error u in x = 4

Figure 2.6: Error of the Velocities of theBC Type 1, 2, 3 and 4 for N = 3200

because they are influencer variables of the problem, since it allows us to show the precision of the method and shows us the behavior of the problem. In addition, it is crucial to observe how the application of different types of boundary conditions affects the obtained values form the MAPS application. The figure 2.7 shows the reconstruction of the derivatives in the entrance, half and exit of the channel, besides the figure 2.9-2.12 shows the reconstruction of the traction, in type 1 we obtained more imprecise values while for the other types these are improved.

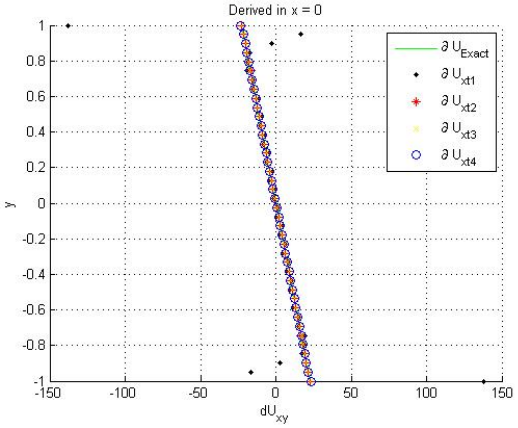

(a) Derivative in x = 0

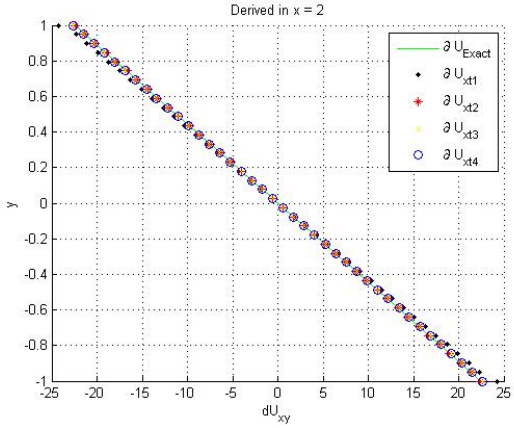

(b) Derivative in x = 2

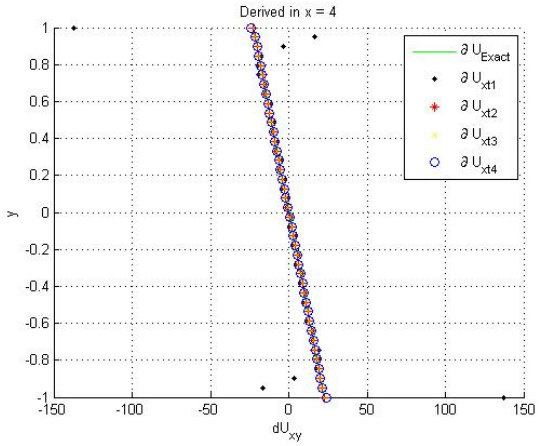

(c) Derivative in x = 4

Figure 2.7: Derivatives of BC for N = 3200

For condition type 2 and 4 similar results were obtained for traction and pressure reconstruction, in the figure 2.13 the reconstructed pressure for condition type 1, 2, 3 and 4 are shown, in which it can be evidenced as at the entrance of the channel it takes the value of 100 at the entrance until reaching the exit with a value of 10, thus fulfilling

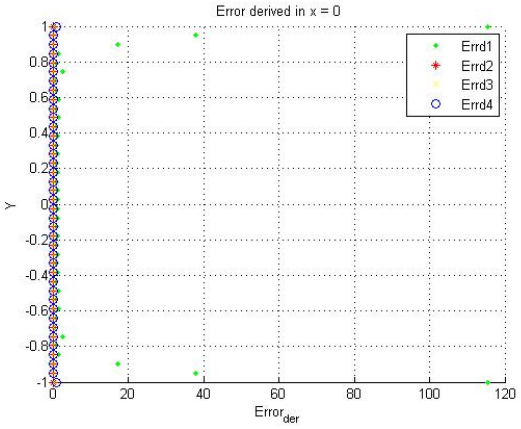

(a) Error du in x = 0

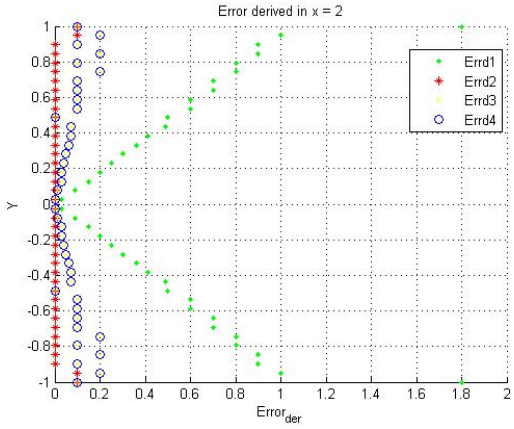

(b) Error du in x = 2

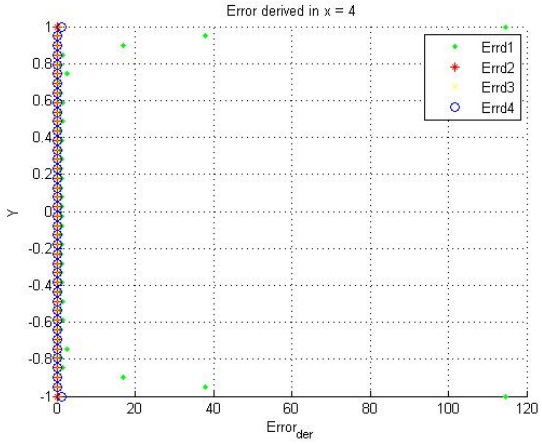

(c) Error du in x = 4

Figure 2.8: Error of the derivatives of the BC Type 1, 2, 3 and 4 for N = 3200

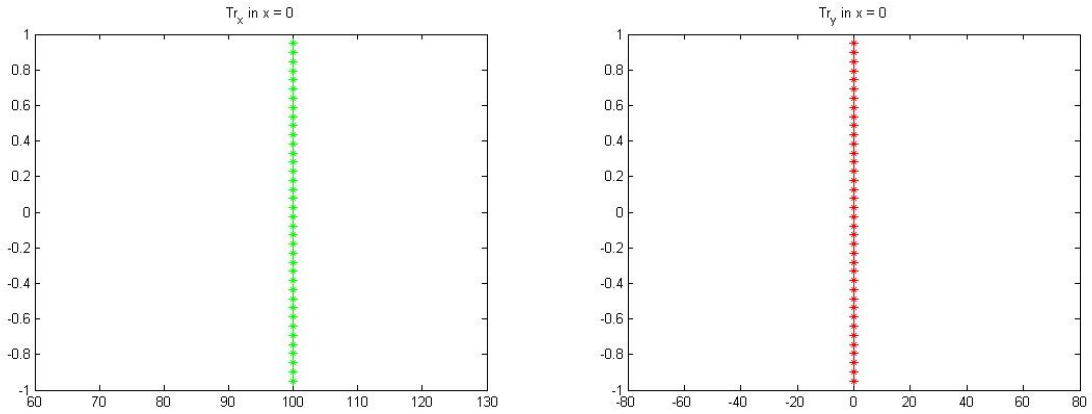

(a) (b)

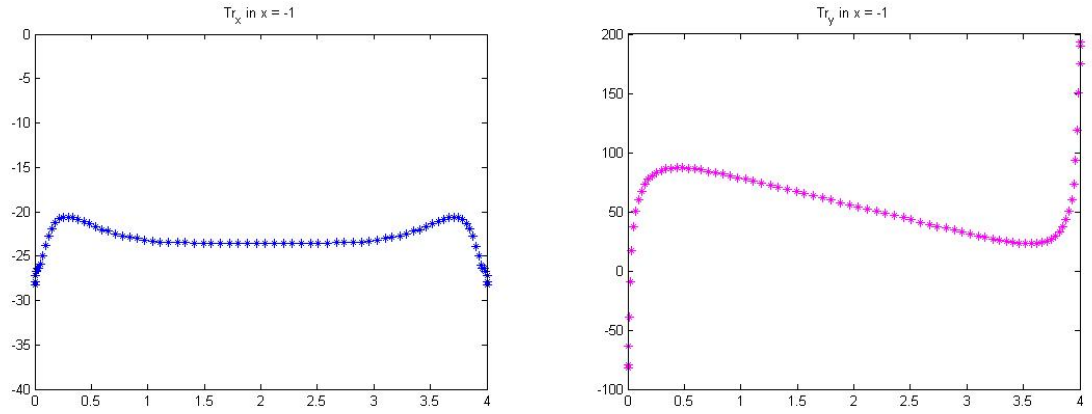

(c) (d)

Figure 2.9: Traction BC Type 1, Adaptive discretization in x

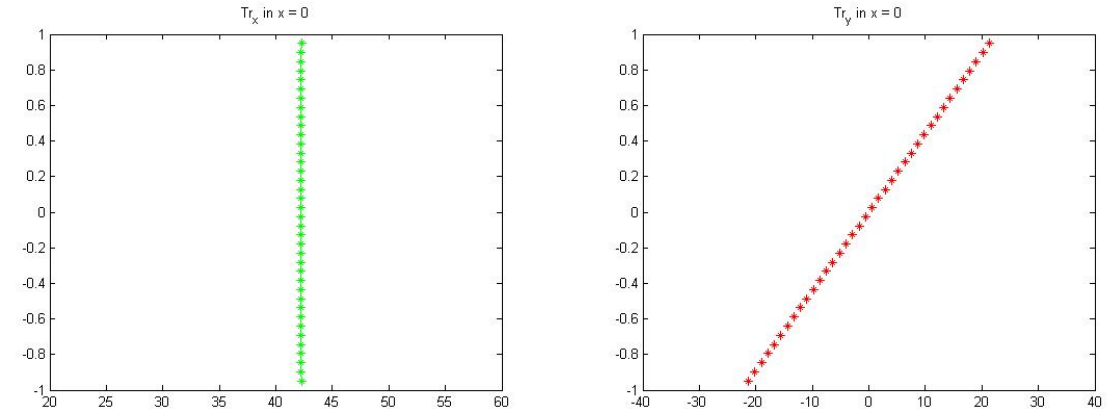

(a) (b)

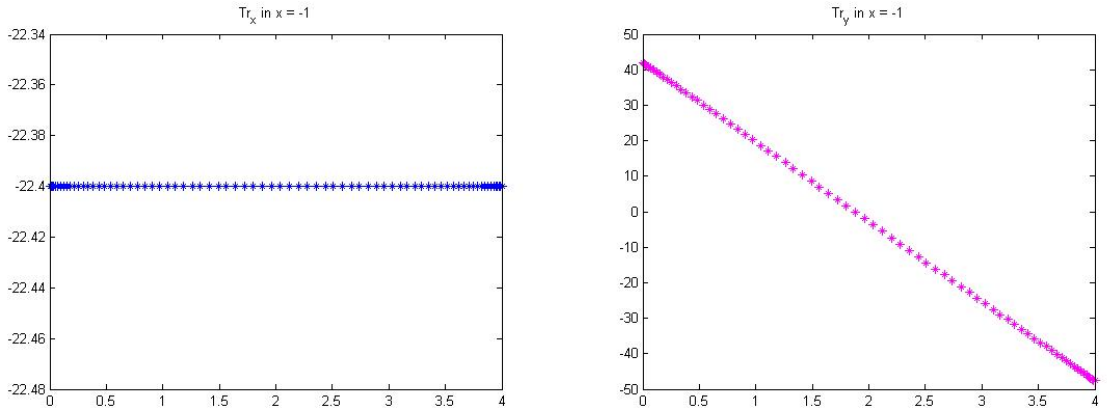

(c) (d)

Figure 2.10: Traction BC Type 2, Adaptive discretization in x

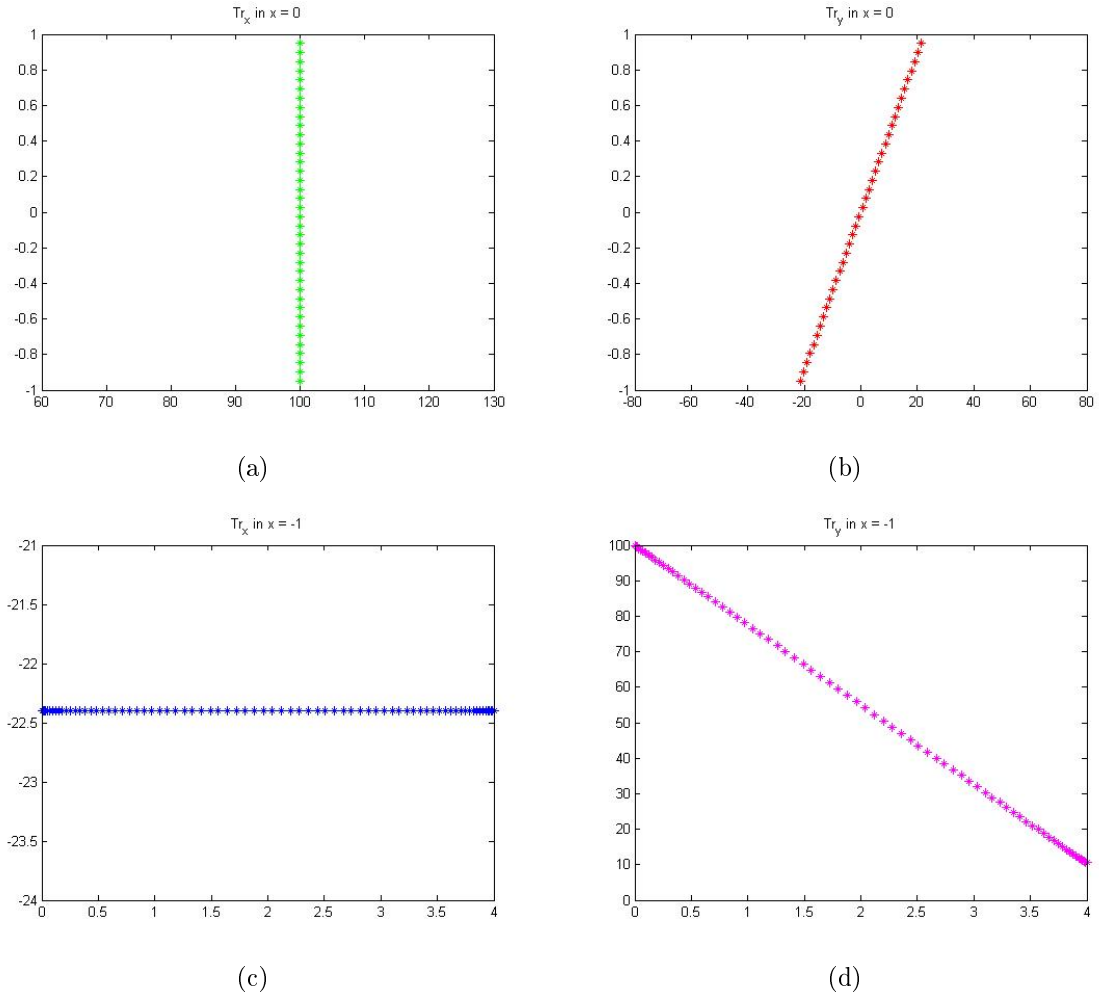

(a) (b)

(c) (d)

Figure 2.11: Traction BC Type 3, Adaptive discretization in x

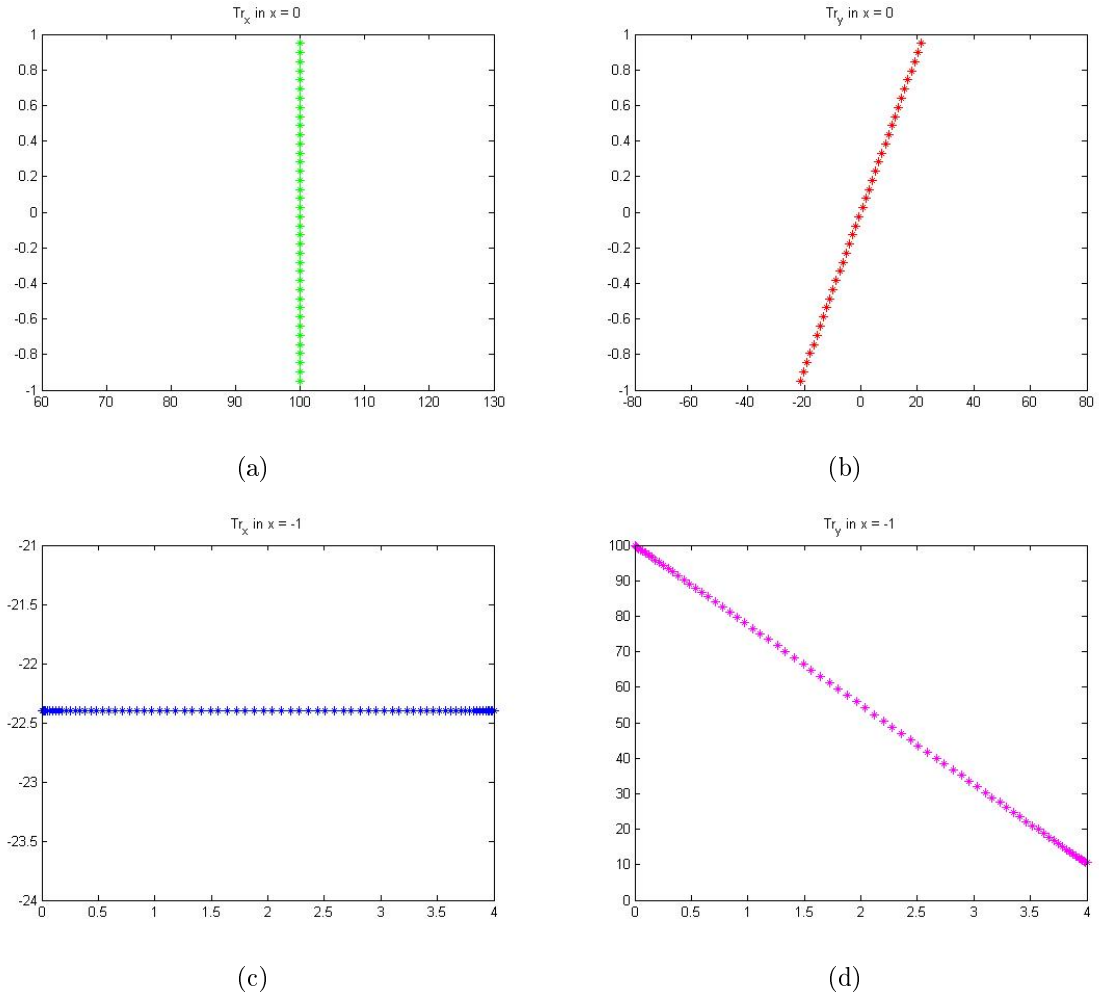

(a) (b)

(c) (d)

Figure 2.12: Traction BC Type 4, Adaptive discretization in x

	Uniform			
N	Type 1	Type 2	Type 3	Type 4
450	3.74×10^{-1}	2.22×10^{-3}	2.52×10^{-2}	3.36×10^{-2}
800	7.86×10^{-2}	2.09×10^{-4}	1.52×10^{-2}	1.29×10^{-2}
1800	2.84×10^{-2}	4.72×10^{-14}	9.23×10^{-3}	9.17×10^{-3}
3200	4.18×10^{-2}	7.89×10^{-14}	5.19×10^{-3}	5.20×10^{-3}

Table 2.2: RMSE error discretization uniform

the pressure gradient. Although in the reconstruction of the pressure of the condition type 2 at the entrance of the channel has the value of 40.3 and at the exit of the channel it has the value of -49.1 the pressure gradient is fulfilled.

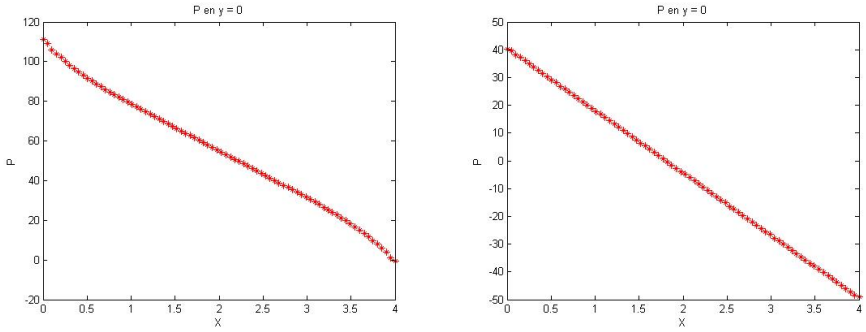

(a) Pressure BC Type 1

(b) Pressure BC Type 2

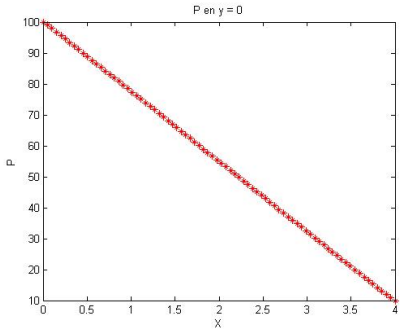

(c) Pressure BC Type 3

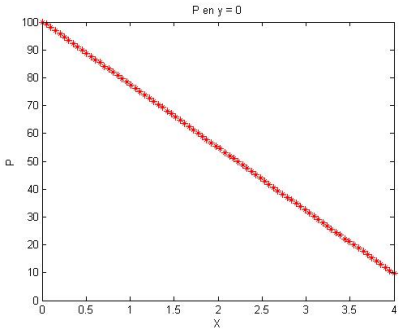

(d) Pressure BC Type 4

Figure 2.13: Pressure in $y = 0$ for N = 3200, Uniform discretization

In the figure 2.14, the RMSE variation is shown according to the node distribution N, in which it can be seen as in figure refErrRMSE-N (b) the error is stabilized for the BC type 1 and manages to improve the error for the other BC.

Finally in the table 2.2 and table 2.3, it is shown the RMSE error obtained with the

	Refined x			
N	Type 1	Type 2	Type 3	Type 4
450	4.25×10^{-2}	2.14×10^{-3}	8.48×10^{-4}	8.48×10^{-4}
800	3.99×10^{-2}	2.60×10^{-4}	3.99×10^{-4}	3.99×10^{-4}
1800	4.13×10^{-2}	2.56×10^{-12}	4.65×10^{-12}	3.81×10^{-12}
3200	4.05×10^{-2}	4.46×10^{-12}	7.92×10^{-12}	1.06×10^{-11}

Table 2.3: RMSE error discretization refined in x

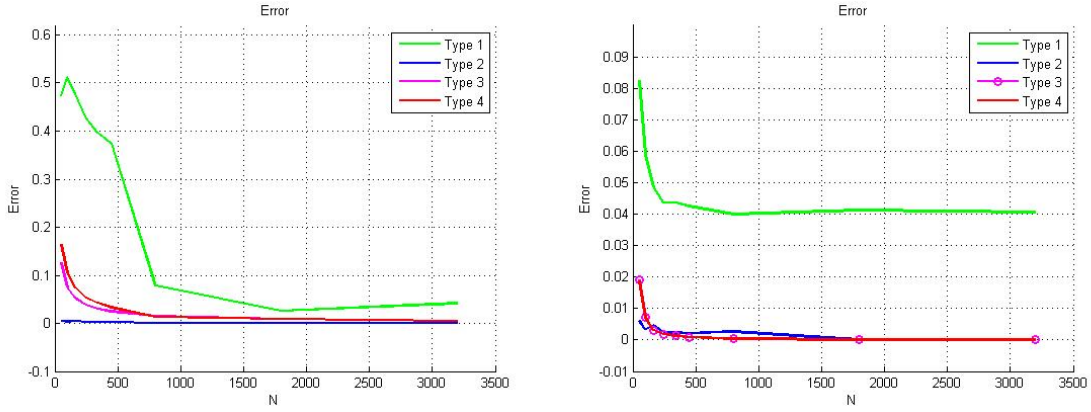

(a) (b)

Figure 2.14: RMSE error vs N in a) Uniform discretization, and b) adaptive discretization in x

different types of boundary conditions, this is calculated for the uniform and refine.

According to the results obtained above, it shows the importance of selecting the correct boundary conditions when solving a PDE problem. For Type 2 and 4, good approximations of the solution are obtained, so they cannot be ruled out, however, the Type 3 condition shows consistent results and according to the physics of the problem.

2.2 Problem 2: Laminar Convective flow between parallel plates

Given an energy balance at steady state within the laminar boundary layer is given by:

$$\rho c_p \left(u_x \frac{\partial T}{\partial x} + u_y \frac{\partial T}{\partial y} \right) = \kappa \left(\frac{\partial^2 T}{\partial x^2} + \frac{\partial^2 T}{\partial y^2} \right) + \mu (\frac{\partial u_x}{\partial y})^2 \tag{2.7}$$

Considering a fully developed fluid, if neglecting the effects of friction and axial condition, see the figure 2.15, and assuming that T is independent of 'y', the energy balance equation is reduced to:

$$\frac{\partial^2 T}{\partial y^2} = 0 \tag{2.8}$$

with boundary conditions

$$T = T_0, \quad x = x_0 \tag{2.9}$$

$$T = T_1, \quad x = -x_0 \tag{2.10}$$

So, integrating to equation (2.2) we have the expresión

$$T = \frac{T_0 - T_1}{2x_0}x + \frac{T_0 - T_1}{2} \tag{2.11}$$

In its dimensionaless form, with $T_m = \frac{T_0 - T_1}{2}$ we have

$$\frac{T - T_m}{T_1 - T_m} = -\frac{x}{x_0} \tag{2.12}$$

Now, the moment equation is given by:

$$\mu\nabla^2 u - \nabla p = -\rho\beta g(T - T_m) \tag{2.13}$$

which boils down to expression

$$\mu\frac{\partial^2 u}{\partial x^2} + \rho\beta g(T - T_m) = 0 \tag{2.14}$$

whose exact solution is given by

$$u_y = \frac{g\beta x_0^2(T_1 - T_m)}{6\frac{\mu}{\rho}}\left[\left(\frac{x}{x_0}\right)^3 - \left(\frac{x}{x_0}\right)\right] \tag{2.15}$$

Entering the following dimensionaless variables,

$$\widehat{u} = \frac{u_y\rho c_p x_0}{\kappa} \quad \text{dimensionaless velocity} \tag{2.16}$$

$$Gr = = \frac{g\beta x_0^3(T_1 - T_m)}{(\frac{\mu}{\rho})^2} \quad \text{Grashoff number} \tag{2.17}$$

$$\widehat{x} = \frac{x}{x_0} \quad \text{dimensionaless length} \tag{2.18}$$

So we have,

$$\widehat{u} = \frac{1}{6}(Gr \cdot Pr)(\widehat{x^3} - \widehat{x}) \tag{2.19}$$

Where $Pr = \frac{C_p \mu}{\kappa}$ is Prandtl number. Then, the Rayleigh number can be written as the product of the Grashof number and the Prandtl number $Gr \cdot Pr$. This problem is solved in the domain given in figure 2.15 with $\Omega = [-1, 1] \times [0, 2]$, where $x_0 = 1$, $\rho = 1$, $\beta = 0.5$. With the following boundary conditions:

$$u_x = 0, \quad \tau_y = 0 \quad \text{in} \quad y = 0 \tag{2.20}$$

$$u_x = 0, \quad \tau_y = 0 \quad \text{in} \quad y = 2 \tag{2.21}$$

$$u_x = 0, \quad u_y = 0 \quad \text{in} \quad x = -1, 1 \tag{2.22}$$

where τ_y is the 'y' component of traction, in this way we have a boundary condition mixed given by (u_x, τ_y).

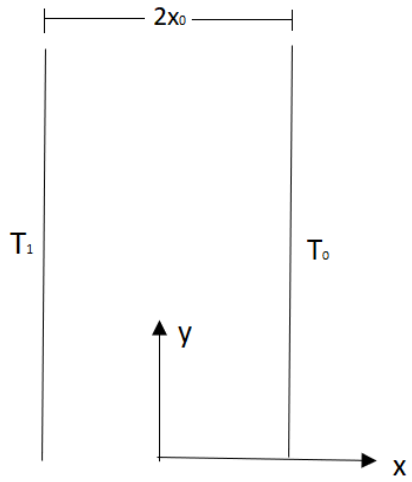

Figure 2.15: 2-D domain for the case of two parallel plates

In figure 2.16, shown the results for $N = 2500$ nodes distributed homogeneously, these are compared to the analytical solution. This was done similarly for the values $Gr \cdot Pr =$

100 see figure 2.17 and $Gr \cdot Pr = 500$ see figure 2.18.

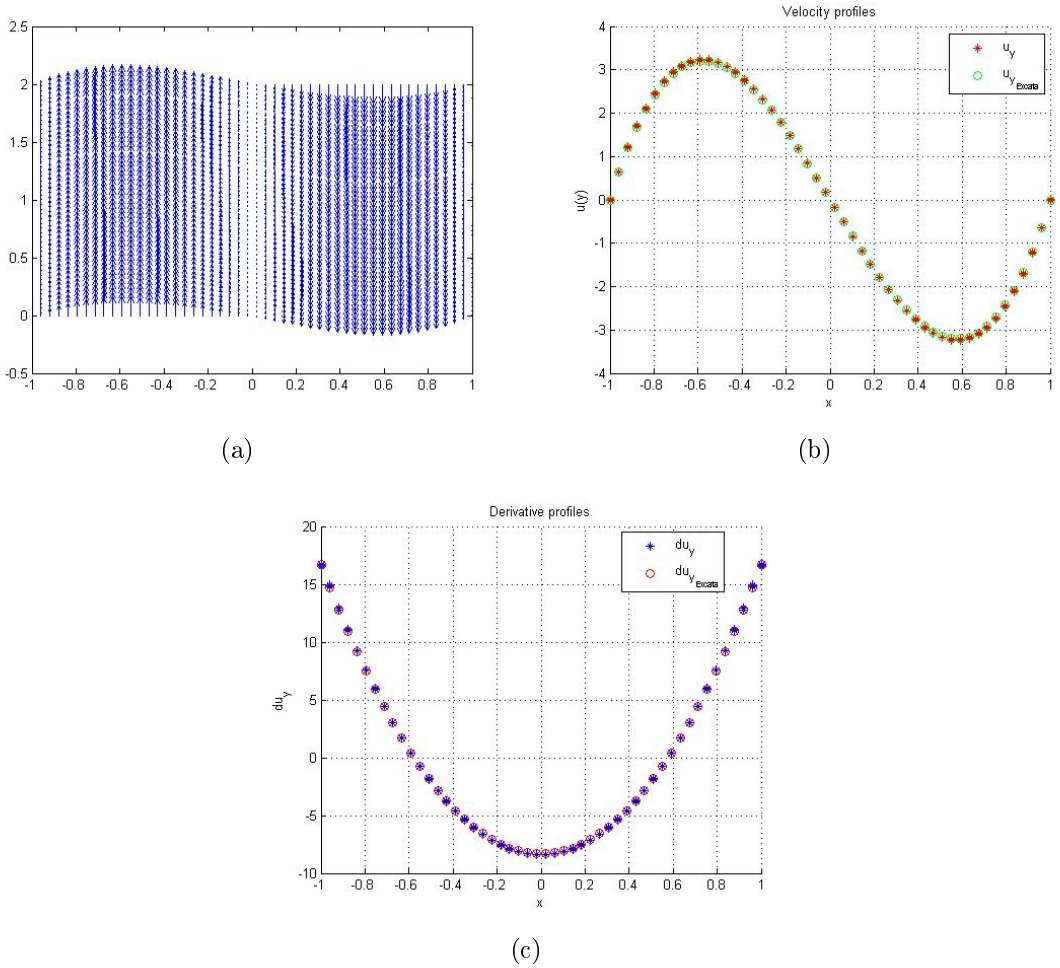

(a) (b)

(c)

Figure 2.16: Figure a) shows the velocity profile, in b) the analytical and numerical solution of the velocity is compared and in c) the value of the analytical derivative is compared with the numerical derivative. This for $Gr \cdot Pr = 50$

We various solutions for $N = 400, 900, 1600$ and 2500 nodes are carried out in order to analyze the effect of nodal distribution on method accuracy, see Table 2.4, where it is shown that the precision of the method does not depend on the characteristics of the fluid in a laminar flow. In figure 2.19 and 2.20 traction in $x = -1$ and $y = 0$ are presented., it could be shown that by the symmetry of the problem, the values of the traction $\tau_x(x = -1) = -\tau_x(x = 1)$ and that $\tau_x(y = 0) = -\tau_x(y = 2)$, so we only show one of them.

Finally, Figure 2.21 presents the behavior of the profiles when varying $Gr \cdot Pr$ for velocity and the derivative.

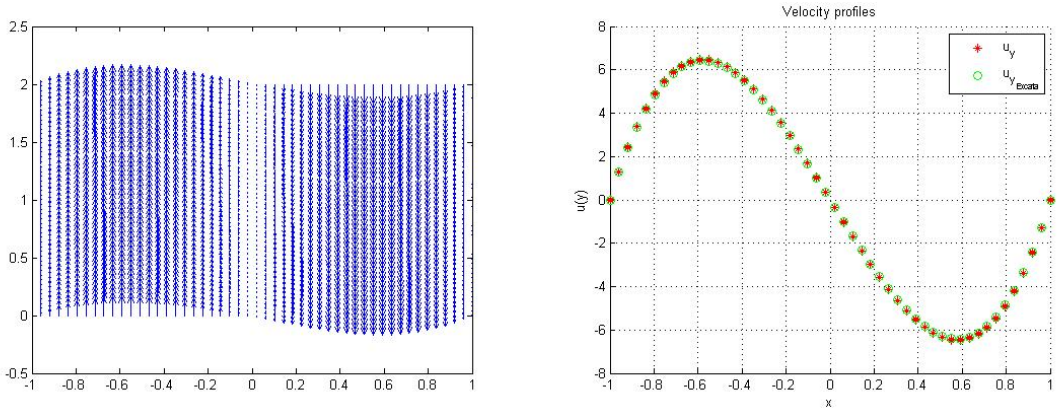

(a)

(b)

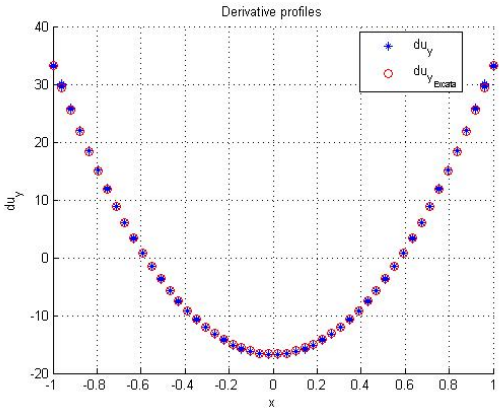

(c)

Figure 2.17: Figure a) shows the velocity profile, in b) the analytical and numerical solution of the velocity is compared and in c) the value of the analytical derivative is compared with the numerical derivative. This for $Gr \cdot Pr = 100$

N \ $Gr \cdot Pr$	50	100	500	Condition of the matrix
400	2.34×10^{-2}	2.32×10^{-2}	2.34×10^{-2}	2.30×10^{7}
900	1.24×10^{-2}	1.30×10^{-2}	1.24×10^{-2}	1.19×10^{8}
1600	8.10×10^{-3}	8.44×10^{-3}	8.10×10^{-3}	1.90×10^{8}
2500	6.04×10^{-3}	6.13×10^{-3}	6.04×10^{-3}	5.41×10^{8}

Table 2.4: RMSE error according to discretization number and GrPr

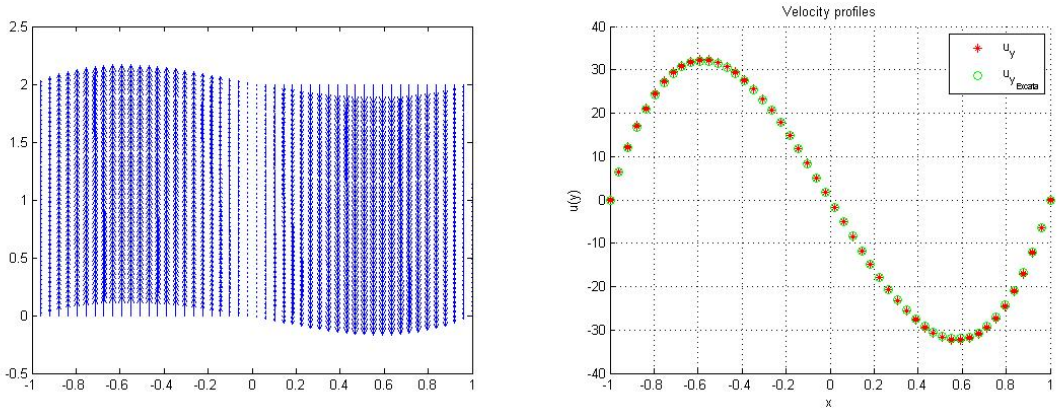

(a) (b)

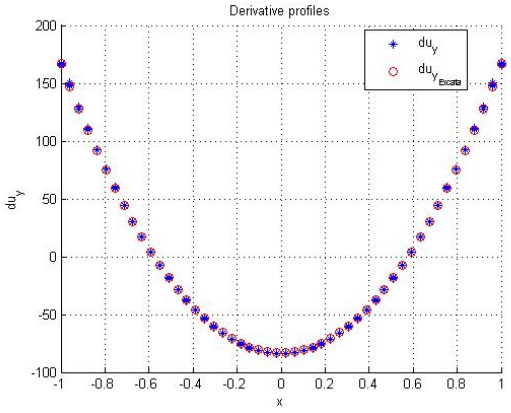

(c)

Figure 2.18: Figure a) shows the velocity profile, in b) the analytical and numerical solution of the velocity is compared and in c) the value of the analytical derivative is compared with the numerical derivative. This for $Gr \cdot Pr = 500$

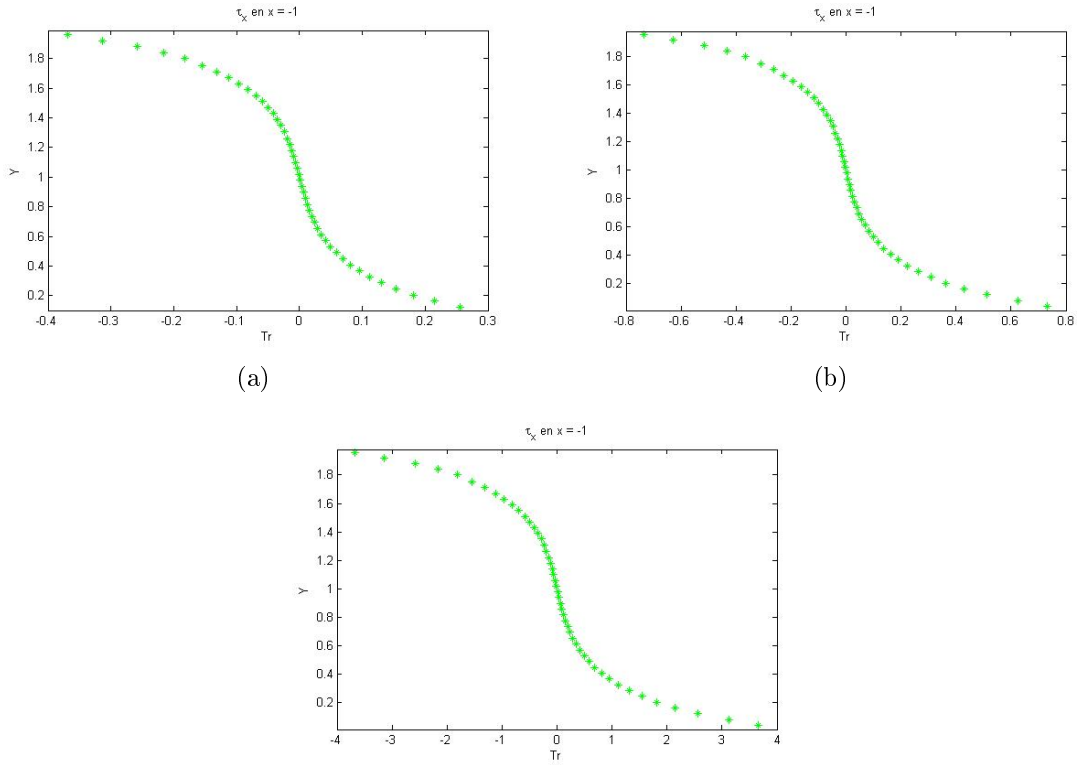

Figure 2.19: Traction for a) $GrPr = 50$, b) $GrPr = 100$, c) $GrPr = 500$ en $x = -1$

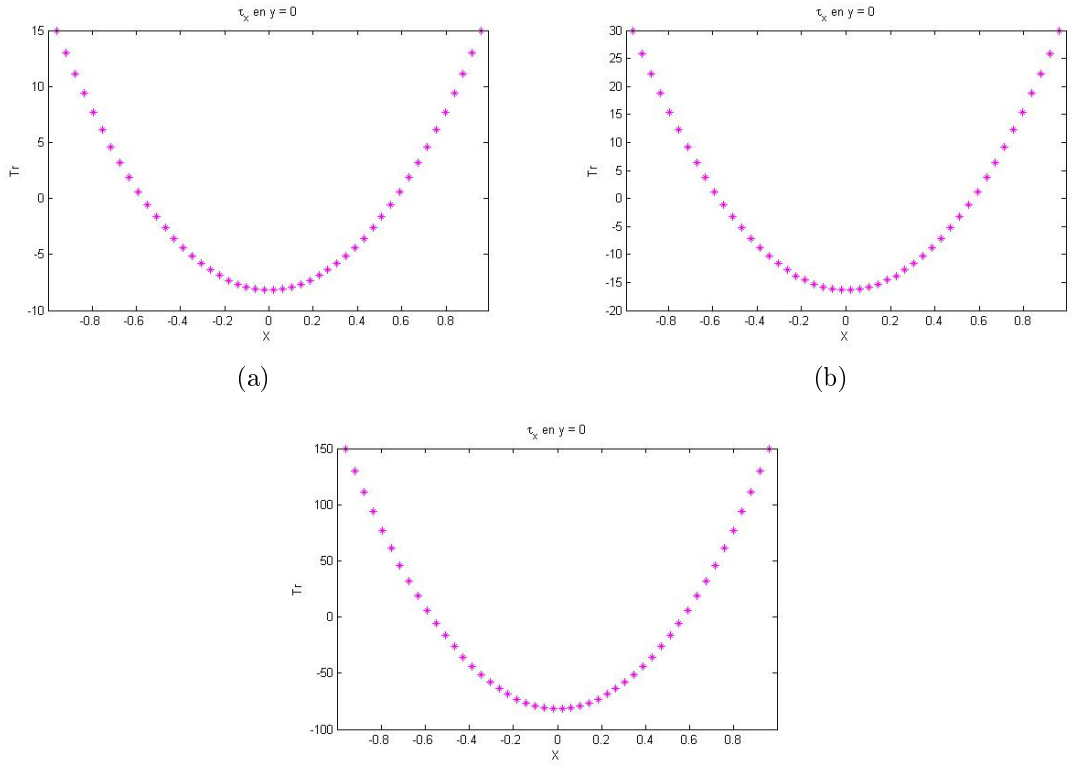

(a) (b)

(c)

Figure 2.20: Traction for a) $Gr \cdot Pr = 50$, b) $Gr \cdot Pr = 100$, c) $Gr \cdot Pr = 500$ en $y = 0$

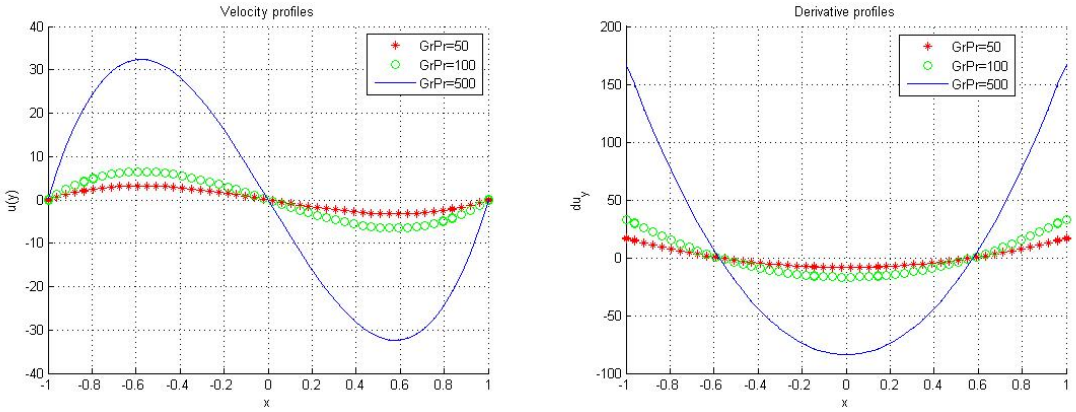

(a) (b)

Figure 2.21: a) Velocity, b) Derivative according to $Gr \cdot Pr$

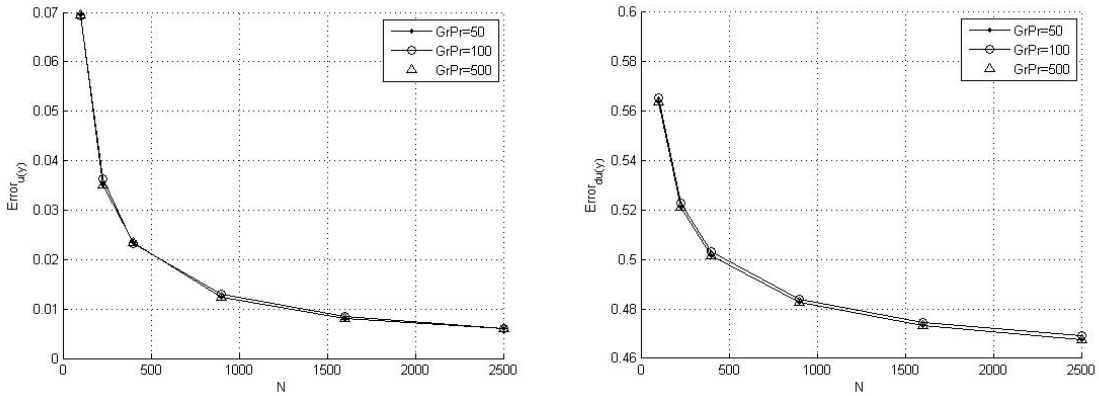

(a)

(b)

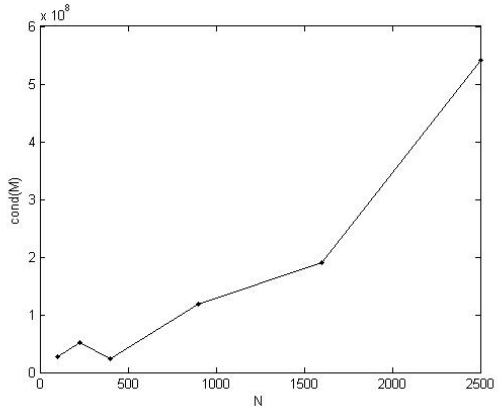

(c)

Figure 2.22: Errors for different discretization points a) Velocity, b) derivative $\frac{du}{dy}$, c) Matrix Condition

2.3 Problem 3: Scalar Problem

It is considered a problem which is taken from[16] which has an elliptic differential equation with scalar coefficient variable given by:

$$\triangle u + \sin(x+y)u + (xy+x^2)\frac{\partial u}{\partial x} + x\sinh(y)\frac{\partial u}{\partial y} = f(x,y) \tag{2.23}$$

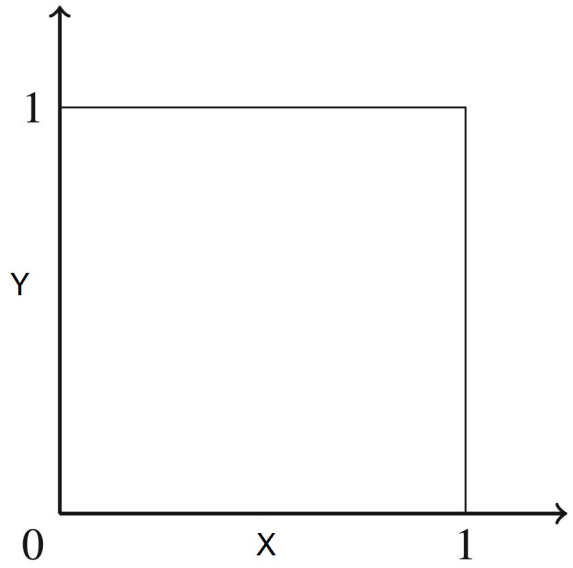

Figure 2.23: Problem domain 3

for this case, we have $f(x,y)$ is given according to the analytical solution is given below:

$$u = y\sin(\phi x) + x\cos(\phi y) \tag{2.24}$$

This problem is solved in the domain shown figure 2.23 and two different boundary conditions are considered for its numerical solution. As in [16] the first one is considered with Dirichlet boundary conditions across the entire boundary of the domain; and the second one with, Neaumann boundary condition in line $y = 0$ and Dirichlet boundary condition in the rest is applied.

The profiles of the solution and its derivatives are shown in figure 2.24 first, the Dirichlet boundary condition is applied and in figure 2.25 Neaumann boundary condition is applied on the line $y = 0$. In the table 2.5, it is possible to see that for the first case the error remains constant, while in the second case, for $N = 441$ the error increases, but this improves as the number of nodes increases ($N = 961$ and $N = 1681$) until the error obtained in the First case, see Table 2.5.

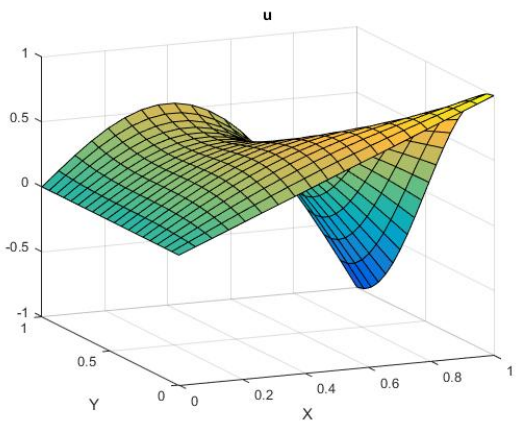

(a) Approximate solution

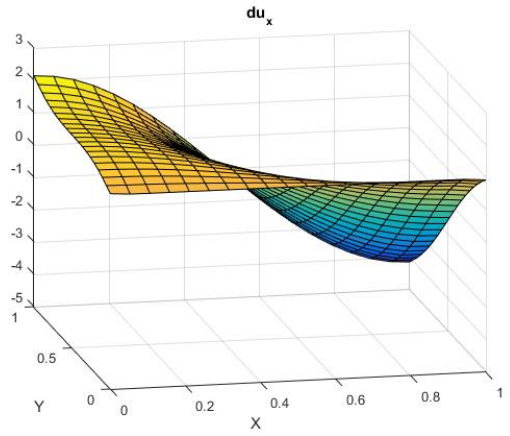

(b) Derivative respect to x

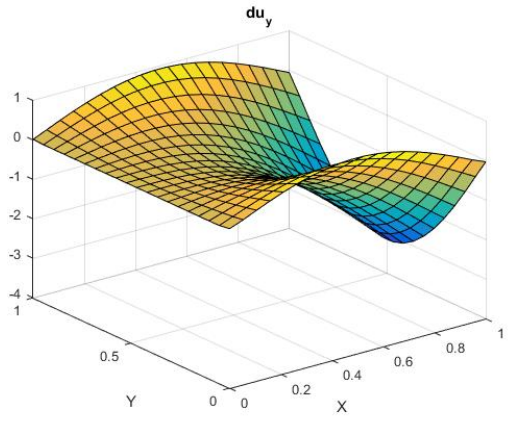

(c) Derivative respect to y

Figure 2.24: Results with BC type Dirichlet: a) Approximate solution, b) Derived in 'x', and c) Derived in 'y'

The table 2.5 shows the RMSE error obtained when solving for $N = 441, 961$ and 1681 for the two cases mentioned above.

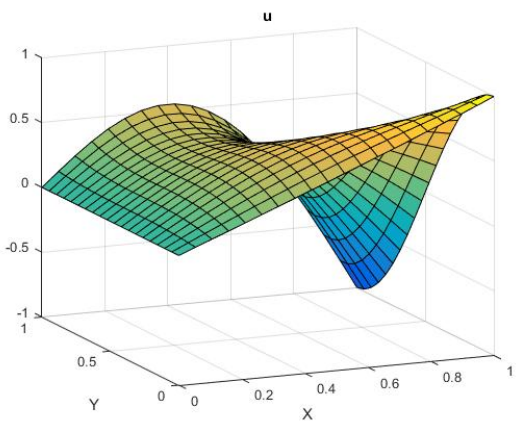

(a) Approximate solution

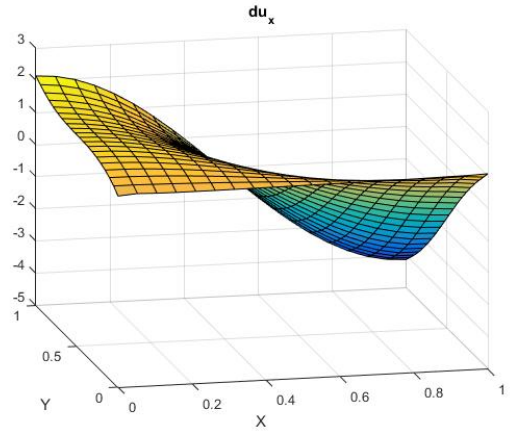

(b) Derivative respect to x

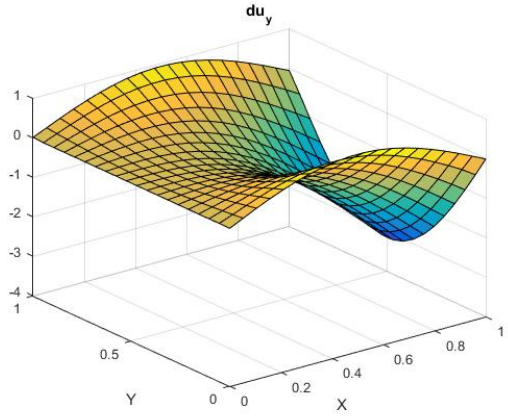

(c) Derivative respect to y

Figure 2.25: Results with BC type Neumann (Mixed): a) Approximate solution, b) Derived in 'x', and c) Derived in 'y'

	Dirichlet		Neumann	
N	u	$\frac{du}{dx}$	u	$\frac{du}{dx}$
441	6.69×10^{-4}	9.43×10^{-3}	1.13×10^{-2}	1.87×10^{-2}
961	2.56×10^{-4}	4.65×10^{-3}	6.01×10^{-3}	9.84×10^{-3}
1681	1.29×10^{-4}	2.77×10^{-4}	3.85×10^{-3}	6.25×10^{-3}

Table 2.5: RMSE error for the solution and its derivative with respect to 'x' according to the type of boundary condition

2.4 Final Remarks

In this chapter, the influence or implications of the boundary conditions when applying the MAPS for the solution of a PDE is shown. In the table 2.2 we see the error obtained for each type of boundary condition applied according to the number of discretization used, where it can be shown that for boundary Type 1 the best approximation that could be achieved was for a discretization of $N = 3200$ nodes with a uniform distribution, this with an RMSE error of 4.18×10^{-2}. This is not appropriate since there is no physical information in the problem to be used and therefore in that case Type 3 would be more convenient..

On the other hand, when performing a distribution of different nodes (see table 2.3) no significant improvement of the error for the type 1 boundary was evidenced, something contrary to what happened with the type 3 boundary that passed from $\epsilon_{err} = 5.19 \times 10^{-3}$ to $\epsilon_{err} = 7.92 \times 10^{-12}$ and the type 4 boundary that passed $\epsilon_{err} = 5.20 \times 10^{-3}$ to $\epsilon_{err} = 1.06 \times 10^{-11}$, this for a discretization of $N = 3200$ node, showing a quite significant improvement when performing an adaptive discretization in x. The above shows how the choice of boundary condition significantly affects the results obtained, also shows that these BCs must be consistent with the physical reality of the problem and can not be imposed arbitrarily.

The table 2.5 shows the RMSE error for solution and the derivative with respect to "x", in which it is evident that if the boundary condition is changed, and the PDE solution remains the same, with a Neumann boundary condition the numerical solution is worse.

Chapter 3

ELECTROKINETIC FLUIDS

In this chapter we try to present and provide an explanation that allows us to understand electro-kinetic fluids, this leads us to understand what electroosmotic flows are. According to [46], electrokinetic effects are important for micro and nanoscale transport applications, as it the case of electroosmosis that allows fluid pumping and flow control using electric fields, which eliminates the need of mechanical pumps or valves with movable components. In addition the speed profiles for electroosmotic flows are mostly uniform.

According to [56], if a stationary solid surface is contact with an aqueous solution and an electric field is applied, excess counter ions in the diffuse layer of the EDL will move, this is called electroosmosis. As the ions move, they drag the surrounding liquid molecules to move with them due to the viscous effect, resulting in a mass liquid movement. Such liquid movement is called electroosmotic flow (see also [71] and [47]).

3.1 The electrical double layer (EDL)

For [36], electrokinetic phenomena occurs due to the double electrical layer (EDL), which is formed as a result of the interaction of the ionized solution with static charges on the dielectric surfaces, generally the solution is electrically neutral although the

Electrostatic charges on the solid surface will attract counterions in the liquid.

Since the ions of opposite charge in the layer protect some of the electrical charges on the surface, the electrokinetic potential quickly falls through the Stern layer. The value of ψ at the edge of the Stern layer is known as potential zeta ζ, see [46]. The distribution of ions in the diffuse layer produces a net electric charge, which is related to the electrokinetic potential through the Poisson equation as:

$$\nabla^2\psi = -\frac{\rho_e}{\varepsilon_0\varepsilon} \tag{3.1}$$

where ψ is the potential of the electric field, ρ_e is the free charge density, ε is the dielectric constants in the middle and ε_0 is the dielectric constants in the vacuum.

Assuming that the equilibrium Boltzmann distribution equation is applicable [56], we have,

$$c_i = c_{i\infty}\exp(-\frac{z_i e\psi}{k_b T}) \tag{3.2}$$

where $c_{i\infty}$ and z_i are the mass ion concentration and the valence of the ith ions; e is the charge of a proton, k_b is the Boltzmann constant, and T is the absolute temperature. The net electric charge density ρ_e is given by

$$\rho_e = \sum_{i=1}^{n} z_i e c_i = e\sum_{i=1}^{n} z_i c_{i\infty}\exp(-\frac{z_i e\psi}{k_b T}) \tag{3.3}$$

Now if $z_i = z = constant$ and we assume a symmetric electrolyte of equal valence that is in equilibrium with the charged surface, what results is the well-known Poisson-Boltzmann equation (P-B)

$$\nabla^2\psi = \frac{2zec_0}{\varepsilon\varepsilon_0}\sinh(\frac{ze\psi}{k_b T}) \tag{3.4}$$

A more general form of the Poisson-Boltzmann equation

$$\nabla^2\psi = -\frac{e}{\varepsilon\varepsilon_0}\sum_{i=1}^{n} z_i c_{i\infty}\exp(-\frac{z_i e\psi}{k_b T}) \tag{3.5}$$

By introducing the dimensionaless the electric potential $\Psi = ze\psi/k_bT$, the Poisson-Boltzmann equation (3.4) can be rewritten as:

$$\nabla^2\Psi = k^2\sinh\Psi \tag{3.6}$$

where $k^2 = \frac{2z^2e^2c_{\infty}}{\varepsilon\varepsilon_0 k_b T}$, is defined as the Debye parameter -Huckel. Now, if the electric potential is small compared to the thermal energy of the ions, that is, ($|ze\psi| < |k_bT|$) thus the function of the right side in 3.6 can be approximated by $\sinh(\Psi) \simeq \Psi$, which transforms the equation (3.6) to

$$\nabla^2\Psi = k^2\Psi \tag{3.7}$$

This result is called in the literature as a linear approximation of Debye-Huckel, whose assumption requires that $\Psi < 25mV$.

3.2 Electrokinetic fluids in a cylindrical microchannel

Consider an electro-osmotic flow of a solution in a cylindrical nanochannel with a circular cross section. It is assumed that the channel wall has a uniform and constant potential load or zeta along the channel, see figure 3.1.

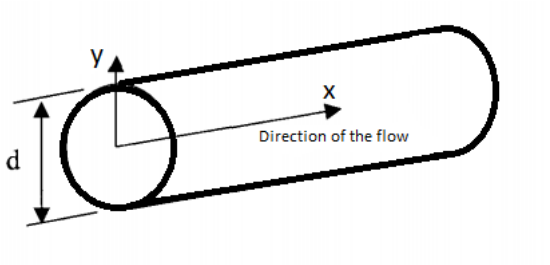

Figure 3.1: Cylindrical Microchannel with circular section

3.2.1 Electrical double layer in a cylindrical microchannel

We have that the electric potential Ψ at any point of the liquid is described by the Poisson equation in the radial direction $'Y'$ and axial direction $'X'$.

$$\frac{1}{Y}\frac{\partial}{\partial Y}\left(Y\frac{\partial \Psi}{\partial Y}\right)+\frac{\partial^2 \Psi}{\partial X^2}=-\frac{\rho_e}{\varepsilon\varepsilon_0} \tag{3.8}$$

If we assume that the Boltzmann distribution is applicable, the concentration of ions for unit volume is of the form

$$c_i = c_{i\infty}\exp(-\frac{z_i e\Psi}{k_b T}) \tag{3.9}$$

The net charge density ρ_e is equivalent to the difference in concentration between cations and anions, like this:

$$\rho_e(Y)=\sum_{i=1}^{n} c_i z_i e = e\sum_{i=1}^{n} z_i c_{i\infty}\exp(-\frac{z_i e\Psi}{k_b T}) \tag{3.10}$$

For a symmetric electrolyte solution, the above equation becomes:

$$\rho_e(Y)=e\sum_{i=1}^{n} z_i c_{i\infty}\exp(-\frac{z_i e\Psi}{k_b T}) = -2ec_\infty \sinh(\frac{e\Psi}{k_b T}) \tag{3.11}$$

Substituting equation (3.11) into equation (3.8), and entering the dimensionless variables.

$$\psi = \frac{e\Psi}{k_b T}, \quad y = \frac{Y}{d}, \quad x = \frac{X}{d}$$

where d is the diameter of the nanochannel, thus we obtain the Poisson-Boltzmann equation for a symmetric electrolyte solution, given by:

$$\frac{1}{y}\frac{\partial}{\partial y}\left(y\frac{\partial \psi}{\partial y}\right) + \frac{\partial^2 \psi}{\partial x^2} = \kappa^2 \sinh(\psi) \tag{3.12}$$

where $\kappa = \left(\frac{2c_\infty e^2 d^2}{\varepsilon\varepsilon_0 k_b T}\right)^{1/2}$ It is the Debye-Huckel parameter. Taking into account the symmetry of EDL equation (3.12) it with non-dimensional boundary conditions

$$y = 0, \quad \frac{\partial \psi}{\partial y} = 0 \tag{3.13}$$

$$x = 0, \quad \frac{\partial \psi}{\partial x} = 0 \tag{3.14}$$

$$y = 1, \quad \psi = \frac{e\zeta}{k_b T} \tag{3.15}$$

$$x = 1, \quad \frac{\partial \psi}{\partial x} = 0 \tag{3.16}$$

where ζ is the zeta potential.

3.2.2 Electrokinetic flow field in a cylindrical microchannel

The flow of the electrolyte solution is determined by the momentum and mass conservation equations,

$$\rho\left[\frac{\partial\vec{u}}{\partial t}+\vec{u}\cdot\nabla\vec{u}\right]=-\nabla P+\mu\nabla^2\vec{u}+E\rho_e \tag{3.17}$$

$$\nabla\cdot\vec{u}=0 \tag{3.18}$$

where $\vec{u}$ is the velocity vector, μ is the viscosity, ρ is the density of the fluid, ρ_e is the net local charge density and E is the force of the applied electric field.

If we assume the steady state and fully developed flow, then the velocity components satisfy $u=u(x,y)$ and $v=w=0$, in terms of the radial coordinate $'y'$ and component axial $'x'$, the equation of momentum (3.17) is reduced to:

$$\mu\frac{1}{y}\frac{\partial}{\partial y}\left(y\frac{\partial u}{\partial y}\right)+\frac{\partial^2 u}{\partial x}=\nabla P-E\rho_e \tag{3.19}$$

For a simple electro-osmic flow there is no pressure along the capillary, that is ∇P is zero. On the other hand for a pressure-driven flow, $E_z=0$. Otherwise, the field strength would change in different sections of the nanochannel. This implies different velocity fields in different sections of the flows. However, for incompressible liquids, the condition of continuity requires a constant flow through the channel, then the pressure gradient is required to satisfy the condition of continuity.

Now substituting (3.11) in equation (3.19) and entering the dimensionless variables $\overline{u}=\frac{ud}{D}$, $\overline{y}=\frac{y}{d}$ y $\overline{x}=\frac{x}{d}$, where D is the diffusion coefficient, we obtain an equation for a symmetric electrolyte solution, given by:

$$\frac{1}{\overline{y}}\frac{\partial}{\partial \overline{y}}\left(\overline{y}\frac{\partial \overline{y}}{\partial \overline{y}}\right)+\frac{\partial^2 \overline{u}}{\partial \overline{x}}=G1E\sinh(\psi) \tag{3.20}$$

where $G1=\frac{2c_\infty ed^3}{\mu D}$ is a dimensionless number, see[56]. It is subjected to symmetric and non-slip boundary conditions:

$$y = 0, \quad \frac{\partial u}{\partial y}=0 \tag{3.21}$$

$$x = 0, \quad \frac{\partial u}{\partial x}=0 \tag{3.22}$$

$$y = 1, \quad u=0 \tag{3.23}$$

$$x = 1, \quad \frac{\partial u}{\partial x}=0 \tag{3.24}$$

3.3 Electrokinetic fluids in a rectangular microchannel

In this section, we intend to examine the numerical solutions of the Poisson-Boltzmann equation and the momentum equation for electroosmotic fluid in rectangular nanochannels. In this case the EDL field is two-dimensional and will affect the flow field.

3.3.1 Electrical double layer in a rectangular microchannel

We consider a nanochannel $2W$ wide, $2H$ high with a length L, as shown in Figure 3.2. The EDL field of a rectangular section is described by the Poisson equation (3.3.1).

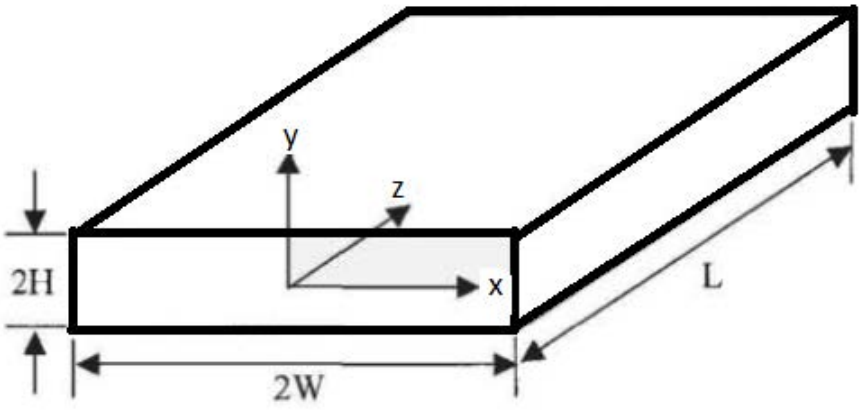

Figure 3.2: Rectangular Microchannel

$$\frac{\partial^2 \Psi}{\partial Y^2} + \frac{\partial^2 \Psi}{\partial X^2} = -\frac{\rho_e}{\varepsilon \varepsilon_0} \tag{3.25}$$

If assuming that the Boltzmann distribution is applicable. The net charge density expressed in terms of the Boltzmann distribution, which for a symmetric electrolyte is given by:

$$\rho_e = -2c_\infty ze \sinh\left(\frac{ze\Psi}{k_b T}\right) \tag{3.26}$$

In this way, by substituting in the Poisson equation we obtain the PoissonBoltzmann equation in two dimensions:

$$\frac{\partial^2 \Psi}{\partial Y^2} + \frac{\partial^2 \Psi}{\partial X^2} = \frac{2c_\infty ze}{\varepsilon \varepsilon_0} \sinh\left(\frac{ze\Psi}{k_b T}\right) \tag{3.27}$$

Together with the following symmetric boundary conditions:

$$Y = 0, \quad \frac{\partial \Psi}{\partial y} = 0 \tag{3.28}$$

$$X = 0, \quad \frac{\partial \Psi}{\partial x} = 0 \tag{3.29}$$

$$Y = H, \quad \Psi = \zeta \tag{3.30}$$

$$X = W, \quad \Psi = \zeta \tag{3.31}$$

Now applying the following dimensionaless variables

$$y = \frac{Y}{D_h} \tag{3.32}$$

$$x = \frac{X}{D_h} \tag{3.33}$$

$$\psi = \frac{ze\Psi}{k_b T} \tag{3.34}$$

where $D_h = \frac{4HW}{H+W}$ is the hydraulic diameter.

Then, the Poisson-Boltzmann equation and boundary conditions are transformed into:

$$\frac{\partial^2 \Psi}{\partial Y^2} + \frac{\partial^2 \Psi}{\partial X^2} = (\kappa D_h)^2 \sinh(\psi) \tag{3.35}$$

where $\kappa = \left(2c_\infty z^2 e^2 / \varepsilon \varepsilon_0 k_b T\right)^{1/2}$ it is the Debye-Huckel parameter. Besides the dimensionaless parameter κD_h is often referred to as the electrokinetic diameter. The corresponding non-dimensional boundary conditions are:

$$y = 0, \quad \frac{\partial \Psi}{\partial y} = 0 \tag{3.36}$$

$$x = 0, \quad \frac{\partial \Psi}{\partial x} = 0 \tag{3.37}$$

$$y = H, \quad \Psi = \frac{ze\zeta}{k_b T} = \zeta^* \tag{3.38}$$

$$x = W, \quad \Psi = \frac{ze\zeta}{k_b T} = \zeta^* \tag{3.39}$$

3.3.2 Electrokinetic flow field in a rectangular microchannel

Consider a steady state flow, fully developed in two dimensions, then the velocity components are reduced to $u = u(x, y)$ y $v = w = 0$. Also, replacing ρ_e the equation (3.17) becomes:

$$\mu \left(\frac{\partial^2 u}{\partial y^2} + \frac{\partial^2 u}{\partial x^2} \right) = \left(2c_\infty ze \sinh(\frac{ze\Psi}{k_b T}) \right) E \tag{3.40}$$

This complemented with symmetric boundary conditions

$$y = 0, \quad \frac{\partial u}{\partial y} = 0 \tag{3.41}$$

$$x = 0, \quad \frac{\partial u}{\partial x} = 0 \tag{3.42}$$

$$y = H, \quad u = 0 \tag{3.43}$$

$$x = W, \quad u = 0 \tag{3.44}$$

Now entering the dimensional variables:

$$\overline{u} = \frac{u}{U} \tag{3.45}$$

$$\overline{E} = \frac{EL}{\zeta} \tag{3.46}$$

where U is the reference velocity and the distance L between the two electrodes. So we have the following equation:

$$\frac{\partial^2 \overline{u}}{\partial \overline{y}^2} + \frac{\partial^2 \overline{u}}{\partial \overline{x}^2} = M\overline{E}\sinh(\psi) \tag{3.47}$$

where $M = \frac{2c_\infty z e \zeta D_h^2}{\mu U L}$ and the boundary conditions are given by:

$$\overline{y} = 0, \quad \frac{\partial u}{\partial \overline{y}} = 0 \tag{3.48}$$

$$\overline{x} = 0, \quad \frac{\partial u}{\partial \overline{x}} = 0 \tag{3.49}$$

$$\overline{y} = \frac{H}{D_h}, \quad \overline{u} = 0 \tag{3.50}$$

$$\overline{x} = \frac{W}{D_h}, \quad \overline{u} = 0 \tag{3.51}$$

3.4 Numerical Results

In this section, the MAPS is used to solve the problem posed in [79], in which they propose an analytical approach to an electro-kinetic flow problem affected by Joule

heating. A fully developed electroosmotic and pressure-driven combined flow in the z direction of a Newtonian liquid is solved in the computational domain given in Figure 3.3. The computational domain is given in 3.3,

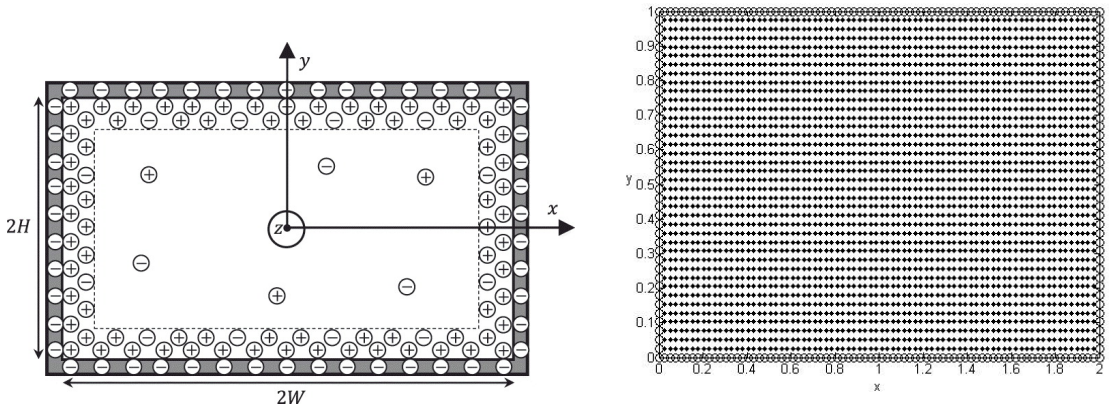

(a) (b)

Figure 3.3: a) Domain of the problem (see [79]) and b) Discretization

The equations to be solved are given by the distribution of the electric potential which is given by the Poisson-Boltzmann equation in the form [94]

$$\frac{\partial^2\psi}{\partial x^2}+\frac{\partial^2\psi}{\partial y^2}=\frac{2zen_0}{\varepsilon}\sinh(\frac{ez\psi}{K_B}T) \tag{3.52}$$

Defining the Debye Huckel parameter $\kappa=(2n_0e^2z^2/\varepsilon k_BT)^{-1/2}$ and entering the dimensional variables $\psi^*=ez\psi/k_BT$, $x^*=x/H$, $y^*=y/H$ and $y^*=y/H$ y $K=H/\kappa$, the equation is in the dimensional form

$$\frac{\partial^2\psi^*}{\partial x^{*2}}+\frac{\partial^2\psi^*}{\partial y^{*2}}=K^2\sinh(\psi^*) \tag{3.53}$$

Together with dimensionaless boundary conditions

$$\frac{\partial\psi^*}{\partial x^*}|_{x^*=0}=0,\quad \psi^*|_{x^*=\alpha}=\zeta^*,\quad \frac{\partial\psi^*}{\partial y^*}|_{y^*=0}=0,\quad \psi^*|_{y^*=1}=\zeta^* \tag{3.54}$$

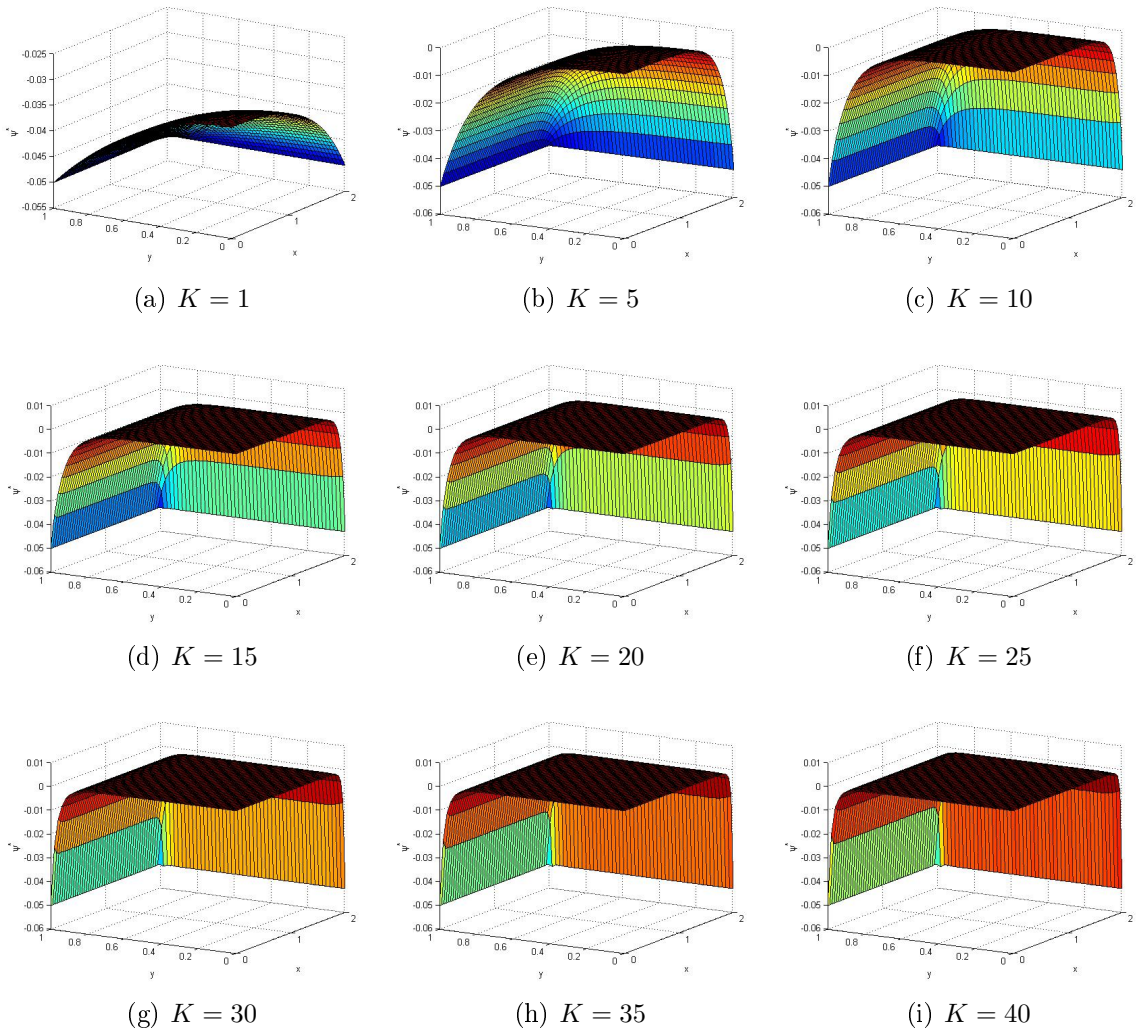

(a) $K = 1$ (b) $K = 5$ (c) $K = 10$

(d) $K = 15$ (e) $K = 20$ (f) $K = 25$

(g) $K = 30$ (h) $K = 35$ (i) $K = 40$

Figure 3.4: The figure shows the numerical profiles of the dimensional potential for different values of K

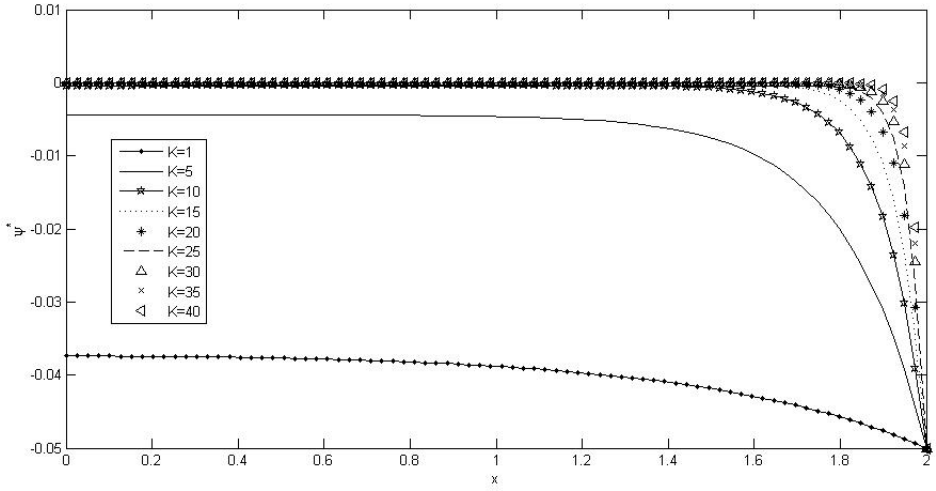

(a)

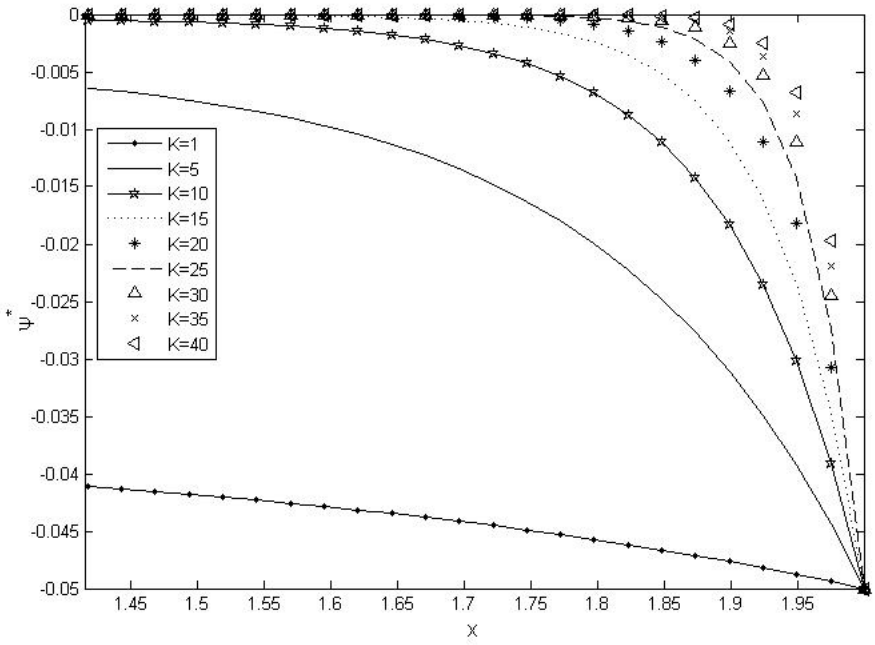

(b) Amplification between 1.4 to 2

Figure 3.5: Electric potential for different K, in $y = 0.5$

where $\alpha = W/H$ and $\zeta^* = ez\zeta/k_BT$. The analytical solution is the following expression:

$$\psi^* = \zeta^* \frac{\cosh(Ky^*)}{\cosh K} + 2\zeta^* K^2 \sum_{n=0}^{\infty} \frac{(-1)^n \cosh(\beta_n x^*) cos(\gamma_n y^*)}{\gamma_n \beta_n^2 \cosh(\beta_n \alpha)} \tag{3.55}$$

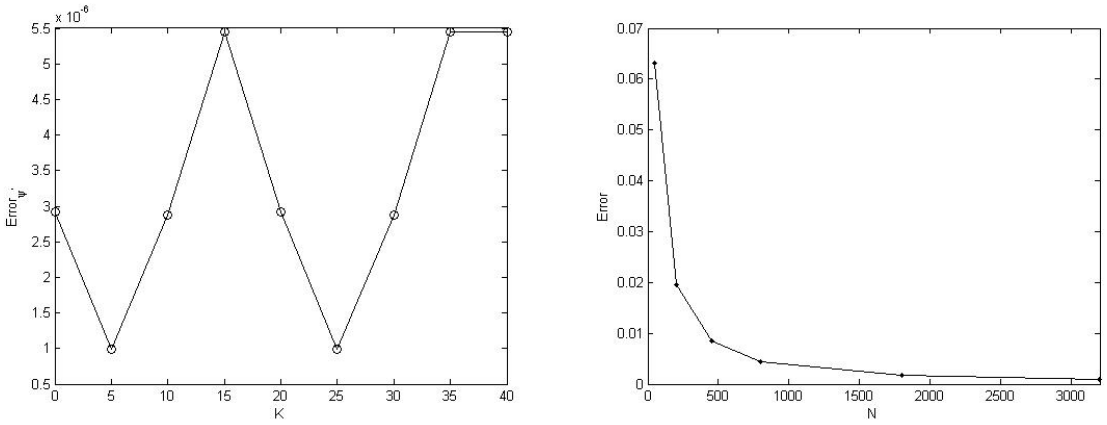

(a) Error vs K

(b) Error vs N

Figure 3.6: Error

Strong effects of constant K can be seen in the numerical profiles of the potential which are shown in figure 3.4. It is also observed that the electrical double layer only exists near the wall. According to [95] microchannel flows, the potential of EDL in the corner regions is expected to cause strong resistance to flow. Figure 3.5 shows the profiles of the potential at $y = 0.5$ where it is possible to see the effects suffered at the corners for the profile of the potential and in figure 3.6 a), the errors obtained in different values of K (see [2]), while in figure 3.6 b), error analysis is shown according to the discretion used different discretizations used for $K = 40$.

The velocity distribution of a mixed electroosmotic and pressure-driven fluid is reduced to the expression given by:

$$\mu \left(\frac{\partial^2 u}{\partial x^2} + \frac{\partial^2 u}{\partial y^2} \right) = \frac{\partial p}{\partial z} - \rho E_z \tag{3.56}$$

where $E_z = -d\phi/dz$ It is the external applied electric field. The momentum equation in the dimensional form can be rewritten as

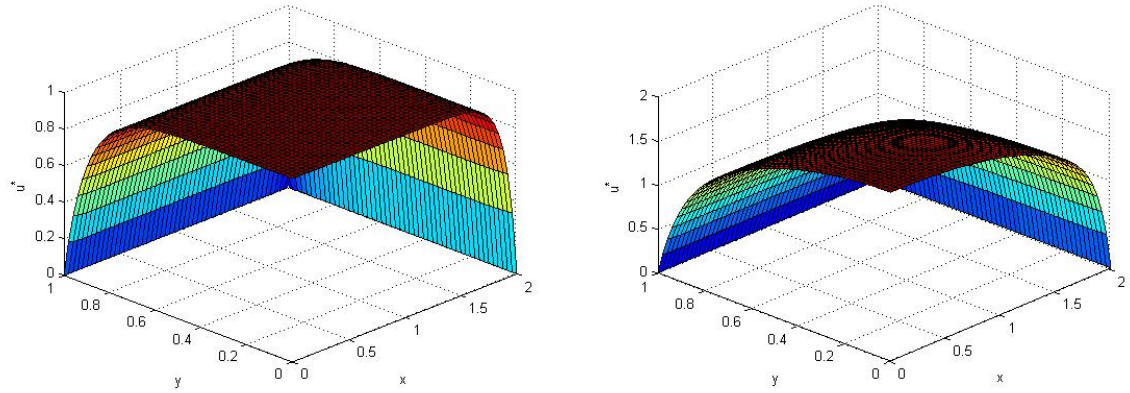

(a) $\Gamma = 0$

(b) $\Gamma = 1$

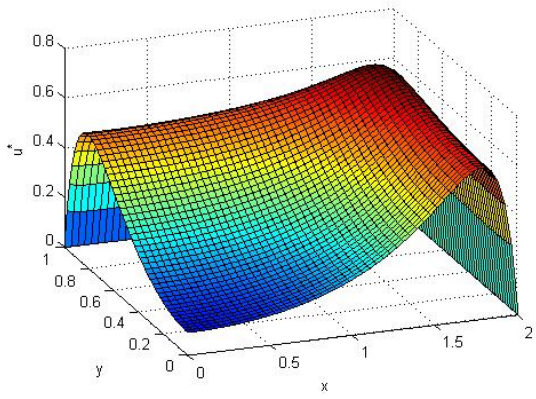

(c) $\Gamma = -1$

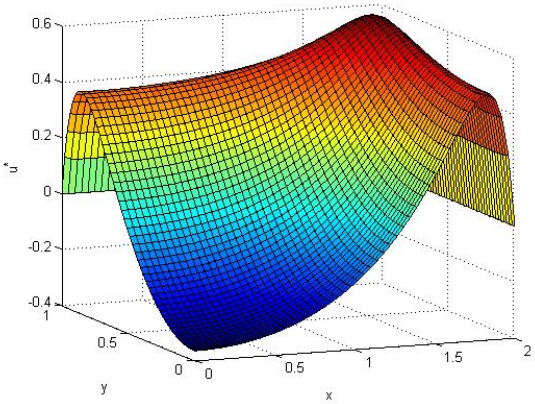

(d) $\Gamma = -1.5$

Figure 3.7: The figure shows the distribution of the dimensionaless velocity for the case where $\alpha = 2$, $K = 10$ and values of $\Gamma = 0, 1, -1$ y -1.5

$$\frac{\partial^2 u^*}{\partial x^{*2}} + \frac{\partial^2 u^*}{\partial y^{*2}} = -2\Gamma - \frac{K^2}{\zeta^*}\psi^* \tag{3.57}$$

where $u^* = u_z/u_{HS}$, here $u_{HS} = -\varepsilon\zeta E_z/\mu$ is called the Helmholtz-Smoluchowski electroosmotic velocity, according to [79], it is the maximum possible electroosmotic velocity. $\Gamma = u_{PD}/u_{HS}$ is the velocity scale relationship with $u_{PD} = -H^2(\partial p/\partial z)/2\mu$ representing the pressure-driven speed. This is complemented by the dimensional boundary conditions given by

$$\frac{\partial u^*}{\partial x^*}|_{x^*=0} = 0, \quad u^*|_{x^*=\alpha} = 0, \quad \frac{\partial u^*}{\partial y^*}|_{y^*=0} = 0, \quad u^*|_{y^*=1} = 0 \tag{3.58}$$

Equation (3.57) has the following expression as an analytical solution

$$u^* = 1 + \Gamma(1 - y^*) - \frac{\psi^*}{\zeta^*} - 4\Gamma \sum_{n=0}^{\infty} \frac{(-1)^n \cosh(\gamma_n x^*)\cos(\gamma_n y^*)}{\gamma_n^3 \cosh(\gamma_n \alpha)} \tag{3.59}$$

In addition, the average speed in the section of the channel is given by

$$u^*_{av} = \frac{1}{\alpha}\int_0^1 \int_0^\alpha u^* dx^* dy^* \tag{3.60}$$

Figure 3.7 presents the distribution of the dimensional velocity for different values of Γ. When $\Gamma = 0$, there is a purely electroosmotic fluid which is moved by the application of the external electric field. In the case $\Gamma = 1$ a combined fluid is obtained in the presence of a pressure gradient whose result is an overlap of electroosmotic and pressure-driven velocity profiles. When $\Gamma = -1$ a pressure opposes the fluid and delays the flow. Figure 3.8 shows the profiles of the dimensional velocities at $y^* = 0.5$ together with the error obtained when it is comparing with the analytical solution. It is observed, as the forces of the electric field is limited to the regions of the wall, this affects the flow velocity profile as seen in Figure 3.8.

Finally, the energy conservation equation in terms of temperature and including the

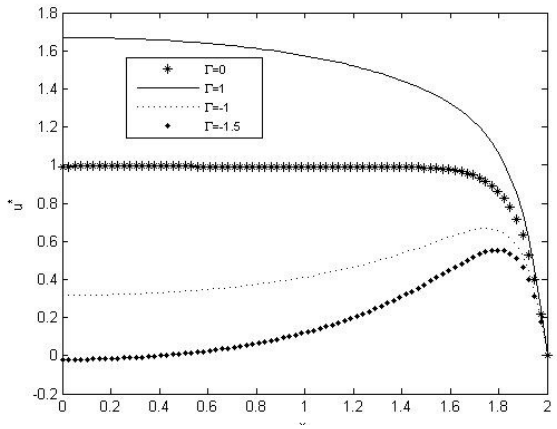

(a)

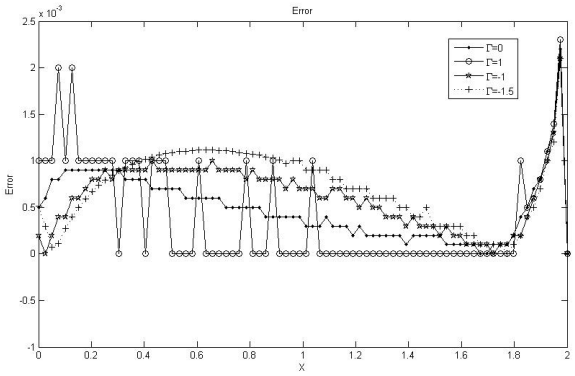

(b)

Figure 3.8: a) dimensional velocity profiles for different Γ y b)RMSE Error

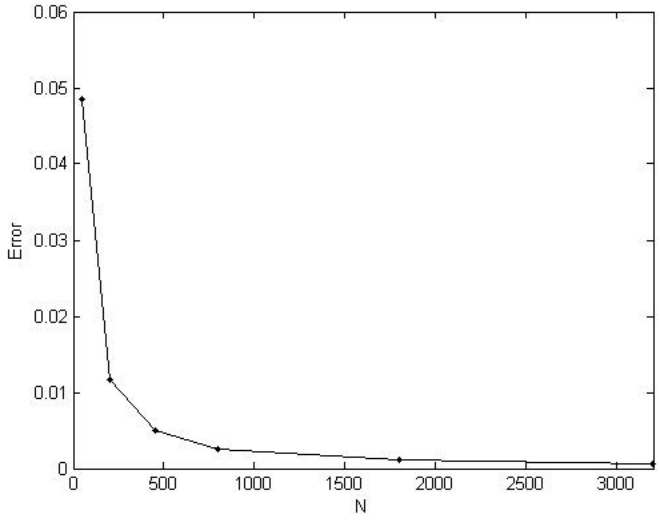

Figure 3.9: Velocity error vs N, for $\Gamma = 1$

effects of Joule heating, is given by

$$\rho c_p \frac{DT}{Dt} = \nabla \cdot (k \nabla T) + s \tag{3.61}$$

where c_p is the specific heat at constant pressure, k the thermal conductivity and $s = E_z^2/\sigma_0$ the volumetric heat generation rate due to Joule heating. Then, energy equation in dimensionaless form is

$$\frac{\partial^2 \theta^*}{\partial x^{*2}} + \frac{\partial^2 \theta^*}{\partial y^{*2}} = \frac{u^*}{u^*_{av}}(1 + 1/\alpha + S) + S \tag{3.62}$$

where $S = \frac{E_z^2 H}{q_{av}\sigma_0}$ is the dimensionless Joule heating parameter, see [58, 78]. with boundary conditions

$$\frac{\partial \theta^*}{\partial x^*}|_{x^*=0} = 0, \quad \theta^*|_{x^*=\alpha} = 0, \quad \frac{\partial \theta^*}{\partial y^*}|_{y^*=0} = 0, \quad \theta^*|_{y^*=1} = 0 \tag{3.63}$$

Which has as an analytical solution the expression given by

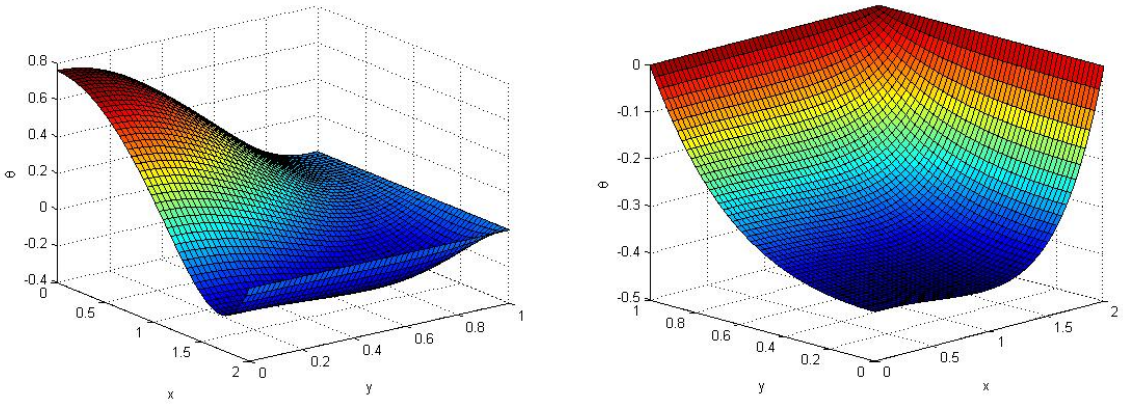

(a) $S = 1$ (b) $S = -1$

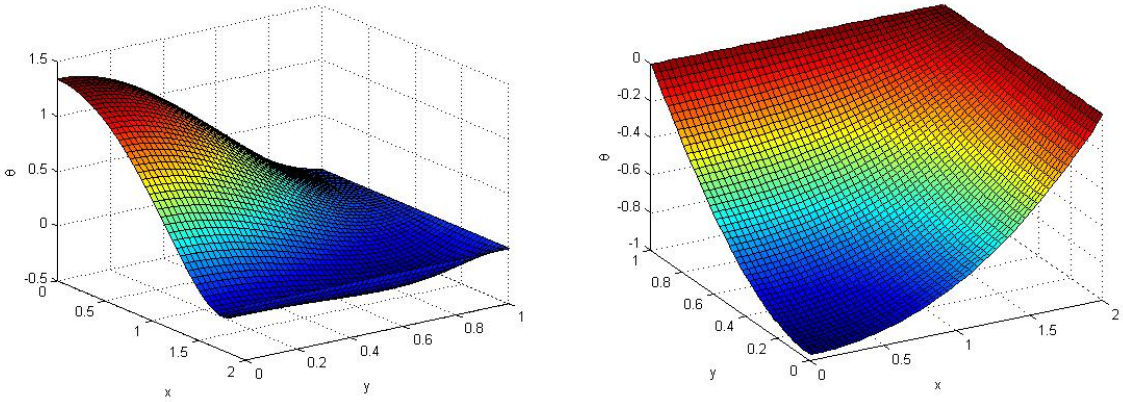

(c) $S = 2$ (d) $S = -2$

Figure 3.10: Dimensionless temperature for the case where $\alpha = 2$, $K = 20$, $\Gamma = -1.5$ and values of $S = 1, -1, 2$ y -2

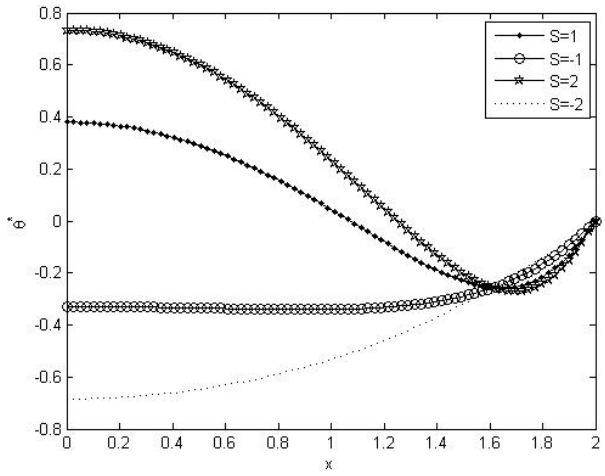

(a)

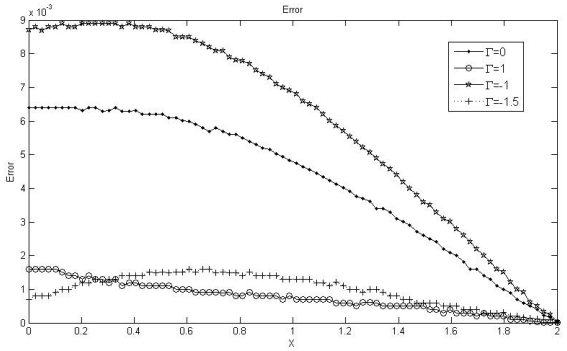

(b)

Figure 3.11: a) Dimensionaless temperature profiles for different S and b)Error RMSE

$$\theta = A_1 + A_2 y^{*2} - A_3 y^{*4} - \frac{(1 + 1/\alpha + S)}{u^*_{av} K^2} \frac{\psi^*}{\zeta^*} + \sum_{n=0}^{\infty} \left[B_n \frac{\cosh(\gamma_n x^*)}{\cosh(\gamma_n \alpha)} - C_n \frac{x^* \sinh(\gamma_n x^*)}{\cosh(\gamma_n \alpha)} \right] \cos(\gamma_n y^*) \tag{3.64}$$

Where the coefficients A_1, A_2, A_3, B_n and C_n are defined below according to [78] as:

$$A_1 = \frac{(1 + 1/\alpha + S)}{u^*_{av}} (1/K^2 - 5\Gamma/12 - 1/2) \tag{3.65}$$

$$A_2 = \frac{(1 + 1/\alpha + S)}{2u^*_{av}} (1 + \Gamma) - S/2 \tag{3.66}$$

$$A_3 = \frac{(1 + 1/\alpha + S)\Gamma}{12u^*_{av}} \tag{3.67}$$

$$B_n = \frac{2S(-1)^{n+1}}{\gamma_n^3} + \frac{2(1 + 1/\alpha + S)(1)^n}{u^*_{av}\gamma_n^3} \left[1 + \frac{\Gamma\alpha}{\gamma_n} \tanh(\gamma_n \alpha) + \frac{2\Gamma}{\gamma_n^2} \right] \tag{3.68}$$

$$C_n = \frac{2\Gamma(1 + 1/\alpha + S)(-1)^n}{u^*_{av}\gamma_n^4} \tag{3.69}$$

Then the average temperature in its dimensionaless form is given by

$$\theta_{av} = \frac{\int_0^1 \int_0^\alpha u^* \theta dx^* dy^*}{\int_0^1 \int_0^\alpha u^* dx^* dy^*} = \frac{\int_0^1 \int_0^\alpha u^* \theta dx^* dy^*}{\alpha u^*_{av}} \tag{3.70}$$

In the figure 3.10, distribution of the dimensionless temperature for different values of the S is presented. It can be observed that for negative values of S ($S = -1$, $S = -2$) the temperature difference between the center and the walls of the microchannel is large, while this is getting large ($S = 2$) this difference decreases, as it is shown in figure 3.11. A clear for cases of $S = -2$ and $S = 2$, it is a clear trends of heating and cooling of the microchannel surface, respectively. The eletroosmotic fluid generates a

Joule heating that dissipates through the walls, because of this the heat flow in the walls is negative, for more details see [78].

3.5 Final Remarks

In this chapter a study on electrokinetic fluids for microchannels was presented, as an overview of the theoretical foundations that support the problem and model to be solved. This corresponds to a validation problem, where two types of pressure-driver flow fluids and electrosmotic flows were considered for rectangular and cylindrical microchannels, and solved a model for the distribution of potential, velocity, coupled to the energy equation where dissipation is analyzed through the walls of the heat flow generated. In addition, it was solved for a non-linear differential Poisson-Boltzman equation, where Newton Raphson's method was applied to solve the non-linearity which allows to obtain a robust scheme

Chapter 4

ELECTROKINETIC FLUIDS IN NANOCANALS OF A PEM MEMBRANE

In this section, a model for electro-kinetic flow in a cylindrical nanochannel (from [9]) is solved by means of the MAPS. The domain is a nanochannel that has a uniform charge density σ_s on the walls, due to the concentration of protons c found within the channel. The models that are solved are a simplification for a nanopore in electrolyte membranes of polymers such as Nafion.

4.1 Governing equations

In order to solve this problem, it is assumed that the flow moves in the axial direction x due to the application of an external electric field and a pressure gradient. The concentration of protons c and the electric potential ψ and the fluid velocity is denoted by $u = u(x, y)$ and the external electric field E applied is constant.

The solution of our problem is carried out in two dimensions, that is to say that both the radial component $'y'$ and the axial direction $'x'$ are taken into account, see figure

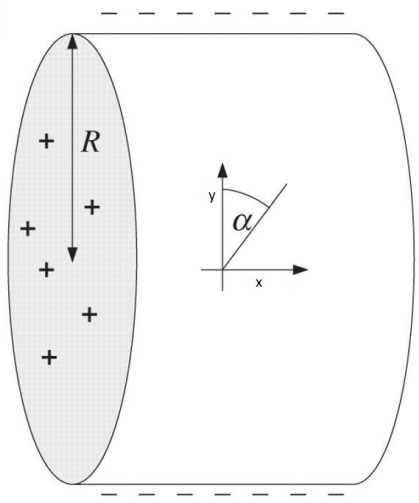

Figure 4.1: Cylindrical nanochannel

4.1. According to this, the system of equations of the model to be solved is given by:

$$\frac{1}{y}\frac{d}{dy}(y\frac{d\psi}{dy}) + \frac{d^2\psi}{dx^2} = -\frac{qc}{\epsilon\epsilon_0} \tag{4.1}$$

Using the Boltzmann distribution equation, the concentration of protons is determined by

$$c(y) = c_0 e^{-q\bar{z}\psi(y)/k_B T} \tag{4.2}$$

Then the Poisson equation becomes the Poisson-Boltzmann equation, so

$$\nabla^2\psi + \frac{1}{y}\frac{d\psi}{dy} = -\frac{qc_0}{\epsilon\epsilon_0} e^{-q\bar{z}\psi/k_B T} \tag{4.3}$$

Here $\Delta\psi = \frac{d^2\psi}{dy^2} + \frac{d^2\psi}{dx^2}$. Now introducing the dimensionaless variable $\widehat{\psi} = -\frac{q\psi}{k_B T}$, $\widehat{y} = y/R$ we have to

$$\nabla^2\widehat{\psi} + \frac{1}{\widehat{y}}\frac{d\widehat{\psi}}{d\widehat{y}} = \lambda e^{\widehat{\psi}} \tag{4.4}$$

Where λ It is a dimensionaless parameter $\lambda = \frac{R^2q^2c_0}{\epsilon\epsilon_0 k_B T}$. According to [8] λ is restricted in the range $0 \leq \lambda < 8$ and with $c_0 = \frac{8\sigma_s}{R^2q^2c_0/\epsilon\epsilon_0 k_B T - 4qR}$

This is complemented with symmetric boundary conditions in their non-dimensional form given by:

$$\frac{d\widehat{\psi}}{d\widehat{y}} = 0 \quad at \quad \widehat{y} = 0 \tag{4.5}$$

$$\frac{d\widehat{\psi}}{d\widehat{y}} = \frac{\lambda}{2(1-\lambda/8)} = -\frac{\lambda\sigma_s}{qRc_0} \quad at \quad \widehat{y} = R \tag{4.6}$$

$$\tag{4.7}$$

$$\frac{d\widehat{\psi}}{d\widehat{x}} = 0 \quad at \quad \widehat{x} = 0 \tag{4.8}$$

$$\frac{d\widehat{\psi}}{d\widehat{x}} = 0 \quad at \quad \widehat{x} = L \tag{4.9}$$

$$\tag{4.10}$$

The flow field is given by the Stokes equation of the form,

$$\mu\frac{1}{y}\frac{d}{dy}(y\frac{du}{dy}) + \mu\frac{d^2u}{dx^2} - \frac{dP}{dx} = -qc(y)E \tag{4.11}$$

Here the pressure gradient $dp/dx = P$ is constant, using the non-dimensional variable $\widehat{y} = y/R$ and $\widehat{x} = x/R$, we have to

$$\nabla^2 u + \frac{1}{\widehat{y}}\frac{du}{d\widehat{y}} = -\frac{qc(y)ER^2}{\mu} + \frac{PR^2}{\mu} \tag{4.12}$$

Complemented with symmetric boundary conditions given by

$$\frac{du}{d\widehat{y}} = 0 \quad at \quad \widehat{y} = 0 \tag{4.13}$$

$$u = 0 \quad at \quad \widehat{y} = R \tag{4.14}$$

$$\frac{du}{d\widehat{x}} = 0 \quad at \quad \widehat{x} = 0 \tag{4.15}$$

$$\frac{du}{d\widehat{x}} = 0 \quad at \quad \widehat{x} = L \tag{4.16}$$

$$\tag{4.17}$$

In equation (4.1) q is the charge of the electron, D is the proton diffusion coefficient, c_0 is the concentration of protons in the center of the channel and F is the Faraday counter.

According to [9] and [8], the analytical solution for the electrical potential is given by:

$$\psi(y) = -\ln\left[\left(1 - \frac{\lambda}{8}y^2\right)^2\right] \tag{4.18}$$

So, the concentration of protons is,

$$c(y) = \frac{c_0}{(1 - \lambda y^2/8)^2} \tag{4.19}$$

and the analytical solution of the Stokes equation,

$$u(y) = \frac{2qc_0ER^2}{\lambda\mu} \ln\left[\frac{1-\lambda y^2/8}{1-\lambda/8}\right] - \frac{PR^2}{4\mu}(1-y^2) \tag{4.20}$$

4.2 Resultados

4.2.1 Cross section of radius R for a nanochannel

The model given by the equations (4.1) and (4.1) is solved using the MAPS, and the parameters used were the following:

* $T = 353K$, $\epsilon = 45$, $q = 1.6 \times 10^{-19}C$
* $\sigma_s = -q/(1 \times 10^{-9})^2 = -0.16C/m^2$
* $R = 1 \times 10^{-9}m$
* $D = 7.5 \times 10^{-10}m^2/s$, $\epsilon_0 = 8.8854 \times 10^{-12}C^2/(Nm^2)$, $\mu = 3.35 \times 10^{-4}Pas$
* $E = 0.1/50 \times 10^{-6}V/m = 2000V/m$

In figure 4.2, the comparison of the analytical solution with the numerical solution is shown, for a uniform discretization of 2500 points, for this case a value of $\lambda = 1$ was used. Figure 4.3 shows the results obtained for the electric potential for different values of λ.

The electro-osmotic velocity is calculated for a pressure gradient P constant to a value of 100 atmosphere which is equivalent to $10 \times 10^{10}Pa/m$. The figure 4.4 the speed profile shown compared with the analytical solution 4.20 and the relative error of this calculation.

Figure 4.5 shows the velocity profiles for different values of λ which shows their dependence on this non-dimensional parameter. In table 4.2.1, we show the RMSE errors

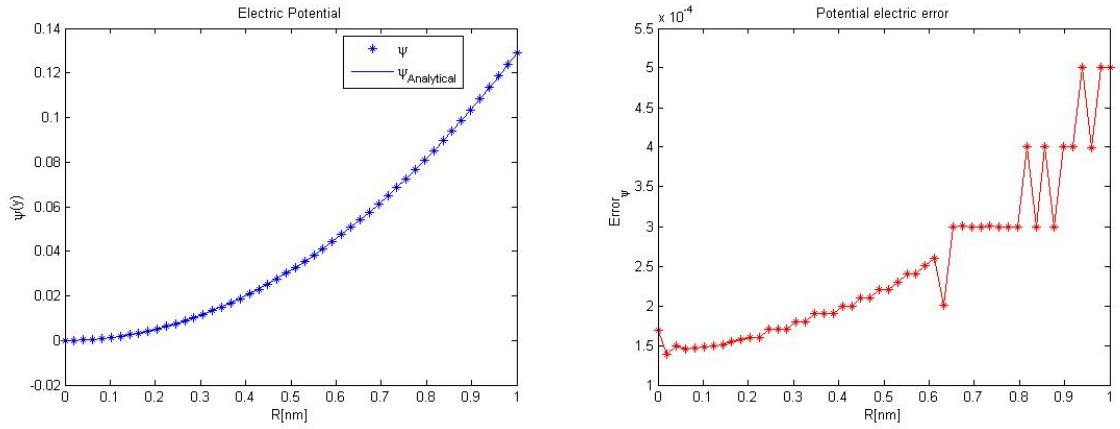

(a) (b)

Figure 4.2: a) comparison of the numerical solution and the analytical solution of the electric potential, in b) The error for a discretization of N = 2500

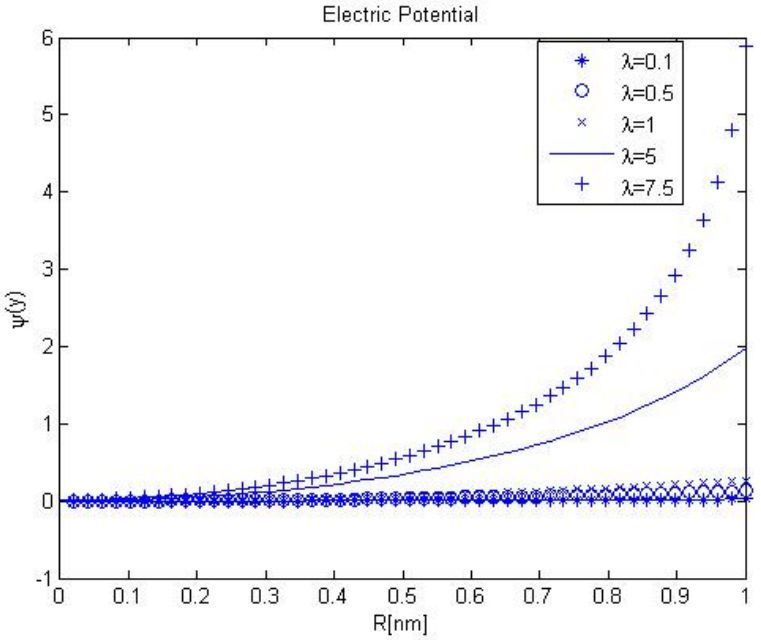

Figure 4.3: Electrical potential for different values of λ and N=2500

obtained for discretizations of $N = 900$ and $N = 2500$, taking different values of λ for the electric potential and electro-osmotic velocity. The variation of the parameter λ, for the potential increases the resistance in the walls of the nanochannel which leads to an increase in velocity, a situation that is generated to maintain the flow of protons through the nanochannel.

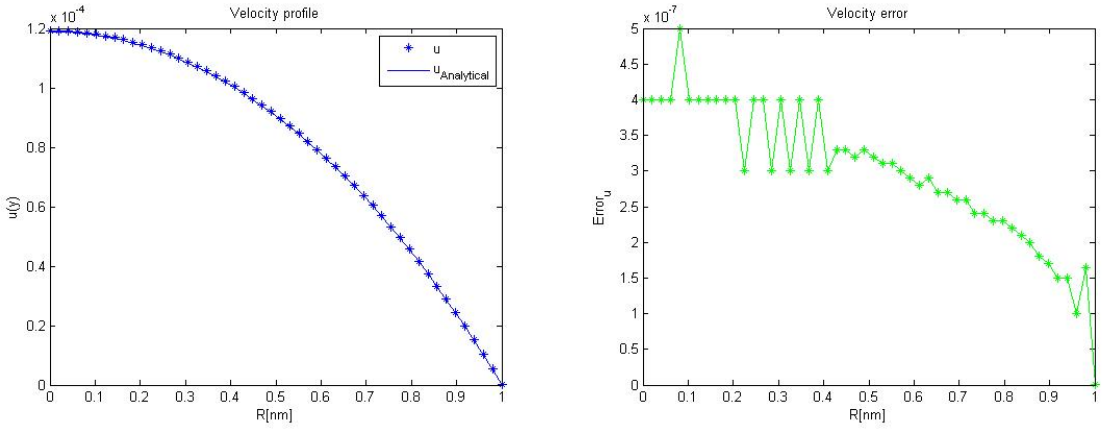

(a) (b)

Figure 4.4: a) comparison of the numerical solution and the analytical solution of the velocity, in b) The error for a discretization of N = 2500

	Potential		Velocity	
λ \ **N**	900	2500	900	2500
0.1	2.30×10^{-3}	1.60×10^{-3}	5.97×10^{-5}	2.74×10^{-5}
0.5	4.31×10^{-4}	1.60×10^{-4}	6.20×10^{-5}	2.74×10^{-4}
1.0	1.50×10^{-3}	5.18×10^{-4}	6.31×10^{-5}	2.88×10^{-5}
5.0	1.13×10^{-2}	5.10×10^{-3}	8.41×10^{-5}	3.76×10^{-5}
7.5	7.20×10^{-2}	3.30×10^{-2}	2.73×10^{-4}	1.15×10^{-4}

Additionally, in table 4.2.1 it shows that there are no significant variations in reference to the number of nodes used, however it is appreciated that for high values of λ the error increases situation that arises due to the resistances in the walls.

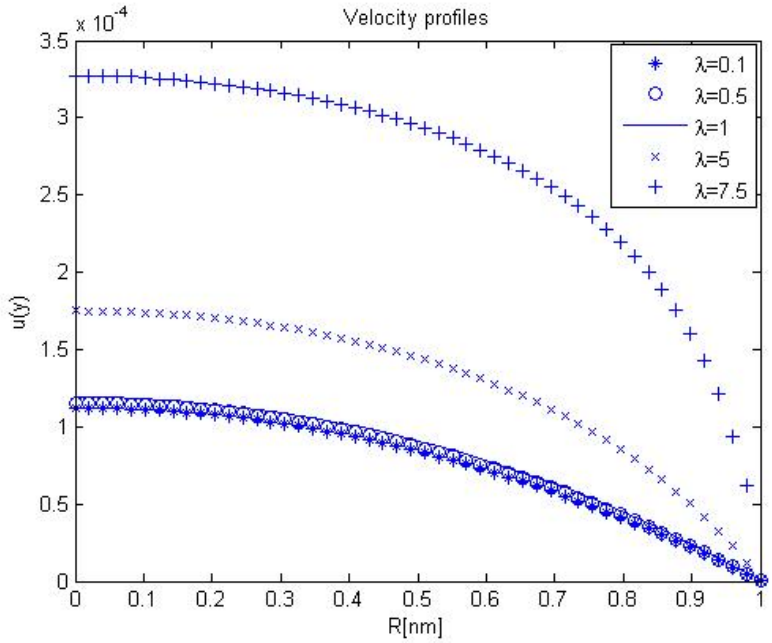

Figure 4.5: Velocities profiles for different values of λ and N=2500

4.2.2 Two cylindrical nanochannels

In this section, the conductivity between two cylindrical nanochannels in connection in a PEM membrane is studied. Two nanochannels a length of $10nm$ and a diameter of $2nm$ are considered, which are assumed to be joined by the superposition of the membrane layers. Two cases are taken into account, one where the nanochannels are perfectly aligned and another in which there is a shift in the interfaces of the two, as shown in 4.6.

This problem is solved in two dimensions in Cartesian coordinates along the two nanochannels.

For this case, the model is solved in Cartesian coordinates in two dimensions that is similar to that presented in equations (4.1) and (4.1), but with boundary conditions,

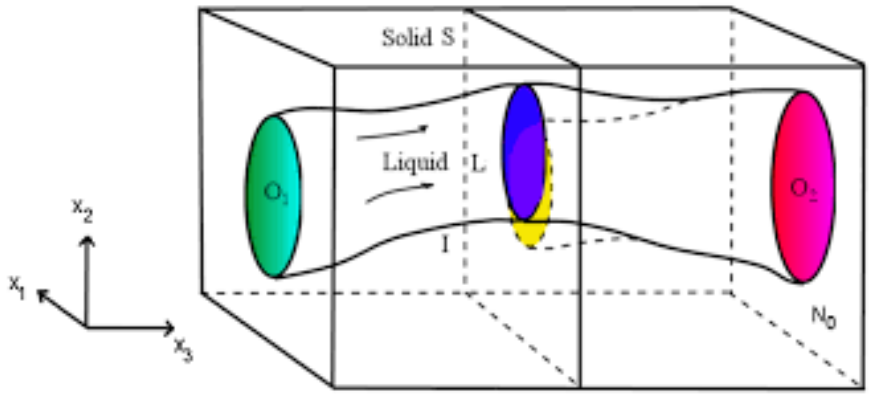

Figure 4.6: Nanochannel: where L is liquid, O_1 is inlet, O_2 is outlet, S is solid and I is free interface between liquid and solid, see [49]

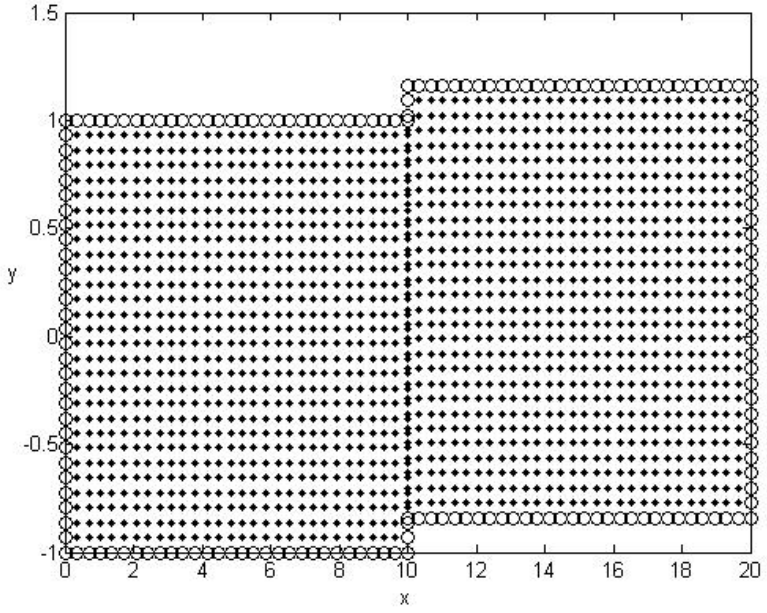

Figure 4.7: Discretizacion

$$\frac{\partial \psi}{\partial n} = \frac{\sigma_0}{\varepsilon_0 \varepsilon_r}, \quad \text{on} \quad I \tag{4.21}$$

$$\frac{\partial \psi}{\partial n} = (-1)^i E_{ext}, \quad \text{on} \quad O_i, i = 1, 2 \tag{4.22}$$

For the electric potential and with,

$$u = 0, \quad \text{on} \quad I \tag{4.23}$$

$$\frac{\partial u}{\partial n} = 0, \quad \text{on} \quad O_i, i = 1, 2 \tag{4.24}$$

For velocity. First, the case is presented when the two nano channels are perfectly aligned as shown in Figure 4.8.

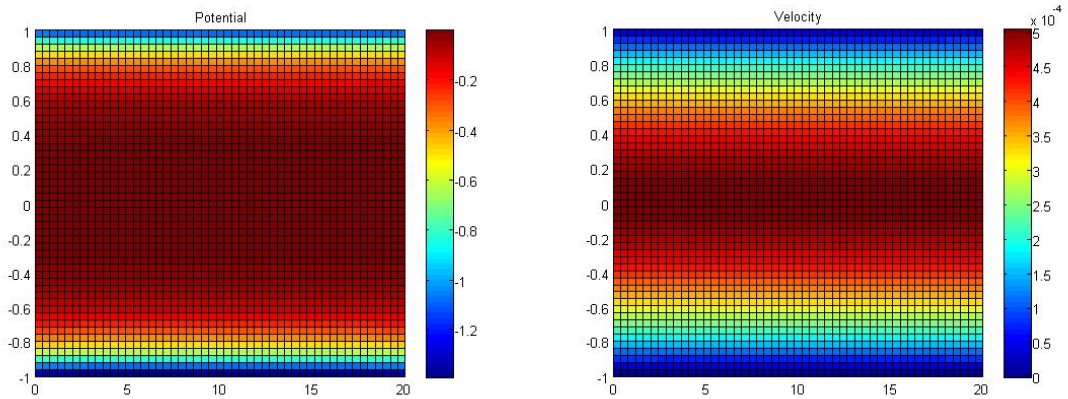

(a) (b)

Figure 4.8: Straight nanochannel result a) electric potential, b) electro-osmotic velocity

For the ideal case of two perfectly aligned nano channels, no electro-osmotic resistance is presented, which allows free fluid mobility. In Figure 4.8 a) the constant potential is maintained at the boundary and in the liquid-solid interface, and it only shows variation as it approaches the center of the nano channel, in Figure 4.8 b) it is observed that the velocity is zero in the boundary and it is increasing towards the center of the channel until reaching its maximum value.

The results in Figure 4.8, that at the interface of the two nano channels there is no resistance to the fluid and therefore there is no electro-osmotic resistance, which would allow a good functioning of a PEM membrane.

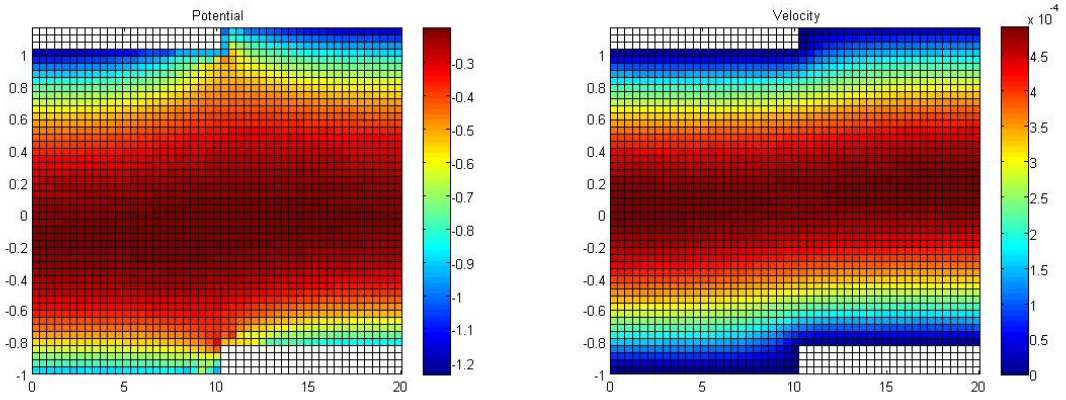

(a) (b)

Figure 4.9: Nanocanal with jump a) electric potential, b) electro-osmotic velocity

Secondly, a case is solved where the nano channels have a slight displacement forming a step or jump class, as shown in Figure 4.9. In Figure 4.9 a) the electrical potential is kept constant at the boundaries of Cana nano channel, however there is a variation in the interface between the two nano channels, in Figure 4.9 b) a velocity profile is formed that is maintained constant and compliance with boundary conditions is observed, however a decrease in fluid velocity is observed

The previous results show a resistance that occurs at the interface of the nano channels, a variation that is evidenced by a decrease in fluid velocity. According to [49], he considers that this variation in velocity is due to an electro-osmotic resistance that is generated between the two nano channels. In the operation of the fuel cell, an increase in pressure would be carried out to maintain the speed of the fluid, but according to [53] and [10], this could generate that in the PEM membrane the jump or step is greater, which leads to another decrease in speed.

On the other hand, we find that the flow of protons is large near the pore wall. Which agree well with the results of the literature. Hence, we believe that the objectives set out in this work are met, since a powerful and robust mesh-free numerical scheme is developed, which solves a mixed electro-kinetic flow problem and identifies the causes of electro resistance -osmitica on the interface of two nano channels.

4.3 Final Remarks

In this section, the MAPS was applied for the solution of an electrokinetic model of a PEM membrane in a fuel cell. In the first, a cross-section of a nanochannel was resolved, the λ parameter is varied for the electrical potential and the incidence of the double electrical layer on the nanochannel wall is determined. In the figure 4.3 it is observed that for small values of λ, the potential exerts little resistance to the flow and as it grows there is an increase in resistance, a situation that is due to the polarity of the wall, see [56]. The equations of potential and velocity are coupled, and an increase in potential was observed represented in a decrease in velocity, a more pronounced profile is obtained as shown in the figure 4.5. This situation is due to the opposition exerted by the double electrical layer to the passage of proton flow through the membrane nanochannels.

In the second problem, it resolved the electrokinetic model between two cylindrical nanochannels connected to each other of a PEM membrane. In the results obtained it is observed that it maintains the trend reported in the literature. In addition, the results of the cross-section can be affirmed that the electrochemical resistance reported in the literature is probably due to the resistance exerted by the double electrical layer on the walls of the nanochannels causing the speed decrease, a situation that worsens when the offset between the nanochannels is greater. For the electric potential it is solved for a non-linear differential Poisson-Boltzman equation, where Newton Raphson's method is applied to solve the nonlinearity of the model.

CONCLUSIONS AND FURTHER WORK

CONCLUSIONS

A meshless method scheme of approximate particular solutions (MAPS)was developed, which is implemented to solve scalar and vector problems. For this, two generic codes were developed, the first with particular Poisson solutions for scalar problems and the second with a particular solution of the Stokes equation system to solve flow in a channel and in two parallel plates, both cases with MQ function as RBF. A two-dimensional Poisson equation with Dirichlet boundary condition and an inhomogeneous momentum equation in two dimensions are solved, respectively.

The MAPS was implemented to solve two initial problems: first a 'Slit Flow' channel and then a convective laminar flow between two parallel plates and additionally an elliptical differential equation with variable coefficients. The influence of the type of boundary conditions on the Approximate Particular Solutions Method for both vector and scalar problems was determined. In the case of vector problems, the analysis was performed for Dirichlet, traction and mixed boundary conditions, while the scalar problem was performed for Dirichlet and Neumann conditions. In all cases, the care that should be taken in the selection of the type of boundary condition was shown, was found that the MAPS has a good behavior for mixed boundary conditions between Dritchlet and traction, which shows better results and stability.

During application of the MAPS to solve the problem of the 'Slit Flow' in the channel,

was performed for two types of discretization: uniform and refined toward axis 'x'. For the Type 1 boundary condition, no significant differences were found when using a uniform discretization and then a refined discretization. Something contrary to what happened with the boundary condition Type 3, in which the error step $\epsilon_{err} = 5.19 \times 10^{-3}$ to $\epsilon_{err} = 7.92 \times 10^{-12}$ and the boundary condition Type 4 step from $\epsilon_{err} = 5.20 \times 10^{-3}$ to $\epsilon_{err} = 1.06 \times 10^{-11}$, improving results in these problems and showing that these boundary conditions must be consistent with the physics of the problem.

Study of electro-kinetic fluids is carried out. These phenomenons are very important for applications in various chemical and biomedical analysis subjects. In addition to the great development in research topics of mechanical engineering and fuel cells type PEM. The MAPS was implemented for solution of eletrokinetic fluid in micro and nanochannels for electroosmotic and pressure-driven fluids, obtaining satisfactory results where evidencing the efficiency and simplicity of the solution method. These results were compared and validated with the respective analytical solutions reported in the literature, convergence analyzes performed according to the type of discretization show how quickly the MAPS achieves stability in the error.

It is important to keep in mind that electrokinetic fluids were solved for a nonlinear Poisson-Boltzman differential equation, where Newton Raphson's method was applied to solve nonlinearity which allows to obtain a robust scheme, which was later used for the solution of the model in the PEM membrane.

After solving solve electrokinetic flows method efficiently, we studied the application of the method to the problem of electroosmotic flow in cylindrical nanochannels in PEM membrane. Results were obtained for a mixed flow (pressure-driven and electroosmotic) based on a system of two coupled equations for fluid velocity and potential. The results obtained follow the trend reported in the literature, for two important cases analyzed: the first case in which has two perfectly aligned nanochannels and the second case where a slight shift in the interface of the two nanochannels. Results that allow us to show the good behavior of the MAPS for the solution of this type of problems.

A numerical method of radial basis functions with approximate particular solutions was developed which was used to solve the Stokes flow problem and for the electrical potential this in a PEM membrane of a fuel cell. The hypothesis at the beginning of this work is validated and shown that the developed method is accurate and efficient

to solve electrokinetic flows and nonlinear coupled equations. easy deployment, robust and consistent method was achieved.

FURTHER WORK

The solution method developed here shows similar results to those reported in the literature, although the capabilities of this solution method have been demonstrated in this work and in previous research, It is recommended to continue with this type of research.

One of the aspects to analyze is the type of discretization to be used. Significant changes were found in the results according to the assigned nodal distribution, this without leaving the issue of bad conditioning of the matrix when trying to improve the results by increasing the number of nodes In this work, only particular solutions were used using the multicadric RBF, although some works have already used another type of RBFs such as [84] that uses trigonometric basis functions to solve PDEs. It is important to keep in mind that there is still much to investigate to find formulations of the particular solutions for each RBF that is used. From there, for future work, an implementation of the Local MAPS could be carried out and the behavior in the interface of the two nano channels can be observed in more detail.

Regarding the application to electrokinetic fluids in the proton exchange membrane (PEM), a study that takes into account the concentration of protons given by the Nernst-Planck equation would be important, this coupled with the equations of the electric potential and the fluid velocity Since, for reasons of time it was not taken into account in this work. Similarly, a formulation of the MAPS could be worked on for a three-dimensional problem that would be easy to apply due to the characteristics of the method.

The method presented can be used for solving similar problems solved in this work, even with a higher degree of complexity provided they are similar models.

SCIENTIFIC PAPERS

The following scientific papers have been developed, submitted for publication and/or published during the accomplishment of the present PhD work:

- D.A. Castro, N. Caruso, M. Portapila, W. Florez, Method Approximate Particular Solutions for the solution of electro-kinetic fluids in Micro and Nanochannels, Tecciencia (Accepted)
- D.A. Castro, N. Caruso, M. Portapila, W. Florez, The influence on the different boundary conditions on Method Approximate Particular Solutions in scalar and vector problems (article in preparation)
- D.A. Castro, N. Caruso, M. Portapila, W. Florez, Solution of a flow problem between and the interface of two nanochannels in a PEM membrane of a fuel cell by means of Method Approximate Particular Solutions (article in preparation)

Additionaly, the following works have been presented in international conferences:

- D.A. Castro, W. Florez, H.V. Martinez, H. Power, Study and Modeling of Conductivity and Geometric Deformation in the Nanoporos Interface in a PEM Membrane. Internal colloquium on Biofuels and nanomaterials for energy storage, Medellin, 2016.
- D.A. Castro, W. Florez, Method Approximate Particular Solutions for Solution of Electrocinetics Fluids in Nanocanales, CIFASIS-CONICET-UNR international seminar, Rosario, Argentina, 2018.
- D.A. Castro, N. Caruso, M. Portapila, W. Florez, Method Approximate Particular Solutions for the solution of electro-kinetic fluids in Micro and Nanochannels, XII Congreso Colombiano de Métodos Numéricos, Bogotá, 2019.

Bibliography

[1] C. Arntsen, J. Savage, Y.-L. S. Tse, and G. A. Voth. Simulation of proton transport in proton exchange membranes with reactive molecular dynamics. *Fuel Cells*, 16(6):695–703, apr 2016.

[2] Sarah Arulanandam and Dongqing Li. Liquid transport in rectangular microchannels by electroosmotic pumping. *Colloids and Surfaces A: Physicochemical and Engineering Aspects*, 161(1):89–102, jan 2000.

[3] Behzad Ataie-Ashtiani, Craig T. Simmons, and Adrian D. Werner. Influence of boundary condition types on unstable density-dependent flow. *Groundwater*, 52(3):378–387, may 2013.

[4] Tadashi Awatani, Hiromi Midorikawa, Nobuo Kojima, Jiping Ye, and Curtis Marcott. Morphology of water transport channels and hydrophobic clusters in nafion from high spatial resolution AFM-IR spectroscopy and imaging. *Electrochemistry Communications*, 30:5–8, may 2013.

[5] Balaji. Analysis of flow parameters in fuel cell for efficient power generation. *International Journal of Engineering and Innovative Technology (IJEIT)*, 2(5):160–164, mar 2013.

[6] Roushanara Begum and MZI Bangalee. Effects of different boundary conditions at the surfaces of the extended computational domain in computing the natural convection flow in an open cavity. *Dhaka University Journal of Science*, 64(1):31–37, jun 2016.

[7] P Berg and BE Benjaminsen. Effects of finite-size ions and relative permittivity in a nanopore model of a polymer electrolyte membrane. *Electrochimica Acta*, 120:429–438, 2014.

[8] P. Berg and J. Findlay. Analytical solution of the poisson-nernst-planck-stokes equations in a cylindrical channel. *Proceedings of the Royal Society A: Mathematical, Physical and Engineering Sciences*, 467(2135):3157–3169, jun 2011.

[9] P Berg and K Ladipo. Exact solution of an electro-osmotic flow problem in a cylindrical channel of polymer electrolyte membranes. *Proceedings of the Royal Society of London Series A*, 465:2663–2679, 2009.

[10] Peter Berg, Sven-Joachim Kimmerle, and Arian Novruzi. Modeling, shape analysis and computation of the equilibrium pore shape near a pem–pem intersection. *Journal of Mathematical Analysis and Applications*, 410(1):241–256, 2014.

[11] Gurpreet Singh Bhatia and Geeta Arora. Radial basis function methods for solving partial differential equations-a review. *Indian Journal of Science and Technology*, 9(45), dec 2016.

[12] C. A. Bustamante, H. Power, W. F. Florez, and C. Y. Hang. The global approximate particular solution meshless method for two-dimensional linear elasticity problems. *International Journal of Computer Mathematics*, 90(5):978–993, nov 2012.

[13] CA Bustamante, H Power, YH Sua, and WF Florez. A global meshless collocation particular solution method (integrated radial basis function) for two-dimensional stokes flow problems. *Applied Mathematical Modelling*, 37(6):4538–4547, 2013.

[14] CA Bustamante, Henry Power, and WF Florez. A global meshless collocation particular solution method for solving the two-dimensional navier–stokes system of equations. *Computers & Mathematics with Applications*, 65(12):1939–1955, 2013.

[15] Somchart Chantasiriwan. Cartesian grid methods using radial basis functions for solving poisson, helmholtz, and diffusion–convection equations. *Engineering Analysis with Boundary Elements*, 28(12):1417–1425, dec 2004.

[16] C. S. Chen, C. M. Fan, and P. H. Wen. The method of approximate particular solutions for solving elliptic problems with variable coefficients. *International Journal of Computational Methods*, 08(03):545–559, sep 2011.

[17] Fan C. M. & Wen P. H Chen, C. S. The method of approximate particular solutions for solving certain partial differential equations. *Numerical Methods for Partial Differential Equations*, 28(2):506–522, 2012.

[18] Yuyan Chen and Shuo Zhang. A conservative stable finite element method for stokes flow and nearly incompressible linear elasticity on rectangular grid. *Journal of Computational and Applied Mathematics*, 323:53–70, oct 2017.

[19] A. H.-D. Cheng and J. J. S. P. Cabral. Direct solution of ill-posed boundary value problems by radial basis function collocation method. *International Journal for Numerical Methods in Engineering*, 64(1):45–64, 2005.

[20] Yong Seok Choi and Sung Jin Kim. Electrokinetic flow-induced currents in silica nanofluidic channels. *Journal of Colloid and Interface Science*, 333(2):672–678, may 2009.

[21] A.S. Muleshkov & M.A. Golberg C.S. Chen. The numerical evaluation of particular solutions for poisson's equation - a revisit. *WIT Transactions on Modelling and Simulation*, 25, 1999.

[22] Giulia Deolmi, Wolfgang Dahmen, and Siegfried Müller. Effective boundary conditions: A general strategy and application to compressible flows over rough boundaries. *Communications in Computational Physics*, 21(02):358–400, feb 2017.

[23] Anne-Claire Dupuis. Proton exchange membranes for fuel cells operated at medium temperatures: Materials and experimental techniques. *Progress in Materials Science*, 56(3):289–327, mar 2011.

[24] Michael Eikerling. Theory and modeling of fuel cells: Extravaganza to panacea? *Fuel Cells*, 16(6):663–668, 2016.

[25] Chia-Ming Fan, Chi-Hung Yang, and Wei-Shiang Lai. Numerical solutions of two-dimensional flow fields by using the localized method of approximate particular solutions. *Engineering Analysis with Boundary Elements*, 57:47–57, aug 2015.

[26] Shulu Feng, John Savage, and Gregory A. Voth. Effects of polymer morphology on proton solvation and transport in proton-exchange membranes. *The Journal of Physical Chemistry C*, 116(36):19104–19116, aug 2012.

[27] W.F. Florez and H. Power. DRM multidomain mass conservative interpolation approach for the BEM solution of the two-dimensional navier-stokes equations. *Computers & Mathematics with Applications*, 43(3-5):457–472, feb 2002.

[28] Zhuo-Jia Fu, Wen Chen, and Leevan Ling. Method of approximate particular solutions for constant- and variable-order fractional diffusion models. *Engineering Analysis with Boundary Elements*, 57:37–46, aug 2015.

[29] & Chen C. S. Golberg, M. A. The method of fundamental solutions for potential, helmholtz and diffusion problems. *Boundary integral methods-numerical and mathematical aspects*, pages 103–176, 1998.

[30] JM Granados, CA Bustamante, H Power, and WF Florez. A global stokes method of approximated particular solutions for unsteady two-dimensional navier–stokes system of equations. *International Journal of Computer Mathematics*, pages 1515–1541, 2017.

[31] J.M. Granados, H. Power, C.A. Bustamante, W.F. Flórez, and A.F. Hill. A global particular solution meshless approach for the four-sided lid-driven cavity flow problem in the presence of magnetic fields. *Computers & Fluids*, 160:120–137, jan 2018.

[32] Hywel Morgan; Nicolas G Green. *AC electrokinetics : colloids and nanoparticles.* Microtechnologies and microsystems series, 2. Research Studies Press, 2003.

[33] Alain Gruger, André Régis, Tatiana Schmatko, and Philippe Colomban. Nanostructure of nafion® membranes at different states of hydration. *Vibrational Spectroscopy*, 26(2):215–225, nov 2001.

[34] M. Grujicic and K.M. Chittajallu. Design and optimization of polymer electrolyte membrane (PEM) fuel cells. *Applied Surface Science*, 227(1-4):56–72, apr 2004.

[35] Mohammad Hadigol, Reza Nosrati, and Mehrdad Raisee. Numerical analysis of mixed electroosmotic/pressure driven flow of power-law fluids in microchannels and micropumps. *Colloids and Surfaces A: Physicochemical and Engineering Aspects*, 374(1-3):142–153, jan 2011.

[36] Robert J Hunter. *Zeta potential in colloid science: principles and applications*, volume 2. Academic press, 2013.

[37] Zainuddin Mat Isa and Nasrudin Abdul Rahim. PEM fuel cell model parameters optimization using modified particle swarm optimization algorithm. In *2013 IEEE Conference on Clean Energy and Technology (CEAT)*. IEEE, nov 2013.

[38] J. Jamaati, H. Niazmand, and M. Renksizbulut. Pressure-driven electrokinetic slip-flow in planar microchannels. *International Journal of Thermal Sciences*, 49(7):1165–1174, jul 2010.

[39] Tongsong Jiang, Ming Li, and C. S. Chen. The method of particular solutions for solving inverse problems of a nonhomogeneous convection-diffusion equation with variable coefficients. *Numerical Heat Transfer, Part A: Applications*, 61(5):338–352, mar 2012.

[40] Dalei Jing and Bharat Bhushan. Effect of boundary slip and surface charge on the pressure-driven flow. *Journal of Colloid and Interface Science*, 392:15–26, feb 2013.

[41] Ryan Jorn, John Savage, and Gregory A. Voth. Proton conduction in exchange membranes across multiple length scales. *Accounts of Chemical Research*, 45(11):2002–2010, may 2012.

[42] Ryan Jorn and Gregory A. Voth. Mesoscale simulation of proton transport in proton exchange membranes. *The Journal of Physical Chemistry C*, 116(19):10476–10489, apr 2012.

[43] Yuejun Kang, Chun Yang, and Xiaoyang Huang. Dynamic aspects of electroosmotic flow in a cylindrical microcapillary. *International Journal of Engineering Science*, 40(20):2203–2221, 2002.

[44] E.J. Kansa. Multiquadrics—a scattered data approximation scheme with applications to computational fluid-dynamics—II solutions to parabolic, hyperbolic and elliptic partial differential equations. *Computers & Mathematics with Applications*, 19(8-9):147–161, 1990.

[45] E.J. Kansa and Y.C. Hon. Circumventing the ill-conditioning problem with multiquadric radial basis functions: Applications to elliptic partial differential equations. *Computers & Mathematics with Applications*, 39(7-8):123–137, apr 2000.

[46] George Karniadakis, Ali Beskok, and Narayan Aluru. *Microflows and nanoflows: fundamentals and simulation*, volume 29. Springer Science & Business Media, 2006.

[47] Daejoong Kim and Eric Darve. Molecular dynamics simulation of electro-osmotic flows in rough wall nanochannels. *Physical Review E*, 73(5), may 2006.

[48] Sven-Joachim Kimmerle, Peter Berg, and Arian Novruzi. An electrohydrodynamic equilibrium shape problem for polymer electrolyte membranes in fuel cells. pages 387–396, 2011.

[49] Sven-Joachim Kimmerle, Kehinde Ladipo, Arian Novruzi, and Peter Berg. Contact resistance at pem-pem interfaces: Charged fluid flow between nanochannels. *ECS Transactions*, 59(1):145–159, 2014.

[50] C Kompis and K Malek. Fuel cell modeling strategic roadmap: A systematic approach. *Fuel Cells*, 16(6):760–770, 2016.

[51] S. Soleimani Kutanaei, Naeem Roshan, A. Vosoughi, S. Saghafi, A. Barari, and Soheil Soleimani. Numerical solution of stokes flow in a circular cavity using mesh-free local RBF-DQ. *Engineering Analysis with Boundary Elements*, 36(5):633–638, may 2012.

[52] C. Laberty-Robert, K. Vallé, F. Pereira, and C. Sanchez. Design and properties of functional hybrid organic–inorganic membranes for fuel cells. *Chemical Society Reviews*, 40(2):961, 2011.

[53] Kehinde O Ladipo, Peter Berg, Sven-Joachim Kimmerle, and Arian Novruzi. Effects of radially dependent parameters on proton transport in polymer electrolyte membrane nanopores. *The Journal of Chemical Physics*, 134(7):074103, 2011.

[54] A.R. Lamichhane, D.L. Young, and C.S. Chen. Fast method of approximate particular solutions using chebyshev interpolation. *Engineering Analysis with Boundary Elements*, 64:290–294, mar 2016.

[55] Jacky S.H. Lee, Carolyn L. Ren, and Dongqing Li. Effects of surface heterogeneity on flow circulation in electroosmotic flow in microchannels. *Analytica Chimica Acta*, 530(2):273–282, feb 2005.

[56] Dongqing Li. *Electrokinetics in microfluidics*, volume 2. Elsevier, 2004.

[57] Jichun Li, Alexander H.-D. Cheng, and Ching-Shyang Chen. A comparison of efficiency and error convergence of multiquadric collocation method and finite element method. *Engineering Analysis with Boundary Elements*, 27(3):251–257, mar 2003.

[58] B.C. Liechty, B.W. Webb, and R.D. Maynes. Convective heat transfer characteristics of electro-osmotically generated flow in microtubes at high wall potential. *International Journal of Heat and Mass Transfer*, 48(12):2360–2371, jun 2005.

[59] Ji Lin, Yongxing Hong, Lei-Hsin Kuo, and Chein-Shan Liu. Numerical simulation of 3d nonlinear schrödinger equations by using the localized method of approximate particular solutions. *Engineering Analysis with Boundary Elements*, 78:20–25, may 2017.

[60] Sudharsan Madhavan and Erica M. Cherry Kemmerling. The effect of inlet and outlet boundary conditions in image-based CFD modeling of aortic flow. *BioMedical Engineering OnLine*, 17(1), may 2018.

[61] Nam Mai-Duy and Thanh Tran-Cong. Numerical solution of differential equations using multiquadric radial basis function networks. *Neural Networks*, 14(2):185–199, mar 2001.

[62] Nam Mai-Duy and Thanh Tran-Cong. Mesh-free radial basis function network methods with domain decomposition for approximation of functions and numerical solution of poisson's equations. *Engineering Analysis with Boundary Elements*, 26(2):133–156, 2002.

[63] Gh Mohiuddin Mala, Chun Yang, and Dongqing Li. Electrical double layer potential distribution in a rectangular microchannel. *Colloids and Surfaces A: Physicochemical and Engineering Aspects*, 135(1-3):109–116, 1998.

[64] Lanju Mei, Li-Hsien Yeh, and Shizhi Qian. Buffer anions can enormously enhance the electrokinetic energy conversion in nanofluidics with highly overlapped double layers. *Nano Energy*, 32:374–381, feb 2017.

[65] Gino Moretti. Importance of boundary conditions in the numerical treatment of hyperbolic equations. *Physics of Fluids*, 12(12):II–13, 1969.

[66] D. Nath, M.S. Kalra, and P. Munshi. Numerical simulation of time-dependent navier–stokes and MHD equations using a meshless method based on fundamental

and particular solutions. *Engineering Analysis with Boundary Elements*, 67:81–95, jun 2016.

[67] Wilmer Olivares, Thomas L. Croxton, and Donald A. McQuarrie. Electrokinetic flow in a narrow cylindrical capillary. *The Journal of Physical Chemistry*, 84(8):867–869, apr 1980.

[68] H.M. Park and H.S. Sohn. Measurement of zeta potential of macroscopic surfaces with navier velocity slip exploiting electrokinetic flows in a microchannel. *International Journal of Heat and Mass Transfer*, 54(15-16):3466–3475, jul 2011.

[69] S.J. Peighambardoust, S. Rowshanzamir, and M. Amjadi. Review of the proton exchange membranes for fuel cell applications. *International Journal of Hydrogen Energy*, 35(17):9349–9384, sep 2010.

[70] H. Power and L. C. Wrobel. *Boundary Integral Methods in Fluid Mechanics*. Computational Mechanics, 1995.

[71] R. Qiao and N. R. Aluru. Ion concentrations and velocity profiles in nanochannel electroosmotic flows. *The Journal of Chemical Physics*, 118(10):4692–4701, mar 2003.

[72] PA Ramachandran and K Balakrishnan. Radial basis functions as approximate particular solutions: review of recent progress. *Engineering Analysis with Boundary Elements*, 24(7-8):575–582, 2000.

[73] Antonio Ramos. *Electrokinetics and Electrohydrodynamics in Microsystems*. CISM International Centre for Mechanical Sciences 530. Springer, 1st edition. edition, 2011.

[74] Liqing Ren, Carlos Escobedo-Canseco, and Dongqing Li. A new method of evaluating the average electro-osmotic velocity in microchannels. *Journal of Colloid and Interface Science*, 250(1):238–242, jun 2002.

[75] S. Yu. Reutskiy. Method of particular solutions for solving PDEs of the second and fourth orders with variable coefficients. *Engineering Analysis with Boundary Elements*, 37(10):1305–1310, oct 2013.

[76] S.Yu. Reutskiy. Method of particular solutions for nonlinear poisson-type equations in irregular domains. *Engineering Analysis with Boundary Elements*, 37(2):401–408, feb 2013.

[77] CL Rice and R_ Whitehead. Electrokinetic flow in a narrow cylindrical capillary. *The Journal of Physical Chemistry*, 69(11):4017–4024, 1965.

[78] Arman Sadeghi, Milad Azari, and Suman Chakraborty. H2 forced convection in rectangular microchannels under a mixed electroosmotic and pressure-driven flow. *International Journal of Thermal Sciences*, 122:162–171, dec 2017.

[79] Arman Sadeghi, Yaser Kazemi, and Mohammad Hassan Saidi. Joule heating effects in electrokinetically driven flow through rectangular microchannels: An analytical approach. *Nanoscale and Microscale Thermophysical Engineering*, 17(3):173–193, aug 2013.

[80] M Schmuck and Peter Berg. Effective macroscopic equations for species transport and reactions in porous catalyst layers. *Journal of The Electrochemical Society*, 161(8):E3323–E3327, 2014.

[81] Markus Schmuck. Analysis of the navier–stokes–nernst–planck–poisson system. *Mathematical Models and Methods in Applied Sciences*, 19(06):993–1014, 2009.

[82] Zhi Shi, Yong yan Cao, and Qing jiang Chen. Solving 2d and 3d poisson equations and biharmonic equations by the haar wavelet method. *Applied Mathematical Modelling*, 36(11):5143–5161, nov 2012.

[83] Naohiko Takimoto, Akihiro Ohira, Yuko Takeoka, and Masahiro Rikukawa. Surface morphology and proton conduction imaging of nafion membrane. *Chemistry Letters*, 37(2):164–165, feb 2008.

[84] Zhaolu Tian, Xinxiang Li, C.M. Fan, and C.S. Chen. The method of particular solutions using trigonometric basis functions. *Journal of Computational and Applied Mathematics*, 335:20–32, jun 2018.

[85] Bijay P. Tripathi and Vinod K. Shahi. Organic–inorganic nanocomposite polymer electrolyte membranes for fuel cell applications. *Progress in Polymer Science*, 36(7):945–979, jul 2011.

[86] Heng-Kwong Tsao. Counterion distribution enclosed in a cylinder and a sphere. *The Journal of Physical Chemistry B*, 102(50):10243–10247, 1998.

[87] Heng-Kwong Tsao. Electroosmotic flow through an annulus. *Journal of colloid and interface science*, 225(1):247–250, 2000.

[88] Moran Wang and Qinjun Kang. Modeling electrokinetic flows in microchannels using coupled lattice boltzmann methods. *Journal of Computational Physics*, 229(3):728–744, feb 2010.

[89] Yun Wang, Ken S. Chen, Jeffrey Mishler, Sung Chan Cho, and Xavier Cordobes Adroher. A review of polymer electrolyte membrane fuel cells: Technology, applications, and needs on fundamental research. *Applied Energy*, 88(4):981–1007, apr 2011.

[90] Jing Xie, Shuai Ban, Bei Liu, and Hongjun Zhou. A molecular simulation study of chemical degradation and mechanical deformation of hydrated nafion membranes. *Applied Surface Science*, 362:441–447, jan 2016.

[91] Zhi-Yong Xie, Yong-Jun Jian, and Feng-Qin Li. Thermal transport of magnetohydrodynamic electroosmotic flow in circular cylindrical microchannels. *International Journal of Heat and Mass Transfer*, 119:355–364, apr 2018.

[92] Liang Yan and Fenglian Yang. The method of approximate particular solutions for the time-fractional diffusion equation with a non-local boundary condition. *Computers & Mathematics with Applications*, 70(3):254–264, 2015.

[93] Chun Yang and Dongqing Li. Electrokinetic effects on pressure-driven liquid flows in rectangular microchannels. *Journal of colloid and interface science*, 194(1):95–107, 1997.

[94] Chun Yang, Dongqing Li, and Jacob H. Masliyah. Modeling forced liquid convection in rectangular microchannels with electrokinetic effects. *International Journal of Heat and Mass Transfer*, 41(24):4229–4249, oct 1998.

[95] Da Yong Yang. Analytical solution of mixed electroosmotic and pressure-driven flow in rectangular microchannels. *Key Engineering Materials*, 483:679–683, jun 2011.

[96] Guangming Yao. An improved localized method of approximate particular solutions for solving elliptic pdes. *Computers & Mathematics with Applications*, 71(1):171–184, 2016.

[97] Guangming Yao, CS Chen, Wen Li, and DL Young. The localized method of approximated particular solutions for near-singular two-and three-dimensional problems. *Computers & Mathematics with Applications*, 70(12):2883–2894, 2015.

[98] Andriy Yaroshchuk, Edxon Eduardo Licón Bernal, and Thomas Luxbacher. Electrokinetics in undeveloped flows. *Journal of Colloid and Interface Science*, 410:195–201, nov 2013.

[99] Li-Hsien Yeh, Yu Ma, Song Xue, and Shizhi Qian. Electroviscous effect on the streaming current in a pH-regulated nanochannel. *Electrochemistry Communications*, 48:77–80, nov 2014.

[100] M. Zerroukat, H. Power, and C. S. Chen. A numerical method for heat transfer problems using collocation and radial basis functions. *International Journal for Numerical Methods in Engineering*, 42(7):1263–1278, aug 1998.

[101] Xueying Zhang, Muyuan Chen, C.S. Chen, and Zhiyong Li. Localized method of approximate particular solutions for solving unsteady navier–stokes problem. *Applied Mathematical Modelling*, 40(3):2265–2273, feb 2016.

[102] Cunlu Zhao, Emilijk Zholkovskij, Jacob H. Masliyah, and Chun Yang. Analysis of electroosmotic flow of power-law fluids in a slit microchannel. *Journal of Colloid and Interface Science*, 326(2):503–510, oct 2008.

[103] Huiqing Zhu. The method of approximate particular solutions for solving anisotropic elliptic problems. *Engineering Analysis with Boundary Elements*, 40:123–127, mar 2014.